ROBUST AIR-FUEL RATIO CONTROL FOR COMBUSTION ENGINES

Markus Brandstetter
Clare Hall, Cambridge

ROBUST AIR-FUEL RATIO CONTROL FOR COMBUSTION ENGINES

MARKUS BRANDSTETTER
Clare Hall, Cambridge

A dissertation submitted for the degree
of Doctor of Philosophy

*This document is available in postscript format on the world wide web at the following locations: `http://www-control.eng.cam.ac.uk/mb2/mb2.html` and the control engineering virtual library `http://www-control.eng.cam.ac.uk/Homepage/Papers.html`. For paper copies please e-mail `www-control-admin@eng.cam.ac.uk`.

To Bernd Pischetsrieder,
for the Arthur Anderson Lecture
at Queens' College
on 11th October 1995:
"The Future of the European Car Industry"

ABSTRACT

This thesis is an investigation of the applicability and the potential of robust control techniques for problems associated with transient control of the exhaust emissions from combustion engines. In particular, the problem of air-fuel ratio control in the presence of exhaust gas recirculation is considered, where the primary objective is to minimise the exhaust emissions during transients, while driveability and fuel economy are design constraints.

For that purpose, nonlinear representations of key engine components are re-formulated using linear fractional transformations and aggregated in a robust control framework. Thereby the bilinear transformation with variable sample time is instrumental to account for the periodicity of the event-based processes with engine revolutions. In this way, the basis for control system design and analysis is a set of linear time-invariant models in fixed operating points as well as a linear parameter-dependent system as a continuous function of engine parameters over the operating envelope.

Optimal controllers are designed for different operating points via $\mathcal{H}_\infty$ loop shaping. The control problem is posed by introducing appropriate error and disturbance signals and augmenting the nominal plant with dynamic weighting functions. The weighting functions serve as design parameters. In order to trade off robust stability versus performance, several optimisation problems are posed and evaluated in terms of closed-loop norms, the generalised stability margin and the gap metric. In doing so, feedforward and feedback control are designed separately in a modular approach.

With the support of the Ford Motor Company it was possible to implement robust multi-variable controllers successfully on a series production engine and demonstrate principal benefits with a view to complying with future emissions standards. The implementation is simple and fully transparent by using a block-oriented language on a rapid prototyping system. Both the controller parameters and the internal signals can be accessed, modified and monitored on all levels of the block diagram, from the generic controller structure to the engine interface hardware. Moreover, the flexibility of the computing environment allows for sophisticated experiments, either for the identification of engine parameters or for the evaluation of the control system's performance.

The controller commands the air by-pass valve and the fuel injection time based on measurements of the throttle plate angle, the mass flow of recirculated exhaust gas, the manifold pressure and the exhaust air-fuel ratio. It is embedded in a control scheme which consists of several look-up tables for the calculation of the error signals and the open-loop settings of the actuators in order to separate the static nonlinear behaviour of the engine from the linear dynamics.

The implementation is re-configured easily, and the design process is automated to an extent, that a complete re-design of the controller is possible in the test cell within a couple of hours. Different control schemes were tested on a 1.8l Ford Zetec engine under warm operating conditions.

The development of robust control strategies to complete the new drive cycles successfully is beyond the scope of this work. Superior performance as well as sufficient robustness must first be achieved in single operating points, before the control scheme can be extended to cover the entire operating envelope, either by gain scheduling several controllers between different operating points or with a control design that is genuinely for parameter-varying systems. However, current research is still at the first stage.

As a measure of success twenty representative transient sections were chosen from the new European drive cycle. To evaluate the control system's performance in fixed operating points, the driving scenarios were further simplified, in particular, engine speed is kept constant, while the throttle plate is perturbed. For moderate perturbations of several degrees, the air-fuel ratio is maintained within a band of five percent around the stoichiometric value at all times. Especially the duration of the excursions is reduced significantly in comparison to test data from current engine management strategies.

Keywords: linear fractional transformation, discrete event-based, robust control design, automotive, combustion engines, engine management, air-fuel ratio, $\mathcal{H}_\infty$

PREFACE

This dissertation is the conclusion of three years of research as a research assistant at the Department of Engineering of the University of Cambridge. It was the first research project at the Department in this area, under the sponsorship of the Ford Motor Company, and has grown into a much larger activity, continuing the development of control strategies for a wider range of applications as well as facilitating experimental work at the University.

I would like to thank my co-workers Mr. Andy Scarisbrick, Dr. Robert Dorey, and Mr. Charles Hawkins from the Advanced PowerTrain Systems Development Group (APTSD) within Advanced Vehicle Technologies (AVT) at the Research and Engineering Centre in Dunton for their involvement and co-operation. Moreover, I would like to thank especially Mr. John Varty from European Electronics Operations (EEO) for the test support.

I am very grateful for the opportunities that I was given to travel and to attend conferences. In summer 1995, I was offered to contribute to a series of presentations at the Ford World Headquarters, which were exciting times. I greatly enjoyed the insights into the activities of a global organisation. The financial support by the Ford Motor Company and EPSRC is gratefully acknowledged.

I am pleased to acknowledge Dr. Sanjay Lall for the authorship of the LaTeX style file which was used to typeset this document. Special thanks go to Dr. Thomas Fliegner for his readiness to review quickly revisions of odds and ends of this thesis at the final stage of writing.

Finally, I would like to express my thanks to Professor Keith Glover for his encouragement over the past years and for the beautiful insights into algebra.

As required by University Statute, I hereby declare that this dissertation is not substantially the same as any that I have submitted for a degree at any other university, is the result of my own work, and includes nothing which is the outcome of work done in collaboration except where stated otherwise.

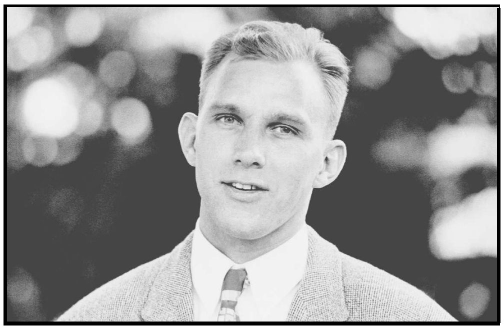

Markus Brandstetter
Auckland Court
Cambridge
December 1996

CONTENTS

1. INTRODUCTION

Undeniably, cars play a prominent role in our lives, whether we like it or not. It should be clear that this is not because the automotive companies are penetrating the markets so relentlessly, but this is because of us. They are quite right, when they say: “Everything we do is driven by you.” It is our Fahrvergnügen and comfort, and that’s nothing bad. However, some might say, that good cars go to heaven and only bad cars go everywhere. This shows how much interest and concern revolve around the car these days.

Automobiles and the pertaining infrastructure form the biggest mass transportation system on earth. They are a hallmark of our modern times, where people are always on the move and goods travel around the globe. The chains of consequences of how our automotive society might develop or how it might have developed without cars are very complex and not fully understood, so many social, political, and economic issues are involved. With regard to automotive design and car production, for example, innumerable technological advances have emerged from the industry and found applications in other areas. That is to say, not only has the automotive industry become a major factor in our economies, but it also provides with its resources the basis for future technological and business innovations.

Beyond research and development, the automobile is a pacemaker in a number of industries. For many companies, radical changes were necessary and continue, to stay in competition. Recent trends include lean production, lean management, and globalisation. There is an enormous thrust to cut cost, to reduce the time to market, and to expand into emerging markets. As a result, major re-organisations and process improvements have already taken place, and many more research and development activities are under way to devise and implement new processes in the spirit of total quality management and with a view to certification.

The opportunities for modern control applications were never greater to improve the vehicle’s overall efficiency and performance. A number of applications are already well established, such as the anti-lock brake system, traction control, or the control of active car suspensions. In view of future safety and emissions regulations, in particular on-board diagnosis and ultra low emissions standards, new engine and powertrain management systems are being developed.

Modern control technology is becoming more and more important for the analysis and design of interactive control systems in order to determine effective mechanisms for their integration, co-ordination and supervision. These issues can be approached from completely different angles, but what is, for example, the most effective mechanism to engage or disengage control systems in different operating modes. Should the engine and powertrain management be centralised or divided into several decentral units? The limitations of the systems currently in production make it necessary to re-consider the underlying hard- and software architecture as well as the methods of strategy development. Simple and transparent control solutions would be very desirable, not at least for easy maintenance and service, with clear-cut interfaces, free connectivity to components from different manufacturers, including the compatibility with related applications.

Allegedly, cars are still a major source of pollutant emissions, putting a severe strain on our environment. At the same time it seems almost impossible to reduce the amount of traffic, if only to a limited extent; on the contrary, both passenger and goods traffic are ever increasing. Moreover, the effects of mass transportation on the environment are not locally confined but extend over the entire globe, whether we consider the changes in the ozone layer of the atmosphere or global warming. The effects can only be seen in the long run, in fact, they are very difficult to predict and can hardly be attributed to individual causes. To what extent our environment is affected by traffic in comparison to other sources of pollution, for instance, in the process of energy production, volcanic eruptions, or even by the cows on our fens, is still very much under debate. At the end of the day the only effective measure is to use the latest technology available in order to minimise the emissions as much as possible at source.

As far as the exhaust emissions from vehicles are concerned, enormous improvements have already been accomplished, especially with the introduction of the catalyst. A reduction of more than 90% was possible by means of exhaust aftertreatment, *i.e.* by converting the components that remain in the exhaust gas in the case of incomplete combustion into harmless by-products. In this way, minimal emissions can be ensured at least in steady-state operation. Yet, the specification of the mixture composition to guarantee a high conversion efficiency of the catalyst is very demanding and not always met, in particular during transient operation. Surprisingly or not, urban air quality has not at all improved as expected [32]. Some people claim that with regard to the influences of automobile traffic the problem is already solved and that it is only a matter of time, until nature recovers.

In principle, new technological developments and innovations are always possible, only because of the cost implications the planning of a legislative framework is necessary to bring them about. Certainly with the announcement of ULEV legislation for the year 2000 many research and development projects were initiated in the area of engine control. The automotive manufacturers are faced with challenging requirements and must provide effective mechanisms for the precise control of the mixture composition during transient engine operation, mainly during acceleration, deceleration, and gear changes, where the current control strategies are insufficient.

For the purpose of control, it is a lot easier to characterise the mixture composition in terms of the so-called air-fuel ratio rather than in terms of the individual exhaust gas constituents: the hydrocarbons, carbon monoxide and oxides of nitrogen. There is a strong correlation between the concentrations of the exhaust gas components and the air-fuel ratio. A necessary condition for complete combustion is that the air-fuel ratio of the charge in the cylinder is stoichiometric, in which case the emissions are minimal.

The closer the air-fuel ratio can be maintained at the stoichiometric value, the better; less emissions will be produced, and the higher the conversion efficiency of the catalyst will be. Except for the mixing of the exhaust gases from different cylinders and the storage effect of the catalyst, the air-fuel ratio originally relates to the charge of an individual cylinder and in that sense evolves as a discrete quantity over time or crank angle. However, it is not sufficient for transient control, to characterise the mixture as merely rich or lean.

The total output of carbon dioxide is a completely different matter and so are particulate emissions. Great efforts are being made to relate engine design parameters formally, for example by the method of quality function deployment, to overall emission levels, driveability, or fuel economy, but this is inherently difficult. No matter how quickly the times are changing, modern automotive engineering and design cannot afford to be conflicting with customer perception in general and with the awareness of environmental issues in particular. In the meantime, customer interest has already shifted back to driveability, and the environmental friendliness of cars is generally assumed.

1.1 Motivation

In mass production the trade-off between product quality and production cost is decisive for economic success or failure. Therefore the final product will always exhibit variations caused by manufacturing tolerances, even if the production process is continually improved. In theory, the variations should be just acceptable, when suitable safety margins are included. However, much more is involved in building an engine, or even a vehicle, than can be predicted from worst-case calculations on the basis of the manufacturing tolerances. This may become apparent all too late in a completely unexpected customer complaint with regard to the cold start behaviour or the sound of the engine. In any case, the variability in the dynamic behaviour of engines is quite noticeable in a fleet of cars.

Moreover, the characteristics of many engine components are changing over the lifetime of a vehicle because of ageing, wear and tear. The temperature drift of the switching point of the exhaust gas oxygen sensor and the carbon build-up in the intake ports are two examples of ageing, which result in significant changes in the dynamic behaviour of the engine, not to speak of partial or complete component failure. Future safety and emissions regulations require durability of the engine's performance over 100,000 miles in addition to significantly lower overall emission levels, or at least safe failure. To prove and certify the technology that is compliant with these future standards is an enormous undertaking, as the necessary data to study the performance degradation as well as other long-term effects over the lifetime of a vehicle are still very limited. More and more intelligent sensors and actuators are introduced to provide the necessary functionality for supervisory control and fault detection in connection with on-board diagnosis [33].

A control system must be able to cope with all kinds of changes, whether they are highly dynamic, slowly varying, or persistent, whether they are known in advance, measured or unknown. From the point of view of control system design the system should be robust, or insensitive, with respect to such changes, which can be interpreted as disturbances to or uncertainty about the behaviour of the system. A model of the system can therefore never be exact; approximations must be made, and model parameters are not known exactly, numerical errors may occur.

If uncertainty is inherent in a system, model-based control on the basis of an inverted model is generally not advisable, since an exact compensation is problematic in the presence of uncertainty. Several types of uncertainty are shown in Figure 1.1. In the simplest case, the model error is additive, see Figure 1.1(a). In Figure 1.1(b) a multiplicative error is assumed at the input of the plant. Both types of uncertainty can also be represented in the much more general case of linear fractional uncertainty as in Figure 1.1(c).

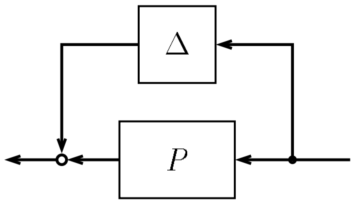

(a) Additive

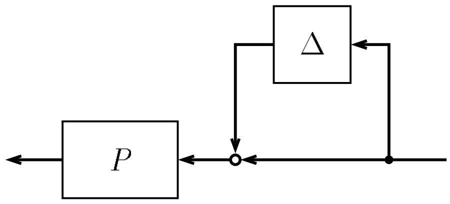

(b) Multiplicative

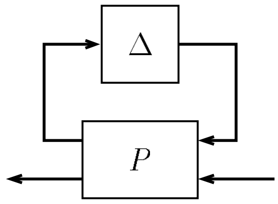

(c) Linear Fractional

Figure 1.1: Types of Uncertainty

A realistic approach to control system design should explicitly account for system uncertainty. In the present case, high performance under nominal operating conditions is not enough; a high level of performance must be sustained in the presence of disturbances and, possibly dynamic, uncertainty over the lifetime of a vehicle.

In the way current engine management systems have evolved it is very difficult to address these issues explicitly. Both the architecture of engine control units and the incident process of strategy development have become so complicated, that it is now very difficult to change their functionality towards these requirements without adverse side effects. Moreover, as it stands, the calibration of engines is a very lengthy process, which involves an enormous amount of human resources, but nevertheless the results may be sensitive to variations in the engine behaviour because of the element of tuning. The assessment of different types of uncertainty is just as comprehensive a task as the evaluation of engine performance over lifetime.

Robust control theory provides a powerful framework to deal with uncertain systems. It is a special feature of robust control that different types of uncertainty, as they arise from different sources, can be treated in a unified way. The fundamental set-up for robust control is the feedback arrangement in Figure 1.2 on the next page, where a linear system M is controlled by a controller K in the presence of perturbations Δ and disturbances d.

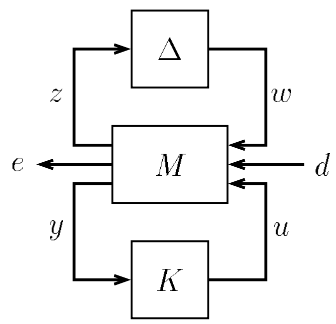

Figure 1.2: Generic Feedback Configuration

We are more specific about the type of system interconnection and the classes of signals and systems in Chapter 3. In the block diagram continuous- and discrete-time signals are not distinguished. Δ may contain known or unknown quantities. The prime motivation for feedback is to reduce the sensitivity of the system to disturbances and uncertainty. In robust control design the desired properties of the system, such as nominal stability and performance ($\Delta = 0$), robust stability, and robust performance, can be characterised in various problem formulations. We are more precise and state what we mean by robustness mathematically in Chapter 3.

Thus an engine control system can be thought of as an uncertain system in the most general sense according to Figure 1.3. As P, which is parameterised by Δ_1, is controlled by K, it behaves under the influence of d according to the performance index e. The controller itself is parameterised by Δ_2, which may include parameters in common with Δ_1. The variations in the plant characteristics as well as the controller function across the operating envelope are described by Δ_1 and Δ_2.

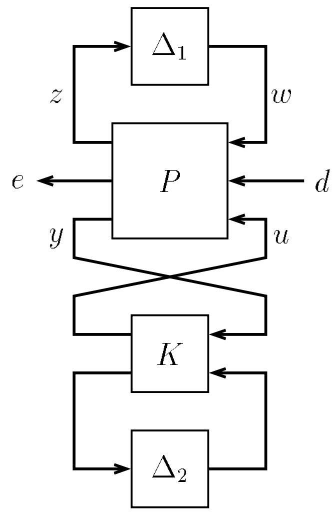

Figure 1.3: Engine Control System

This form of system interconnection is no more general than the set-up in Figure 1.2. In fact, the block diagram can be re-arranged to be of the same form. More specifically, Figure 1.3 shows the starting point for the synthesis of parameter-dependent controllers and gain scheduling via linear fractional transformations [45], which was the theoretical motivation behind this work.

1.2 Objectives

Precise air-fuel ratio control is required during transient engine operation, so that the mixture composition of the exhaust gas stays within narrow bounds around the stoichiometric value under all driving conditions. Then the benefit of the exhaust aftertreatment will be greatest, and the exhaust emissions will be minimal. For that purpose, the process of mixture composition in the intake manifold must be controlled in such a way, as to adjust both the fuel injection and the exhaust gas recirculation precisely to the air flow into the engine in response to the driver's demand.

Finding an appropriate control action is difficult because of the complex nature of engine behaviour. Above all, the engine behaviour changes significantly across the operating envelope. The response time in the intake manifold, for example, varies by two orders of magnitude. Moreover, the flow phenomena in the intake system, including the throttle body, the air by-pass, and the EGR system, are predominantly nonlinear. Finally, the delays that are inherent in the engine operation owing to the spatial distribution of the engine configuration, in particular with regard to the UEGO sensor and the catalyst, limit the use of feedback for transient control.

Optimal control is simple in steady state but generally much more difficult during transient operation, in the presence of disturbances and dynamic uncertainty. Typically, the driving situation is constantly changing in city traffic, which to a large extent consists of quick driving manoeuvres, accelerations and decelerations in between idle motion. In this respect the classical definition of individual operating points seems to be somewhat artificial for the present application, since individual operating points do not really characterise a transient driving situation. On the other hand, further advances in the areas of engine testing and engine modelling are still necessary, before alternative characterisations can be adopted.

We would like to demonstrate significant benefits of robust control techniques in a model-based approach to transient air-fuel ratio control. It is a great challenge to develop new integral control strategies in order to improve the transient performance of engines, to improve the process of strategy development by replacing ad hoc refinements and lengthy calibration, and shorten the development cycle at the same time. We would also like to develop a greater understanding of dynamic engine behaviour, of the fundamental limitations of transient emissions control as well as the limitations of current engine management systems. New concepts are needed for ultra low emissions vehicles to pass federal test procedures. A number of issues that are addressed in this thesis also arise in other engine and powertrain control applications. We would like to indicate the technological requirements for future automotive control systems by the example of a generic control problem.

In this thesis, the focus is on exhaust emissions; other sources of emissions, such as underhood evaporation, are not considered. Therefore the special features that are involved in recycling fuel leakages from various sources, like crankcase ventilation, are excluded from the investigation. The problem of transient air-fuel ratio control is treated for an engine under warm operating conditions, separately from the start-up phase before the light-up of the UEGO sensor and the catalyst. Hence, neither the electrically heated catalyst, nor the concept of exhaust gas ignition is relevant to the subject matter. Since a control-oriented specification of the dynamic behaviour of catalysts is yet to be determined, it is assumed, for the sake of simplicity, that the behaviour is optimal for a constant stoichiometric air-fuel ratio and that any deviations from this value are undesirable. The storage of oxygen in the catalyst does not necessarily imply a requirement for tracking control during transient engine operation.

In particular, a control configuration is considered, where measurements of the throttle plate angle, the mass flow of recirculated exhaust gas, the manifold pressure, and the exhaust air-fuel ratio are available for the control of the air by-pass valve and the fuel injection time. The investigation is based on the 1.8l Ford Zetec engine, which is a four-cylinder series production engine with a sequential fuel injection system.

1.3 Background

The engine management systems of today have evolved over a number of years. The schematic in Figure 1.4 on the next page gives an overview of the many components that are involved in engine control. There are a number of interconnected feedback loops in addition to the subloops of the individual components. Depending on the mode of operation or the operating condition, the interrelationship between the components can be quite different. The principal components which are relevant for air-fuel ratio control are the throttle body, the air by-pass, the EGR system, the intake manifold, the fuel injection system, the cylinders, the exhaust system, and the UEGO sensor. A large part of the control strategies that are implemented in the engine control unit is concerned with steady-state operation only, but, typically, some functions are also included for the compensation of the dynamic processes of the mixture composition in the intake manifold.

The classical approach to air-fuel ratio control was to design simple PI controllers in fixed operating points and to schedule the controller gains across the operating envelope [36]. For the analysis of the closed-loop behaviour in the frequency domain, the nonlinear characteristic of the EGO sensor was represented by a describing function. On the basis of a very simplistic model of the engine processes, a first order time-delay system, the choice of the proportional and integral gains only involved a trade-off between the magnitude and the frequency of the resulting limit cycle. If engines were operated in steady state only, such a control scheme would be completely sufficient. In order to increase the bandwidth of the control system, the use of a Smith predictor was suggested in [36] to compensate the delays inherent in the engine operation.

An even simpler way was found in recent years to replace a number of PI controllers with a single nonlinear controller [15]. In sliding mode control the control problem is formulated in terms of a sliding manifold, which is designed to give global Lyapunov stability. However, in order to determine the control calculations, it is necessary to differentiate the stability condition and to solve for the control inputs by dynamic inversion. The idea was that a switching control would be compatible with the switching characteristic of the EGO sensor. As a matter of fact, the calibration effort is reduced

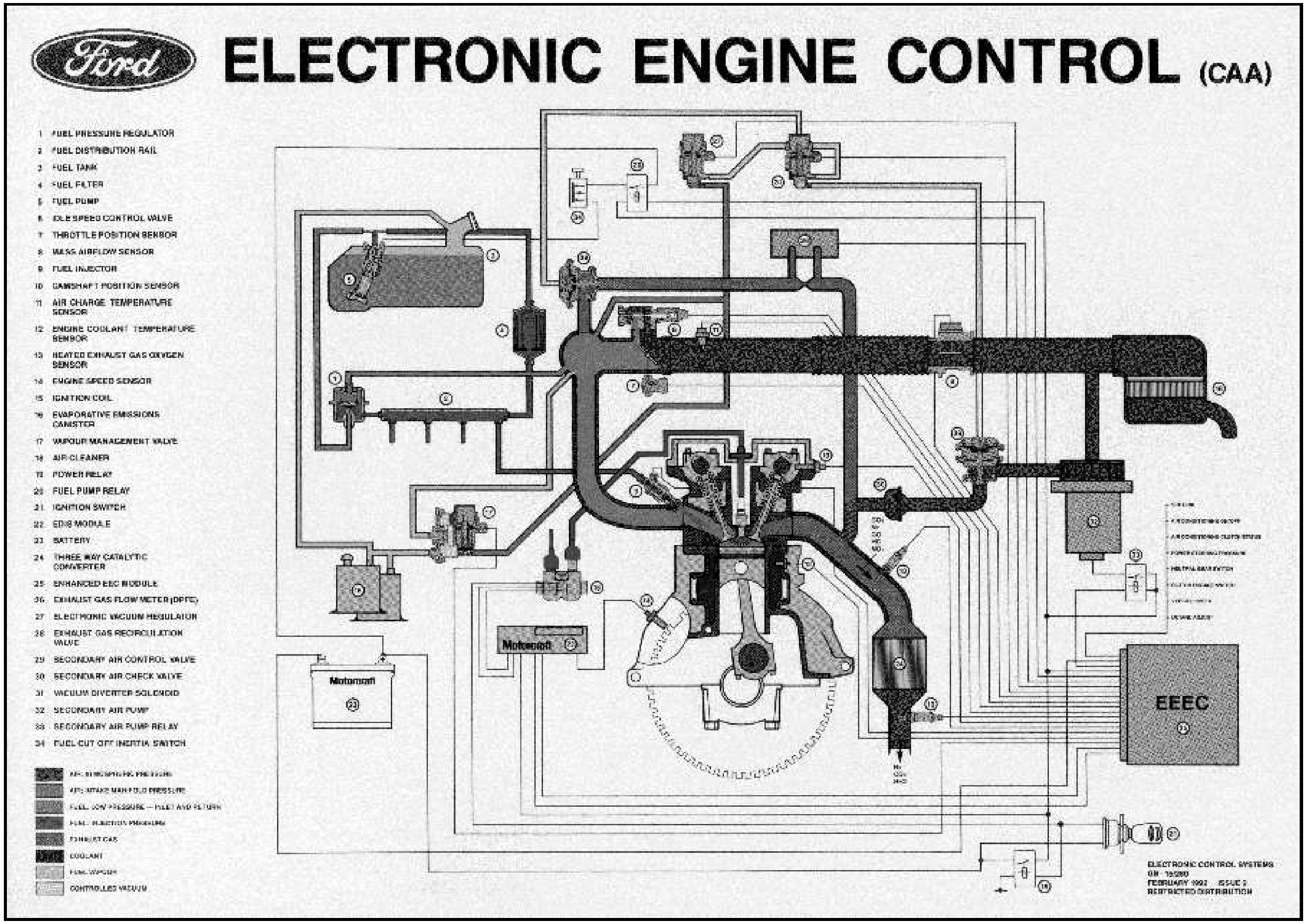

Figure 1.4: Electronic Engine Control

significantly with this approach, but several assumptions in the derivation of the controller are very critical. Just as in the case of [36], there is no great potential for transient control with feedback only.

Yet another alternative with the same scope are neural nets [37, 49]. They exhibit a particularly simple structure and, in principle, do not need any *a priori* information about the system to be controlled. Neural nets are very effective in approximating static nonlinear functions, but in feedback arrangements with dynamic systems their use is not as straightforward and can be problematic. A major limitation in practice is the time it takes to learn the desired behaviour, especially if dynamic processes are involved that are quickly changing. Although the learning capabilities of neural nets may be very appealing with a view to the adaptation to changing requirements over the lifetime of a vehicle, it is difficult to include *a priori* knowledge about the system for the sake of a short learning phase, and often extensive training is required. This is reflected in the approach of [37], where a neural net is trained off-line on the basis of linear measurements of the air-fuel ratio, before it is implemented in a standard configuration with the nonlinear EGO sensor.

More recent approaches address the problem of transient air-fuel ratio control and, in doing so, have several features in common. It is increasingly common to calculate the base values of the engine settings as a function of engine speed and the position of the throttle plate and to replace the air mass flow sensor. The emphasis has shifted from feedback to feedforward control in order to achieve high performance during transient engine operation. With the latest control concepts there is a clear trend away from controllers which require a lot of engine calibration. The design of engine control systems used to be based on continuous-time models, but it is now widely recognised that engine dynamics are best represented in a discrete event-based setting. However, most concepts rely on an electronic throttle to hold the position of the throttle plate constant during the intake stroke, as to ensure a reliable air charge estimation. Typically, they also rely on a wide-range UEGO sensor. In this thesis, the problem of transient air-fuel ratio control is treated as a disturbance rejection problem. As a consequence, an electronic throttle is not necessary.

Initially, engine models for control system design were developed in continuous time [40, 14, 39]. Still they were all mean value models which described the engine behaviour in terms of characteristic values over an engine cycle [28]. A question of immediate interest is how to equip such models with engine data. Both on- and off-line system identification techniques for model-based engine control were investigated in [4, 3]. Particularly the dynamic behaviour of fuel deposits in the intake system has been a much studied problem. In [44], for example, perturbations to the fuel injection time are correlated with the torque response to identify a model with two parameters. A more sophisticated model is proposed in [52].

By means of an observer the states of a system can be re-constructed on the basis of current measurements. In principle, any system can be an observer, if the state estimates are corrected via feedback. A combination of state and parameter estimation is also possible.

A number of observer-based control configurations have been applied to the problem of air-fuel ratio control. In all cases, the air charge in the cylinder is estimated, either in terms of manifold pressure and engine speed [35] or in terms of volumetric efficiency

[53, 6]. In the simplest case, the fuel injection time is calculated by evaluating an inverted model of the process of fuel injection [11, 30, 27].

The most advanced approach so far has been to design a time-varying Kalman filter in order to estimate certain parameters related to the dynamics of fuel injection as well as the dynamics of the oxygen sensor on-line [54, 53, 51]. However, a persistent excitation of the system was necessary for the filter to track the true parameter values. The filter was tuned by the method of covariance matching. Finally, a compensator was adapted with the estimated parameter values to achieve a certain closed-loop behaviour according to a reference model. Alternatively, a linear quadratic Gaussian regulator has been designed by loop transfer recovery on the basis of a linearised model at idle operation [43, 42]. Generally, experimental results are demonstrated in fixed operating points for constant engine speed. The importance of the delays inherent in the system is emphasised in [27]. Moreover, it is claimed in [6, 26] that with the approach described therein a dynamic compensation for the fuel injection is not necessary under warm operating conditions for the most part of the operating envelope, if only the estimates are corrected for the delay in the timing of the fuel injection. Some attempts at cylinder-individual control have also been made [11].

There is yet another line of development in the area of adaptive air-fuel ratio control [21, 20, 1, 13, 12]. At first, a constant gain extended Kalman filter was developed and implemented on a single-cylinder research engine [13, 12]. The control scheme included an integrator that could be reset to speed up the slow integration in the feedback loop. Feedback control relied on the UEGO sensor. Next, the linear sensor was replaced by a series production sensor by embedding a nonlinear model of the sensor in the observer [1]. The idea of integral control via bias estimation was given up, and the integral action was separated from the observer structure. This work was extended to the case of a multi-cylinder engine by incorporating further adaptive features in the feedforward part of the control scheme [21, 20]. The result was a multi-rate control system, where the calculation of the air flow into the engine was oversampled by a factor of four and the calculations of the fuel injection time for the individual cylinders were operated at a four times lower rate in relation to the fundamental sample period. Special attention was given to modelling the cylinder filling. Although $\mathcal{H}_\infty$ controllers admit a representation in observer form, the approach to robust control design is fundamentally different.

1.4 Contribution

The problem of air-fuel ratio control has been studied in a robust control framework. The suitability of robust control techniques and their effectiveness for this application are demonstrated in control system design.

- A uniformly discrete event-based representation of the engine processes is derived for robust control.
- The air by-pass valve as an already existing component is used in a new way for air-fuel ratio control.
- The mechanism of exhaust gas recirculation is also integrated in the air-fuel ratio control scheme.

- Recent advances in robust control theory are applied in the design of multi-variable controllers for transient air-fuel ratio control.
- The concept of discrete parameter-dependent systems which are variable with the sample time is introduced in order to shift seamlessly between system representations in continuous and discrete time.
- Robust multi-variable controllers have been implemented successfully on a series production engine in a vehicle installation.
- A single controller can be optimised to give high performance in a certain operating region, superior to current engine management systems, see Figures 1.5 and 1.6 on the next pages.[1]

[1] A detailed explanation of these diagrams is given in Chapter 5.

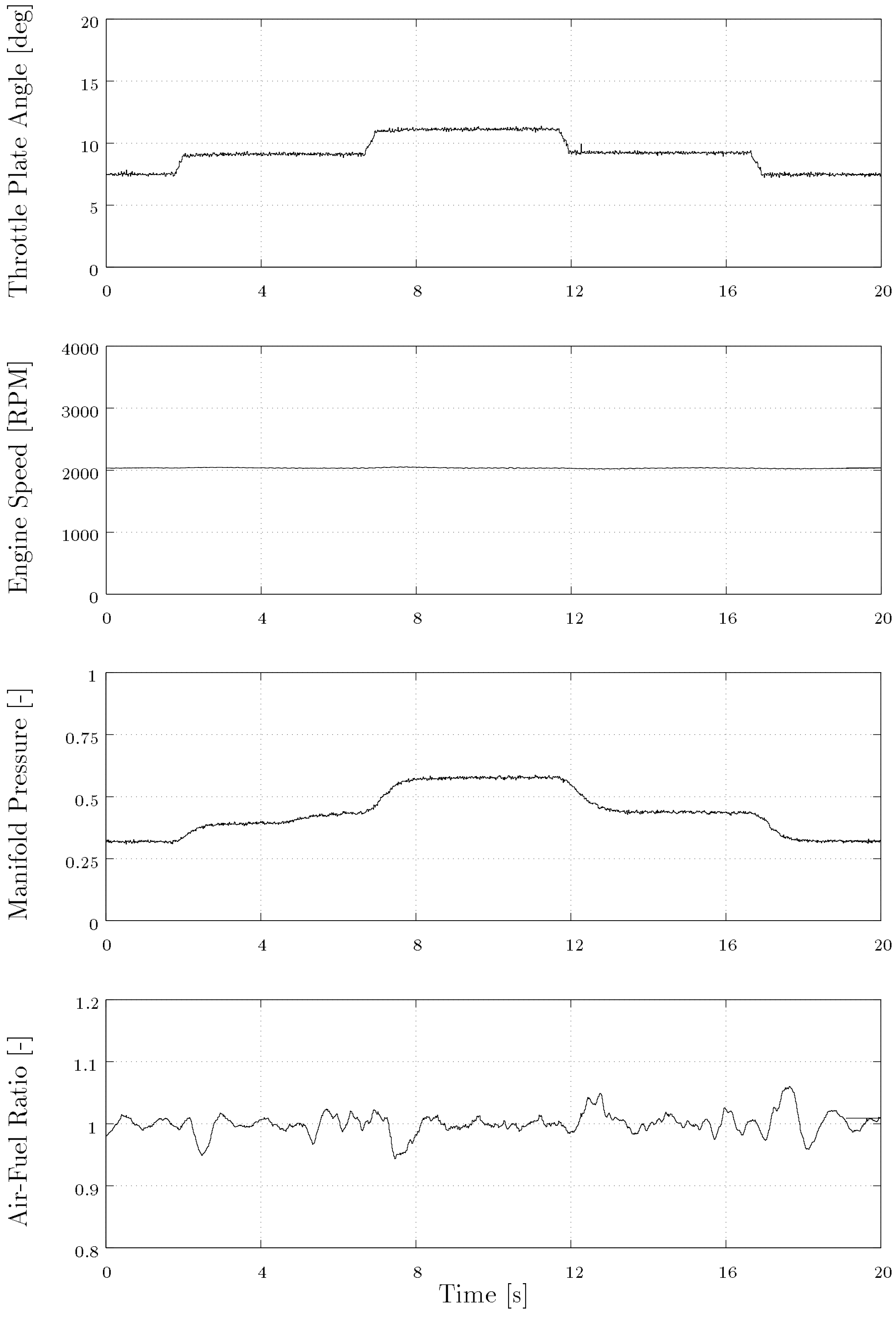

Figure 1.5: Modular Feedforward Design, Measurements

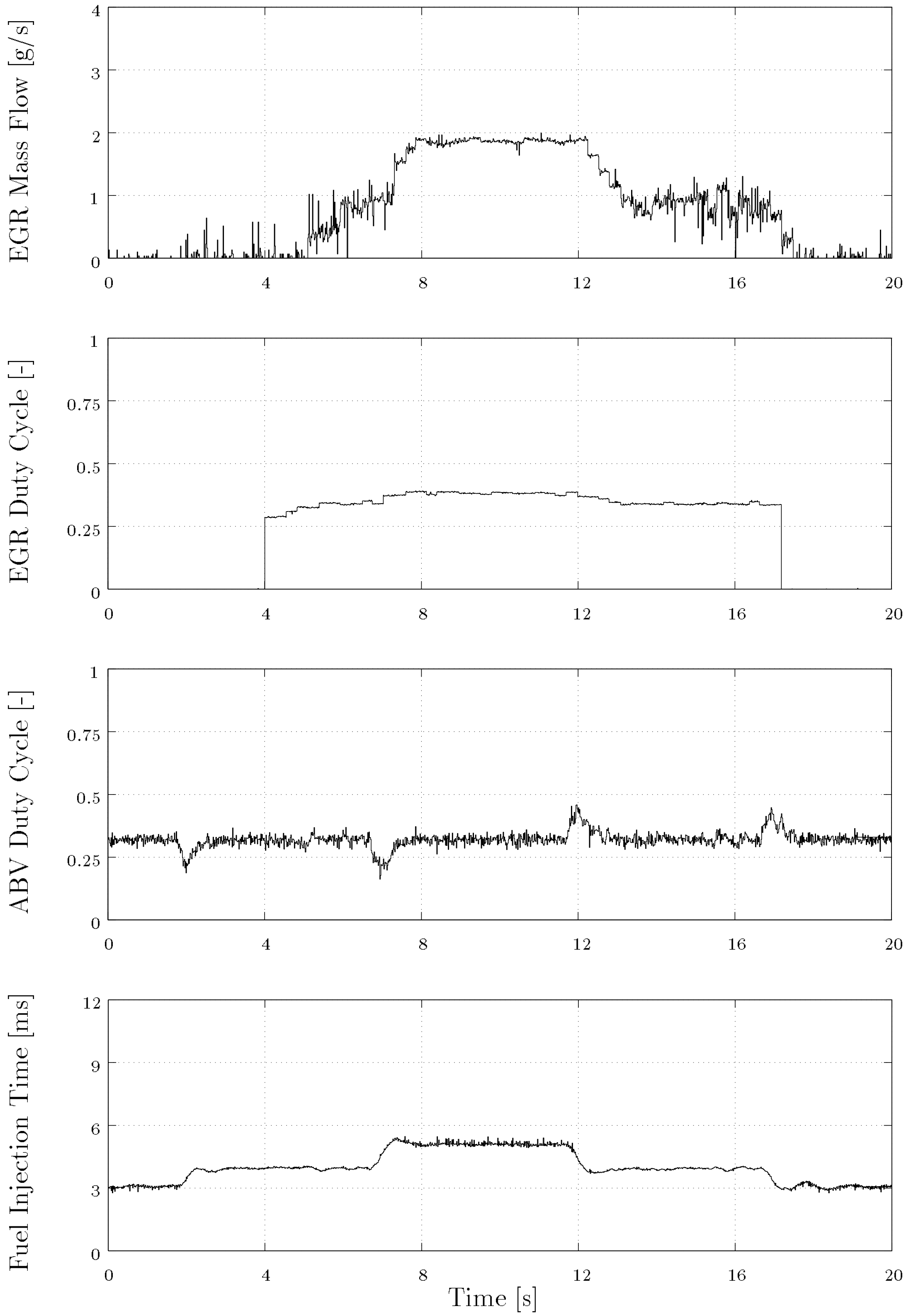

Figure 1.6: Modular Feedforward Design, Control Signals

1.5 Overview

A decisive feature of combustion engines is that their operation is event-based. The operation is also periodic with engine revolutions owing to the periodicity of the combustion cycle. We therefore include the aspect of event-based sampling in the characterisation of the dynamic behaviour of the engine. To this end the following relationship between time and crank angle increments

$$dt = \frac{d\varphi}{6n}, \tag{1.1}$$

is instrumental, where the time t is in seconds, the crank angle φ in degrees, and the engine speed n in RPM. In the case of a four-cylinder engine the fundamental sample period is

$$\Delta\varphi = 180 \ \text{ deg} \ . \tag{1.2}$$

Using the substitution above, the differential equations that constitute an engine model can be integrated with respect to crank angle rather than time. It can also be seen from Equation (1.1) on this page that variations in engine speed will result in variations in the sample time. In this work, engine speed, or equivalently the sample time, will be treated as an exogenous variable to characterise the operating point of the engine as well as the variations of the engine parameters.

The type of interconnection in Figure 1.1(c) on page 4 is called a linear fractional transformation and is defined as

$$\mathcal{F}_u(P, \Delta) = P_{22} + P_{21}\Delta\left(I - P_{11}\Delta\right)^{-1} P_{12} \, . \tag{1.3}$$

It is a generic form of representation for uncertain systems as well as system operations. Typically, P contains the known part of a process, while Δ is unknown, but, more generally, Δ may also contain known quantities. A more complete introduction to linear fractional transformations will be given in Chapter 3.

A variety of concepts in system theory admit representations via linear fractional transformations, such as power series, *cf.* Appendix E, rational functions, and linear systems, whether they are uncertain or parameter-dependent. In the most general case a class of linear parameter-varying systems can be considered, where the parameters are varying in real time. The star product $\mathcal{S}(P, K)$ in Figure 1.3 on page 5, by which we chose to describe an engine control system, consists of two such systems. Linear fractional transformations are fundamental to robust control. In particular, the interconnection of two LFT systems is again a linear fractional transformation. Therefore the set-up in Figure 1.3 is, in principle, the same as in Figure 1.2 on page 5.

Another example of an LFT operation is the bilinear transformation

$$\frac{1}{s} = \frac{h}{2}\frac{z+1}{z-1}, \tag{1.4}$$

which is used in this thesis to switch between continuous and discrete time. In the equation above h denotes the sample time, s is the Laplace variable and z the shift operator. In this way, the discretisation of systems fits seamlessly into the robust control framework. A generalised version of the bilinear transformation is derived in Appendix B in order to include perturbations to the sample time.

After these theoretical highlights the approach to transient air-fuel ratio control in this thesis is in detail as follows.

Chapter 2: Event-Based Engine Model

First, central issues in engine modelling are surveyed in Section 2.1. On this basis, models are derived for the engine components in Section 2.2. The machinery for the model development are linear fractional transformations. In Section 2.3, the component models are aggregated to give a set of discrete event-based models in fixed operating points. Finally, a single parameter-dependent system representation is constructed in Section 2.4.

Chapter 3: Robust Control Theory

This chapter is the control toolbox of this thesis. It provides the control theoretic concepts behind the approach to control design in Chapter 4. All material is taken from the standard literature. The basic system theoretic concepts are introduced in Section 3.1. Section 3.2 contains a brief description of $\mathcal{H}_\infty$ optimal control and two control problem formulations of particular importance. Some approaches to extend the present scope of the thesis are outlined in Section 3.3.

Chapter 4: Control Design

Robust multi-variable controllers are designed on the basis of the models in fixed operating points. Two different control configurations are considered. The control scheme in Section 4.1 includes active EGR control, while in the second configuration in Section 4.2 the EGR system is controlled by an external controller. In both sections the controller development is carried out along similar lines to make comparisons possible. In particular, both control designs are analysed in terms of closed-loop norms and frequency responses, in the gap metric as well as in linear simulation.

Chapter 5: Experimental Results

The two control schemes from the previous chapter were implemented on a series production engine. The experimental set-up and the controller implementation are documented in Section 5.1 and Section 5.2, respectively. The engine test data are presented in Section 5.3. A general interpretation of the data is given in Section 5.4. The chapter is concluded in Section 5.5 with an outlook on the computational requirements for gain scheduling.

Chapter 6: Conclusions

In addition to the thesis summary in Section 6.1, the scientific contribution is discussed in Section 6.2, and a perspective for future research is developed in Section 6.3.

Appendices

In Appendix A a procedure is outlined to compensate static actuator nonlinearities. A bilinear transformation which allows for discrete parameter-dependent systems to be variable with the sample time is derived in Appendix B. For quick reference, two tables in Appendix C allow to interpret the event-based frequency scale that is used in Chapter 4 in terms of physical frequencies and response times. Appendix D contains a description of two gain scheduling schemes which could be used to extend the present scope of the control designs across the operating envelope. An LFT realisation for two-dimensional polynomials is given in Appendix E. Finally, Appendix F contains the formal notation and Appendix G the symbols and acronyms used in this thesis.

2. EVENT-BASED ENGINE MODEL

Models have always been important tools for engineers to study the behaviour of complex systems. Systems are represented in many different ways for a variety of engineering tasks. The range of automotive applications is enormous and still growing. Especially, in the development of engine and powertrain control systems there is a strong demand for dynamic multi-variable models because of the complex interactions between engine, powertrain and vehicle components. However, models are usually for a specific purpose, and the suitability of a model for re-use or its generic value are often not part of the requirements for its development. If the different engineering problems that arise in engine and powertrain control could be solved separately in a modular approach, this would not be an issue, but it is the industrial experience of practical difficulties that creates the demand for compatible models and a common framework. An analysis of different engine configurations and control systems is necessary from a systems perspective, because the way engine management systems have evolved makes it difficult to develop clear-cut control strategies using calibration and tuning techniques only.

In industry there is a great deal of re-thinking in many areas. What are the requirements for the integration, co-ordination and supervision of different control systems? What is an appropriate representation of engine behaviour in this context? Genuinely, the engine is a hybrid system combining continuous flow processes with discrete event-based processes, such as fuel injection and spark ignition.

2.1 Preview

2.1.1 Nonlinear Simulation Model

It would be appropriate to represent these processes with their intrinsic properties in a nonlinear and highly accurate model that would serve as a reference for the specification of the control problem. Control schemes could be implemented with such a model to be verified and evaluated before the implementation on the engine.

Both the implementation of the controller and the implementation of the model should be independent of the software and hardware used. With general-purpose simulation packages this is often only possible to a limited extent, but the architecture of a virtual machine would be ideal, where the functionality of the upper layers of the implementation is independent of the functionality of the lower layers. The same considerations apply to hierarchical or decentral control systems.

As an example the interconnection of the key components for air-fuel ratio control is shown in SIMULINK in Figure 2.1 on the following page. Any of the components could be modified or replaced without affecting the implementation of the other modules. Unfortunately, the functionality of the software tools to implement and simulate hybrid systems is not mature; there are a number of implementational and programming issues with regard to event generation and the event-based execution of program modules that are not readily solved.

2.1.2 Model Validation

The validation of the overall system behaviour, for example over a prescribed drive cycle, is a very hard problem. Model validation is very difficult in general [17]. For realistic problem sizes and data records, model validation in a formal sense is not practical using current computer technology and optimisation algorithms. In the case of nonlinear and hybrid systems the problems are even more complicated.

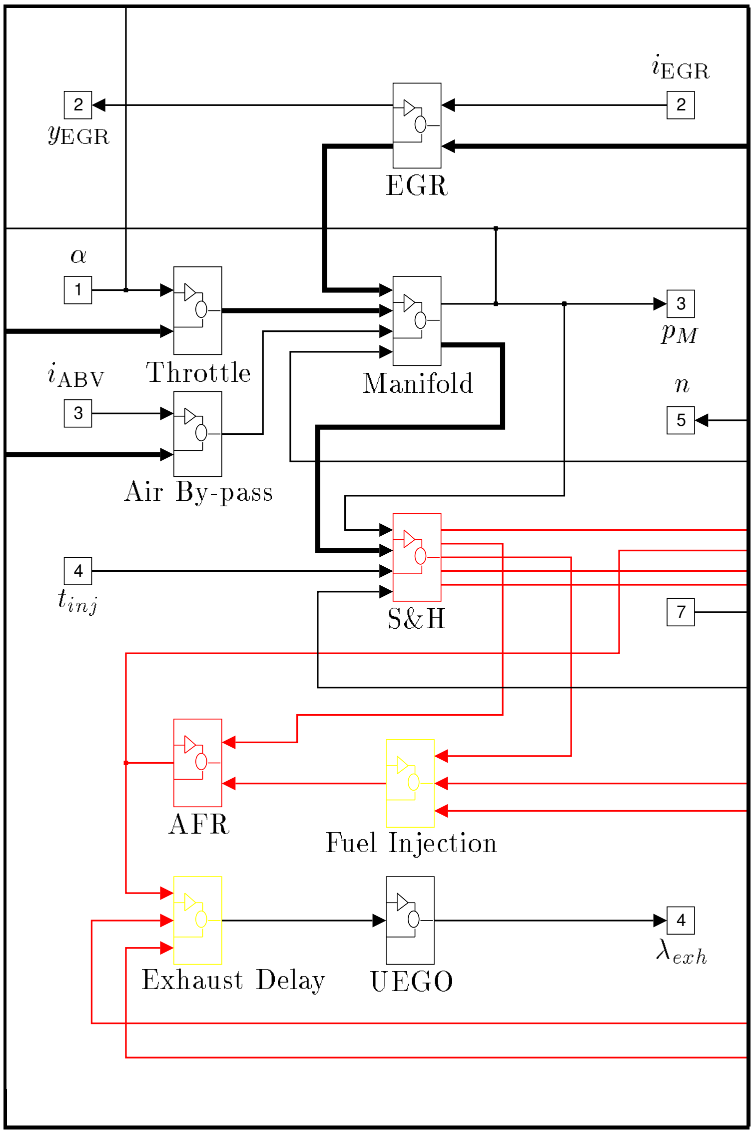

Figure 2.1: Nonlinear Hybrid Engine Model

A more practical approach is to introduce time-domain measures, such as the RMS value or 2-norm of model outputs that can be measured in order to quantify the differences between real and simulated engine behaviour. The assessment becomes somewhat arbitrary though, because a number of issues cannot be resolved in a formal way. For example, what should be the overall measure of success? Can the complexity of the problem be reduced by considering the validation of the subsystems first? How can we attribute discrepancies, as observed in our measures of error, to individual dynamic effects and tune the corresponding model parameters using general nonlinear optimisation? What are the implications for the system identification of engine components for the purposes of control? In addition, it would be very useful to combine the procedures of system identification and model validation. We return to the issues of experimental accuracy and model uncertainty on the basis of the results in Chapter 5.

From our experience the continuous processes are validated more easily than the discrete event-based processes. So far we have only been able to validate certain parts of a nonlinear model that is implemented in SIMULINK. Simulation studies were successful mostly for the subsystems of the intake system. To achieve consistency among all components in steady state is already difficult, because the open-loop settings of the engine were derived from different experiments than the model parameters. For these reasons, it has not been possible to evaluate the control schemes of Chapter 4 in nonlinear hybrid simulations before their implementation on the engine. A full validation of the model over the European drive cycle is part of on-going research.

2.1.3 System Identification

The model that is to be described in this chapter consists of parameter-dependent systems and two-dimensional nonlinear functions, which map the model parameters over the operating envelope. The dynamic systems are linear in the input, the state, and the output respectively, yet their state-space data depends on parameters, which are tabulated in terms of states of the model or exogenous variables. In the construction of the model the dynamics are linearised analytically as far as possible, whereas the local gains are calculated by numerical linearisation of the look-up tables.

The dynamics of the crankshaft are considered to be quasi-stationary due to the large inertia, in comparison to the air and fuel flow processes, and are not modelled explicitly. Therefore engine speed is considered to be a slowly-varying exogenous variable.

Even though the dynamics of the crankshaft are not part of the model, the model is still too large and too complex to be identified as a whole. In spite of the complex interactions between the components of the model, they are therefore treated separately for the purposes of system identification. In view of the additional complexity of engine experiments and limited experimental capabilities, the only way forward was to identify in a simplistic approach the individual components using standard system identification techniques for SISO systems.

The local dynamics were identified for small perturbations around fixed operating points using least squares techniques in the time domain on event-based data records. Neither measurement noise nor system noise were particular issues in the identification process; the measurements were filtered to remove the high-frequency content from the data, *i.e.* the cyclic oscillations and fluctuations of the engine variables. Besides, it would have been beyond the scope of this work to establish the distributions of the model parameters for the individual cylinders. All engine data in this thesis have been produced by, and are presented by courtesy of, the Ford Motor Company.

2.1.4 Model Uncertainty

Uncertainty is always present, or inherent, in complex systems. The basis for the analysis and design of such systems that should be robust with respect to their inherent uncertainty is a mathematical model of the relevant dynamic processes as well as the associated uncertainty.

There are a number of different sources of uncertainty, so that it arises naturally in different locations of a system. One could consider the experimental repeatability and measurement accuracy at the stage of experimentation, the selection of suitable model parameterisations, the confidence in parameter estimates and the interpretation of residuals at the stage of system identification, and the numerical issues of approximation in the model construction.

How the assumptions made and errors incurred at the different stages influence the overall accuracy of the model is difficult to assess. A rigorous error analysis is hardly possible, because the pieces of quantitative information are not readily compatible. However, the effects of all these kinds of errors should be of second order and negligible in comparison to the changes in dynamics as a result of the parameter variations across the operating envelope. Still, it would be very useful, if also such sources of uncertainty could be integrated in a common framework.

We are primarily concerned with the uncertainty in system dynamics, be it constant uncertainty or uncertainty as a result of real-time parameter variations, and would like to represent the different types of uncertainty, as they arise in the engine components, in a unified way; whether it is gain or phase uncertainty as in the case of scalar systems, or more generally, dynamic uncertainty as in the case of multi-variable systems, whether it is unstructured or parametric uncertainty.

In our case, the parameter variations are known in a number of operating points. For simplicity, the ambient conditions, *i.e.* pressure and temperature, are assumed to be constant. With this approach we would like to understand the fundamental limitations of the physical system, the control configuration and the model itself. We would like to analyse the sensitivity of the model to unmodelled dynamics, *e.g.* additional delays, and assess the achievable performance on this basis. The key question is what accuracy of the model is required in the feedforward path for precise air-fuel ratio control.

In this chapter, we focus on engine modelling for the design of robust control systems using $\mathcal{H}_\infty$ synthesis and analysis techniques, such as $\mathcal{H}_\infty$ loop shaping and μ analysis. For that purpose, the nonlinear representations of the key engine components are reformulated using linear fractional transformations in Section 2.2 and aggregated in a robust control framework. We derive a set of linear time-invariant models in fixed operating points (Section 2.3) as well as a linear parameter-dependent system as a continuous function of engine parameters across the operating envelope (Section 2.4).

2.2 Engine Components

The following engine components are modelled in the sequel: throttle body, air bypass, EGR system, intake manifold, fuel injection system, cylinder filling, delays in the exhaust system, and UEGO sensor.

2.2.1 Throttle Body

The primary air supply of the engine is through the throttle body except for idle operation, when the air is supplied through a by-pass. In any case, the key determinant for the throughput of the engine is the air mass flow past the throttle, which is a function of the driver's demand and the pressure ratio across the throttle body.

Ideally, one would therefore like to consider the engine dynamics along air mass flow trajectories or at least along trajectories of the driver's input in terms of the throttle plate angle. However, for historical reasons and because of experimental limitations the development of dynamic engine models has predominantly revolved round steady-state operation to characterise the local dynamics around an equilibrium point. The same approach is adopted here, although the genuine problems of emissions control only arise during transient operation across the operating envelope.

In the present model the throttle plate angle is treated as an exogenous input to the throttle body; in particular, neither the transfer characteristics of the mechanical link between the accelerator-pedal and the throttle plate nor the characteristics of a human driver are considered. The throttle body component is considered to be a purely mechanical system, yet without friction. That is to say, a disturbance to the position of the throttle plate results in an instantaneous change in the air mass flow, not as in the case of electronic throttle control, where the driver's demand is delayed.

Throttle Characteristic

Given the area function

$$A(r,R) = 2R^2\left(\arcsin\sqrt{1-\frac{r^2}{R^2}} - \frac{r}{R}\sqrt{1-\frac{r^2}{R^2}}\right) \tag{2.1}$$

in terms of the radius of the shaft r and the radius of the bore R, the free cross-sectional area of the throttle can be written as

$$A_{\mathrm{TH}} = \begin{cases} A_{\mathrm{TH}\,max} - \frac{b}{R}\cdot A(r,b) & \text{if } 0 \le \alpha < \alpha_{max} \\ A_{\mathrm{TH}\,max} & \text{if } \alpha = \alpha_{max}, \end{cases} \tag{2.2}$$

where

$$A_{\mathrm{TH}\,max} = A(r,R) \tag{2.3}$$

is the maximum area, when the throttle is fully open,

$$b = \frac{\cos(\alpha+\alpha_0)}{\cos\alpha_0}\cdot R \tag{2.4}$$

for short notation, and

$$\alpha_{max} = \arccos\left(\frac{r}{R}\cdot\cos\alpha_0\right) - \alpha_0 \tag{2.5}$$

is the corresponding angle, when the throttle plate lies just within the projection of the shaft. Finally, α_0 is the off-set, when the throttle is closed. For a geometric derivation see [51].

Flow Characteristic

Stationary isentropic flow through an orifice is characterised by the flow function

$$\psi = \begin{cases} \sqrt{\frac{2\kappa}{\kappa-1}\left[\left(\frac{p}{p_0}\right)^{2/\kappa} - \left(\frac{p}{p_0}\right)^{(\kappa+1)/\kappa}\right]} & \text{if } \frac{p}{p_0} \geq \left(\frac{p}{p_0}\right)_{choked} \\ (\psi)_{choked} & \text{if } \frac{p}{p_0} < \left(\frac{p}{p_0}\right)_{choked}, \end{cases} \tag{2.6}$$

where

$$\left(\frac{p}{p_0}\right)_{choked} = \left(\frac{2}{\kappa+1}\right)^{\kappa/(\kappa-1)} \tag{2.7}$$

is the critical pressure ratio, below which the flow is choked, *i.e.* sonic:

$$(\psi)_{choked} = \sqrt{\kappa\left(\frac{2}{\kappa+1}\right)^{(\kappa+1)/(\kappa-1)}}\,. \tag{2.8}$$

κ denotes the ratio of the specific heats of air.

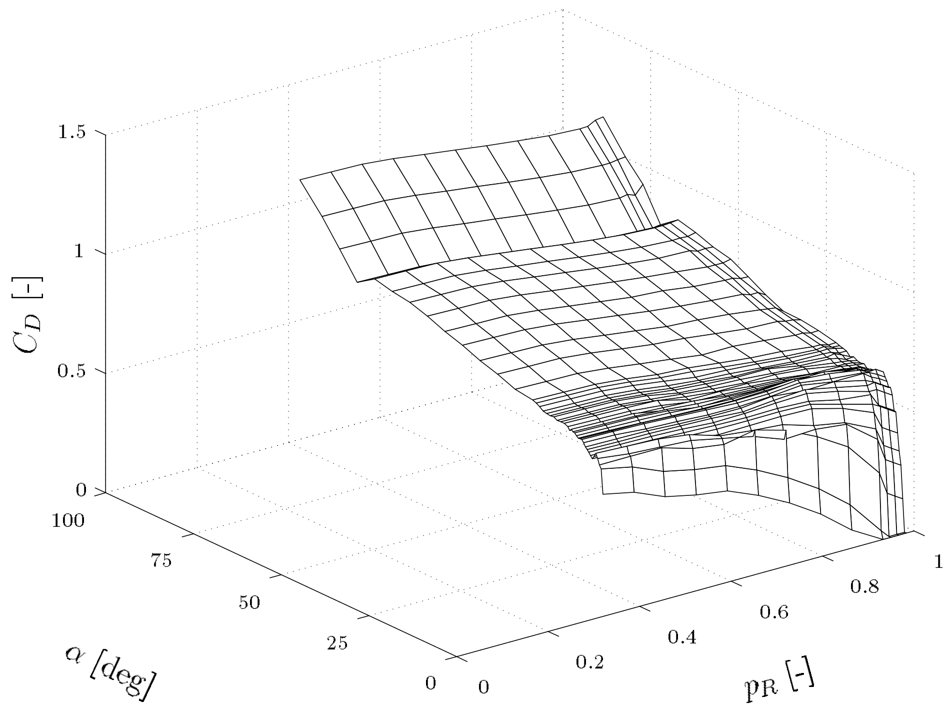

Figure 2.2: Discharge Coefficient

The air mass flow through the throttle body is often represented by a separable function in terms of the throttle plate angle α and the pressure ratio p_R of the pressure in the intake manifold with respect to the ambient pressure. The two-dimensional function is adapted to flow data using the discharge coefficient C_D as a free parameter. With the throttle and flow characteristics as above the air mass flow through the throttle can be expressed as

$$\dot{m}_{A\,\mathrm{TH}} = \frac{C_D A_{\mathrm{TH}}(\alpha) p_0}{\sqrt{\mathsf{R}T_0}} \cdot \psi(p_R)\,. \tag{2.9}$$

The pertaining discharge coefficient is shown in Figure 2.2 on the preceding page. For the sake of simplicity, the ambient pressure p_0 and temperature T_0 are assumed to be constant. R stands for the gas constant of air. A table of the steady-state air mass flow across the operating envelope is used to determine the gradients with respect to the throttle plate angle and the pressure ratio via numerical linearisation, to be included in the model, as well as in the implementation to calculate air mass flow disturbances with respect to the current operating point.

2.2.2 Air By-Pass

It is common practice to use a by-pass to the throttle to control the air flow into the engine during idle operation, when the throttle is closed. To integrate such functionality in the throttle component by means of electronic throttle control has recently become a viable alternative, but this approach is not pursued here.

In the present hardware configuration, the air flow through the by-pass can be regulated with an electromagnetic valve, whose control authority is substantial at low and medium engine loads but less influential at high loads, relative to the primary mass flow through the throttle. It seems advantageous to use the potential of the actuator also outside the idle regime, not only to reject torque disturbances during idle operation but also to moderate the perturbations to the mass flow past the throttle during throttle transients.

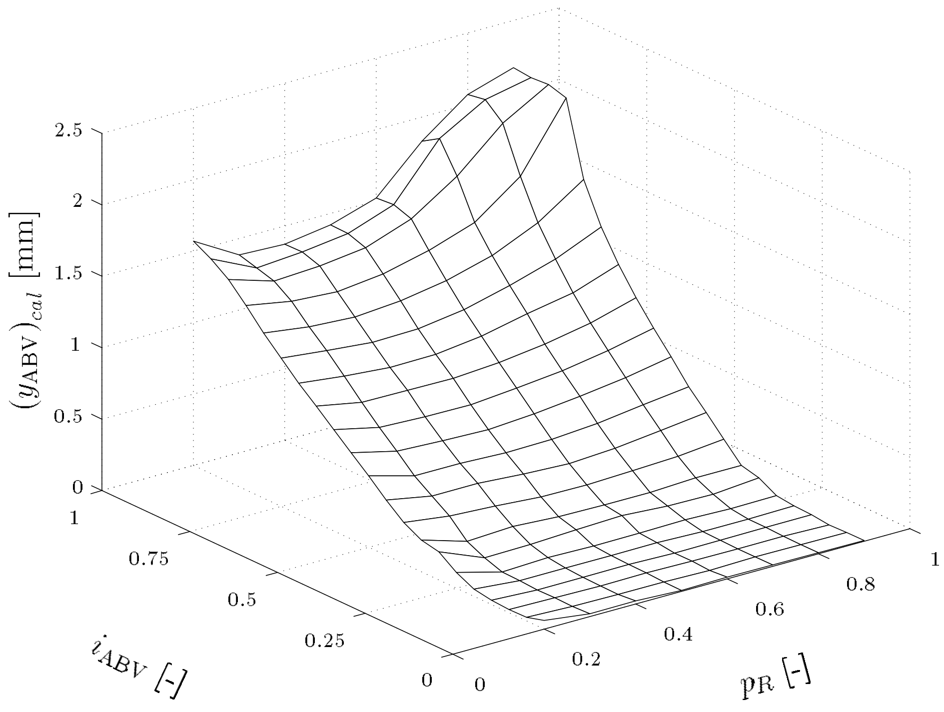

Figure 2.3: Air By-Pass Valve Calibration

Mass Flow Characteristic

For the purpose of system identification, the air by-pass valve is instrumented with a position sensor. The measurement of the valve position is used to calibrate the system in steady state and identify the dynamics of the actuator, yet the measurement is not intended to be used for control.

First, the valve position y_{ABV} is established as a function of the input current i_{ABV} and the pressure ratio p_R with respect to ambient pressure, see Figure 2.3 on the preceding page. The characteristic exhibits a dead band up to 0.25 units of input current and saturates above 0.75. In the active range, however, the local gain is fairly constant and independent of the pressure ratio. Secondly, the nominal air mass flow through the by-pass is determined at a number of operating conditions, as defined by the following equation:

$$\dot{m}_{\text{ABV}} = (\dot{m}_{\text{ABV}})_{cal} \cdot \sqrt{\frac{(T_0)_{cal}}{T_0}} \cdot \frac{p_0}{(p_0)_{cal}} \cdot \frac{\psi}{(\psi)_{choked}}. \tag{2.10}$$

The empirical correction factors account for deviations from the calibration conditions $(p_0)_{cal}$, $(T_0)_{cal}$, and $(\psi)_{choked}$. For simplicity, the ambient conditions are assumed to be constant across the operating envelope, and the flow characteristic is assumed to deviate from choked flow according to Equation (2.6) on page 22. The nominal flow data in Figure 2.4 are calculated, based on these assumptions, simply by solving Equation (2.10) on the current page for $(\dot{m}_{\text{ABV}})_{cal}$.

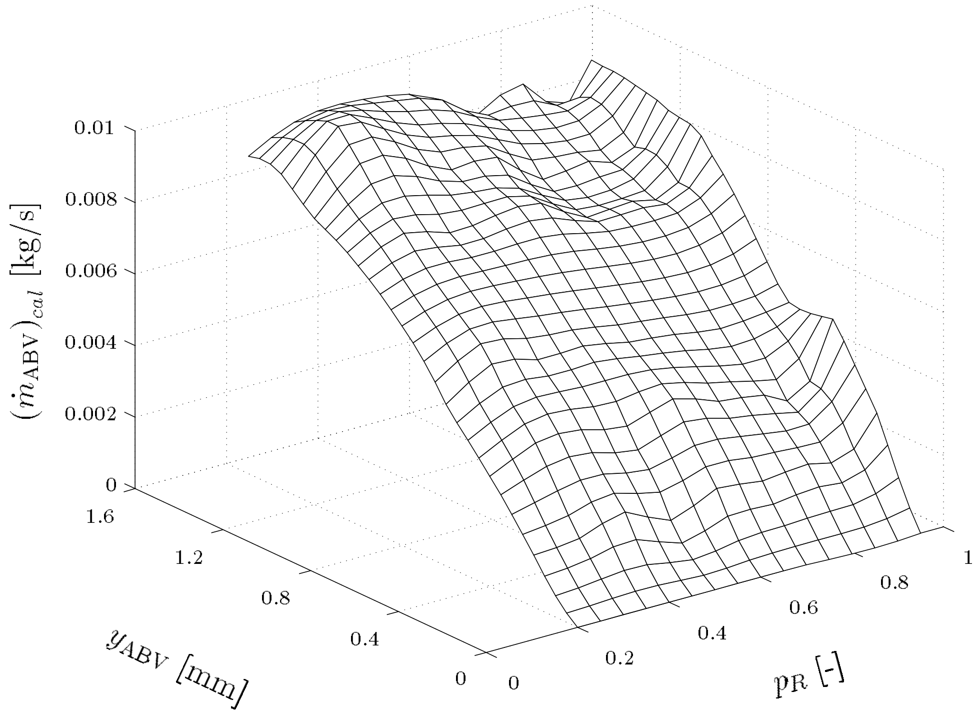

Figure 2.4: ABV Mass Flow Calibration

Thus the steady-state air mass flow can be characterised either in terms of the valve position, or equivalently in terms of the valve input. In the dynamic case the behaviour of the actuator must be included, changes in the flow dynamics, however, need not be considered, as they occur almost instantaneously.

Actuator Model

In identifying the linear dynamics of the actuator, it was necessary to account for the nonlinear input characteristic in Figure 2.3 on page 23. Suitable test signals were constructed by compensating for the effect of the nonlinearity, to identify a second order system as the transfer function from the input current to the valve position,

$$y_{\mathrm{ABV}} = G_{\mathrm{ABV}} i_{\mathrm{ABV}} \, .^{2} \tag{2.11}$$

Its frequency response is shown in the Bode diagram in Figure 2.5.

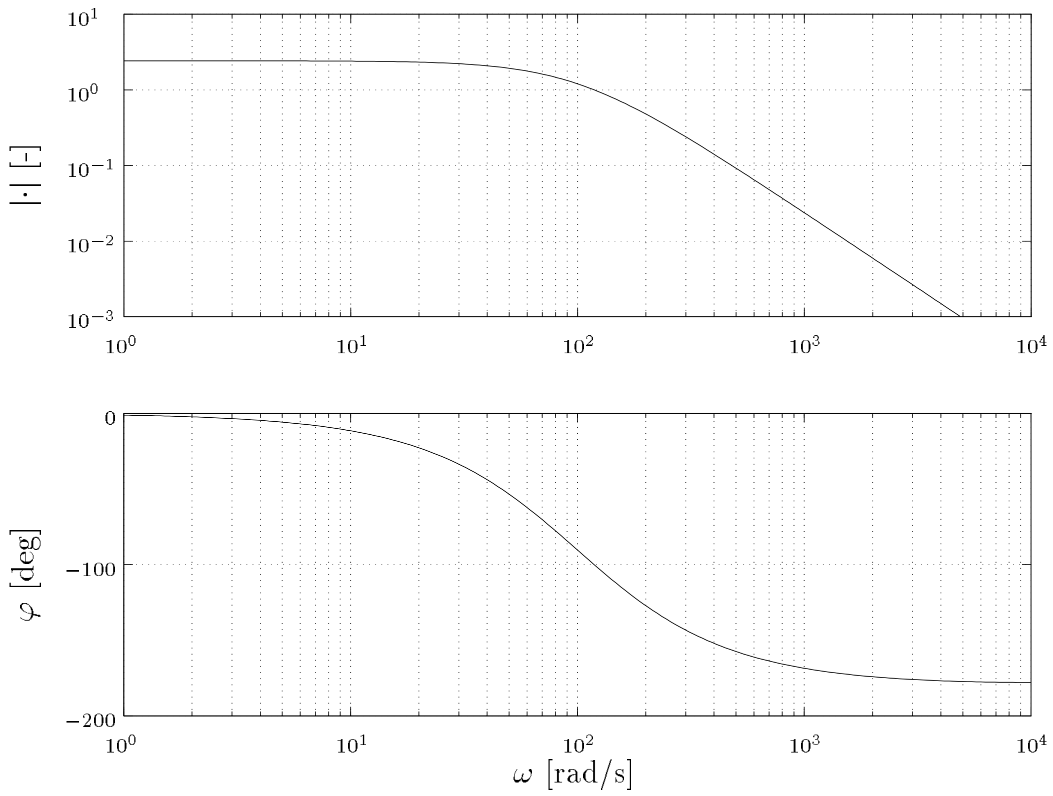

Figure 2.5: ABV Actuator Dynamics

The dynamic part of the model fits in with the nonlinear flow characteristics as in Figure 2.6 on the following page. The static nonlinear block F_1 contains the valve calibration, while F_2 contains the mass flow calibration. For a given input current u and a pressure ratio x, the output of F_1 is the nominal valve position y', of which the process variable p_1 is a dynamic measurement. The process variable p_2, the output of F_2, is the instantaneous air mass flow as a function of the current valve position y and

[2]For the purpose of short notation, although slightly ambiguous, the variable names of the physical signals are also used in the linear case for the corresponding incremental signals. This practice is adopted throughout the thesis.

the state x. (The manifold pressure is treated as an exogenous variable pertaining to a separate process.)

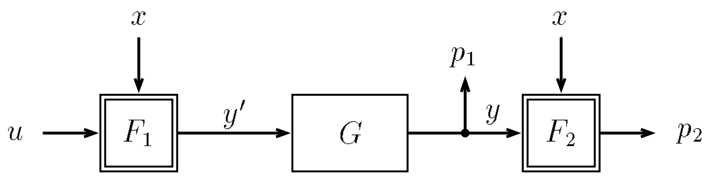

Figure 2.6: Actuator Model

From the point of view of control design a linear, possibly uncertain, model from the input u to the output p_2 would be preferable to the sophisticated model in Figure 2.6. Therefore the nonlinear flow characteristics were linearised by means of static compensation, see Appendix A. Implemented on the engine, the compensator gives an approximately linear actuator behaviour from the input current to the air mass flow

$$\dot{m}_{\mathrm{ABV}} = G_{\mathrm{ABV}} K_{\mathrm{ABV}} i_{\mathrm{ABV}} \tag{2.12}$$

with a nominal gain of $K_{\mathrm{ABV}} = 0.01$. For the subsequent system interconnection, the continuous-time model is discretised according to Appendix B, whereby the system's dynamics are parameterised as a function of the sample time.

2.2.3 Exhaust Gas Recirculation

Exhaust gas recirculation is a common feature of modern combustion engines to reduce the formation of nitrogen oxides in the combustion process. The concentration of nitrogen oxide in the exhaust gas depends strongly on the combustion temperature. For this reason, the combustion temperature is lowered under certain operating conditions by diluting the charge in the cylinder with inert exhaust gas. This is achieved by recirculating exhaust gas into the intake manifold to combine with the air stream.

In engines with variable valve timing it is alternatively possible to create a controlled backflow of exhaust gas into the cylinder during the exhaust stroke, so that there is no need for an external EGR system. In the present hardware configuration, however, the mechanism for exhaust gas recirculation is external: the EGR mass flow into the intake manifold is restricted using an electromagnetic valve. In this way, the exhaust gas recirculation not only affects the combustion process but also the mixture composition in the intake manifold and provides a means for transient air-fuel ratio control.

Mass Flow Characteristic

The approach to modelling and system identification is the same as in the case of the air by-pass valve. In addition, the measurement of the valve position is also available for the EGR control system.

By its very nature exhaust gas recirculation is more complicated than the regulation of the air mass flow through the by-pass. For one thing, the exhaust conditions, which determine the EGR mass flow, cannot be considered to be constant, as they are dependent on the operating point due to the feedback involved. Secondly, the mixing of hot exhaust gas with air in the intake manifold affects the density of the air that is inducted into the cylinder, *cf.* Section 2.2.4.

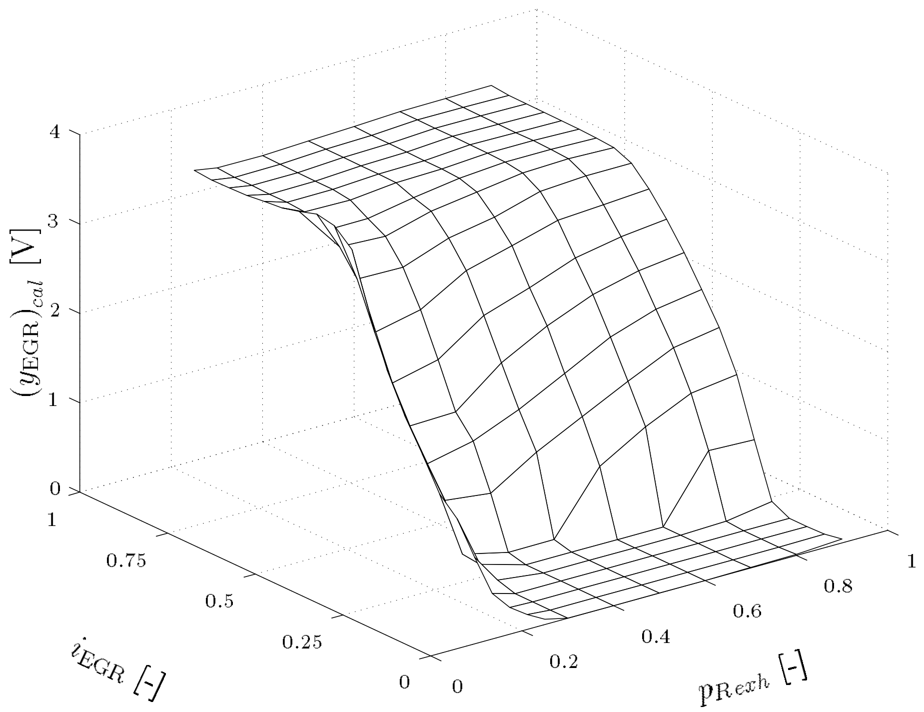

Figure 2.7: EGR Valve Calibration

Therefore, the valve calibration in Figure 2.7 shows the valve position y_{EGR} as a function of the input current i_{EGR} and the pressure ratio $p_{R\,exh}$ with respect to the exhaust pressure p_{exh}. Note that the valve position is in Volts not in millimetres.

For the normalised control input, the same observations can be made as in Section 2.2.2. The characteristic exhibits a dead band up to 0.25 units of input current and saturates above 0.75. In the active range the local gain is fairly constant and independent of the pressure ratio. The defining equation for the EGR mass flow into the intake manifold

$$\dot{m}_{\mathrm{EGR}} = (\dot{m}_{\mathrm{EGR}})_{cal} \cdot \sqrt{\frac{(T_{exh})_{cal}}{T_{exh}}} \cdot \frac{p_{exh}}{(p_{exh})_{cal}} \cdot \frac{\psi}{(\psi)_{choked}} \tag{2.13}$$

is the same as Equation (2.10) on page 24, only the exhaust conditions replace the ambient conditions in the correction factors. The nominal flow data in Figure 2.8 on the following page complete the description of the steady-state behaviour of the EGR system.

The EGR control system is to be designed such that the mass fraction of exhaust gas in the mixture reaches a certain value in steady state, which is in any case less than 20%. There is such a requirement for each operating point, which is easily translated into an absolute mass flow. Then the corresponding valve position is determined according to Figure 2.8 on the next page, and, equivalently, the valve input according to Figure 2.7.

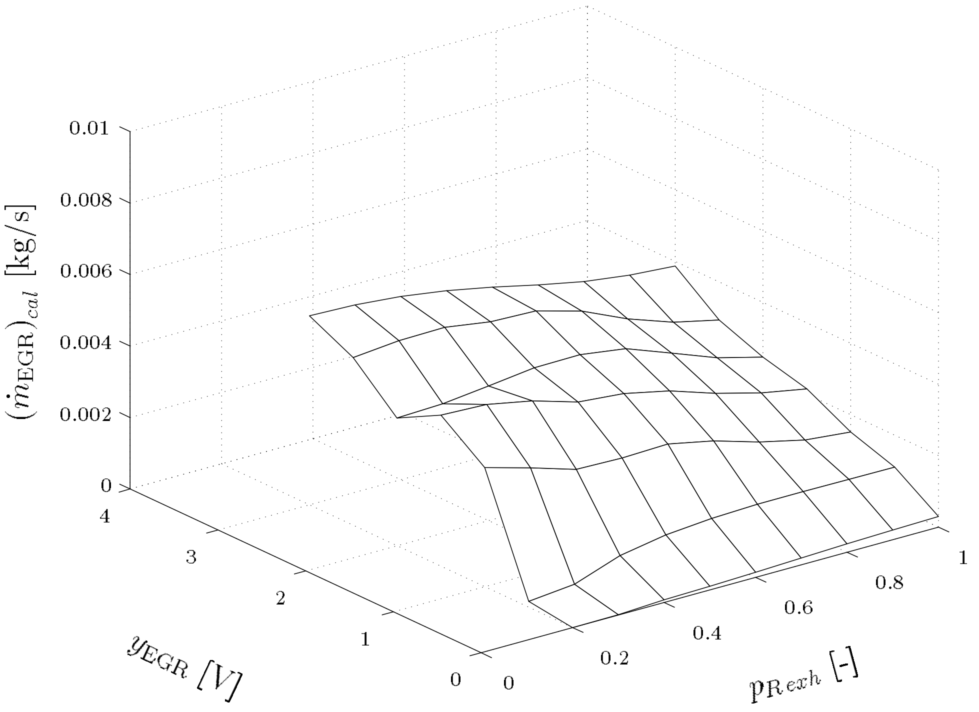

Figure 2.8: EGR Mass Flow Calibration

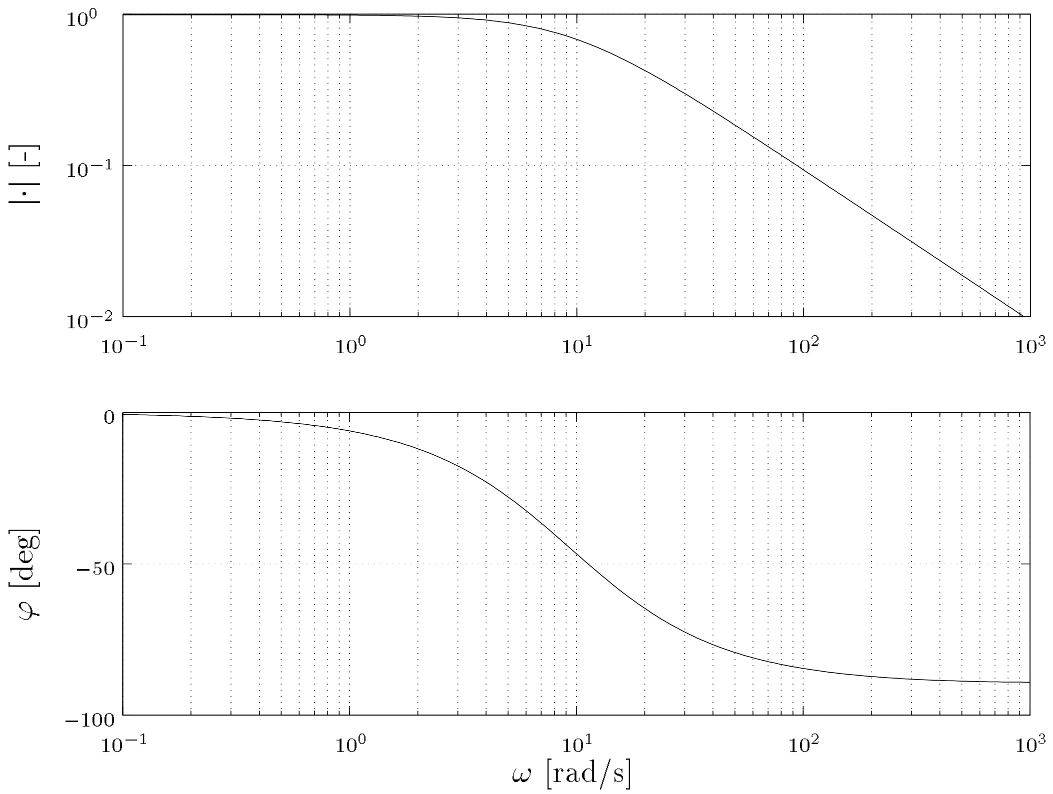

Figure 2.9: EGR Actuator Dynamics

Actuator Model

A first order system, with unity gain, was identified as the transfer function from the input current to the valve position,

$$y_{\mathrm{EGR}} = G_{\mathrm{EGR}} i_{\mathrm{EGR}} \,. \tag{2.14}$$

Its frequency response is shown in the Bode diagram in Figure 2.9 on the preceding page. Note that the nominal gain is already included in the valve calibration. Thus the structure of the actuator model is exactly as in Figure 2.6 on page 26, and the same procedures apply with regard to linearisation and discretisation. Assuming an ideal compensator, the nominal behaviour of the actuator from the input current to the EGR mass flow is given by:

$$\dot{m}_{\mathrm{EGR}} = G_{\mathrm{EGR}} K_{\mathrm{EGR}} i_{\mathrm{EGR}} \,. \tag{2.15}$$

2.2.4 Intake Manifold

The combination of the continuous flow dynamics in the intake manifold with the discrete event-based fuel injection is the key step towards a uniform treatment of the engine processes. For that purpose, we integrate the dynamic equations which represent the intake manifold with respect to crank angle.

Continuity Equation

The model of the intake manifold is based on the continuity equation and the ideal gas law:[3]

$$\frac{dp_M}{d\varphi} = -\frac{\eta_v V_D}{720 V_M} \cdot p_M + \frac{\mathsf{R} T_M}{p_0 V_M \Delta\varphi} (\dot{m}_{A\,\mathrm{TH}} + \dot{m}_{\mathrm{EGR}}) h \tag{2.16a}$$

$$\frac{dp_{\mathrm{EGR}}}{d\varphi} = -\frac{\eta_v V_D}{720 V_M} \cdot p_{\mathrm{EGR}} + \frac{\eta_v V_D}{720 V_M} \cdot \dot{m}_{\mathrm{EGR}} h \tag{2.16b}$$

$$m_A = \frac{\eta_v p_0 V_D \Delta\varphi}{720 \mathsf{R} T_M} \cdot p_M - p_{\mathrm{EGR}} \,. \tag{2.16c}$$

V_D is the engine displacement volume and V_M the volume of intake manifold. R denotes the ideal gas constant of air. In the equations the substitution

$$dt = \frac{d\varphi}{6N} \tag{2.17}$$

has already been made to change from the time to the crank angle domain. The inflows and outflows are integrated over the intake stroke simply by multiplying with the sample time

$$h = \frac{\Delta\varphi}{6N} \,. \tag{2.18}$$

Note that p_M is the ratio of the manifold pressure with respect to ambient pressure. Since the ambient conditions are constant:

$$p_0 = \bar{p}_0 + \hat{p}_0 \cdot 0 \,, \tag{2.19}$$

[3] The filling and emptying model is documented in [31] and [2].

the notation is simplified. We use the volumetric efficiency η_v to define the air charge in the cylinder m_A as an average over one crankshaft revolution. The mathematical treatment of the intake manifold is complicated significantly in the presence of exhaust gas recirculation, as the manifold temperature T_M becomes a function of the rate of recirculation. This affects the partial pressure of air and consequently the air charge that is inducted into the cylinder.

Both the volumetric efficiency and the manifold temperature are determined in steady-state tests over a common set of operating points. Their variations across the operating envelope can be seen in Figure 2.10 and Figure 2.11 on the facing page. Note that the symbol p_R is used instead of p_M in case the manifold pressure ratio is seen as an exogenous variable.

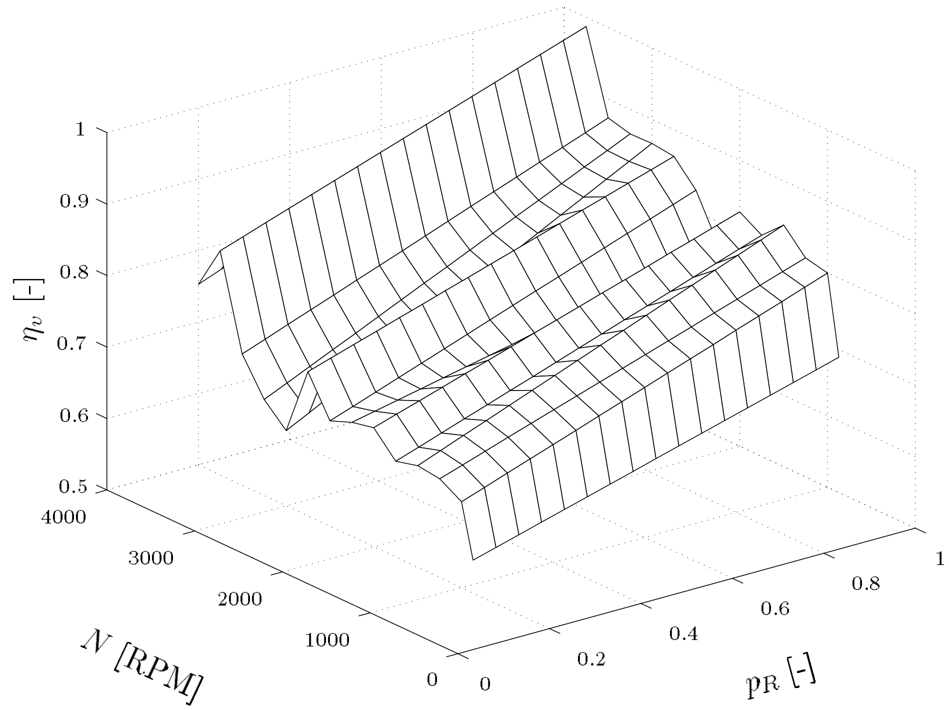

Figure 2.10: Volumetric Efficiency

Typically, a heat balance is not included in control applications, since thermal effects are difficult to quantify in general, and the heat transfer across the wall of an intake port in particular. However, it is common practice to adapt model parameters dependent on engine coolant temperature, see *e.g.* [51]. We introduce a second state p_{EGR} to account for the storage of exhaust gas in the intake manifold, and it is assumed that the flow dynamics of exhaust gas are the same as those of air.[4]

[4]Note that p_{EGR} is not the partial pressure of the exhaust gas but denotes the mass of exhaust gas in the intake manifold. The notation is deliberately inconsistent here, because the EGR mass flow rate into the intake manifold was already denoted $\dot{m}_{\mathrm{EGR}}$.

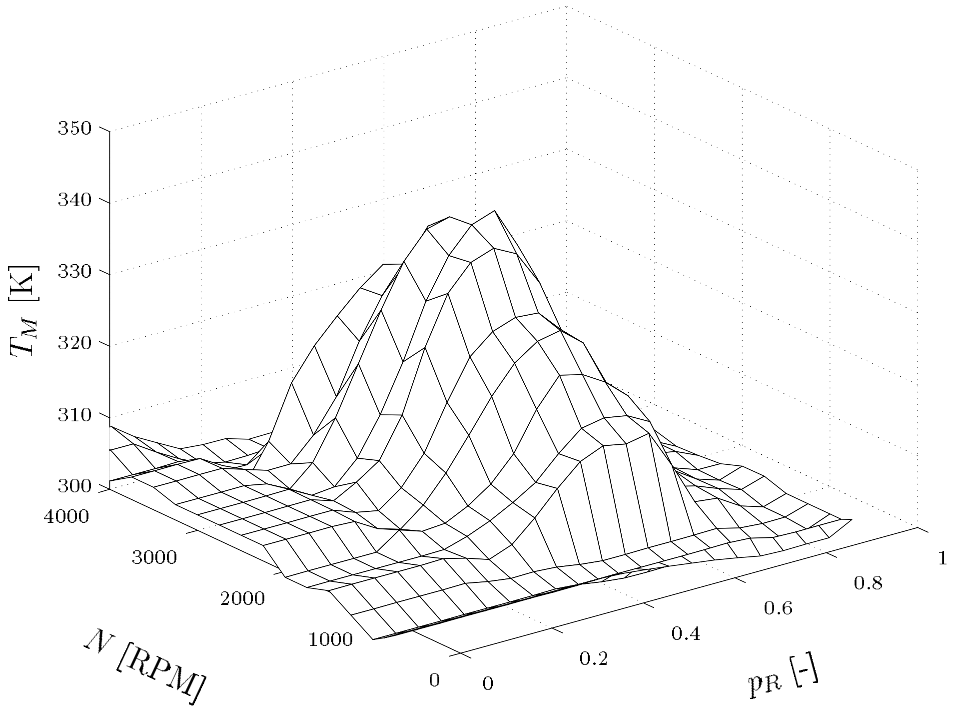

Figure 2.11: Manifold Temperature

LFT Formulation

The parameter variations can be interpreted in different ways. While the parameter η_v determines the response time of the system, the parameter T_M determines the gain, secondary effects of T_M on η_v not considered.

When we consider the dynamics of the system locally for small perturbations around an operating point, the parameter values will lie in a neighbourhood of the corresponding grid point, and the dynamics of the system will be slightly perturbed. On the other hand, changes in dynamics across the operating envelope may result in a behaviour completely different to the local behaviour. In both cases, the variations can be described as parametric uncertainty, to be, without loss of generality, of the form:

$$\alpha = \bar{\alpha} + \hat{\alpha}\delta\alpha\,, \qquad |\delta\alpha| \leq 1\,. \tag{2.20}$$

We would like to represent the set of Equations (2.16) on page 29 via linear fractional transformations as in Figure 2.17 on page 42 to integrate the intake manifold with the other engine components. For that purpose, the following abbreviations are introduced:

$$a = \frac{V_D}{720 V_M}\,, \qquad b = \frac{\mathsf{R}}{p_0 V_M \Delta\varphi}\,, \qquad c = \frac{a}{b}\,. \tag{2.21}$$

Furthermore, the state, the output, and the input of the intake manifold are defined as

$$x = \begin{bmatrix} p_M \\ p_{\mathrm{EGR}} \end{bmatrix}, \qquad y = \begin{bmatrix} p_M \\ m_A \end{bmatrix}, \qquad u = \begin{bmatrix} \dot{m}_{A\,\mathrm{TH}} h \\ \dot{m}_{\mathrm{EGR}} h \end{bmatrix}. \tag{2.22}$$

In this instance, $\dot{m}_{A\,\mathrm{TH}}$ denotes the total air mass flow past the throttle body to save notation. Then the Equations (2.16) can be expanded as follows to allow for parametric uncertainty in the volumetric efficiency and the manifold temperature.

$$\dot{x}_1 = -\bar{\eta}_v a x_1 - \hat{\eta}_v a w_1 + b\hat{T}_M w_3 + b\bar{T}_M(u_1 + u_2) \tag{2.23a}$$
$$\dot{x}_2 = -\bar{\eta}_v a x_2 - \hat{\eta}_v a w_2 + \bar{\eta}_v a u_2 \tag{2.23b}$$
$$z_1 = x_1 \tag{2.23c}$$
$$z_2 = x_2 - u_2 \tag{2.23d}$$
$$z_3 = u_1 + u_2 \tag{2.23e}$$
$$y_1 = x_1 \tag{2.23f}$$
$$y_2 = \frac{\bar{\eta}_v c}{\bar{T}_M} x_1 - x_2 + \frac{\hat{\eta}_v c}{\bar{T}_M} w_1 - \frac{\bar{\eta}_v + \hat{\eta}_v \delta\eta_v}{\bar{T}_M + \hat{T}_M \delta T_M} \frac{c\hat{T}_M}{\bar{T}_M} \delta T_M x_1 \,. \tag{2.23g}$$

These equations are complemented by the definition of the extra inputs

$$w_1 = \delta\eta_v z_1 \tag{2.24a}$$
$$w_2 = \delta\eta_v z_2 \tag{2.24b}$$
$$w_3 = \delta T_M z_3 \,. \tag{2.24c}$$

By introducing a further output

$$z_4 = -\frac{\bar{\eta}_v + \hat{\eta}_v \delta\eta_v}{\bar{T}_M + \hat{T}_M \delta T_M} x_1 \tag{2.25a}$$
$$= \left(-\frac{\bar{\eta}_v}{\bar{T}_M} x_1 - \frac{\hat{\eta}_v}{\bar{T}_M} \delta\eta_v x_1\right) \frac{\bar{T}_M}{\bar{T}_M + \hat{T}_M \delta T_M} \tag{2.25b}$$
$$= -\frac{\bar{\eta}_v}{\bar{T}_M} x_1 - \frac{\hat{\eta}_v}{\bar{T}_M} w_1 - \frac{\hat{T}_M}{\bar{T}_M} \delta T_M z_4 \tag{2.25c}$$

and input

$$w_4 = \delta T_M z_4 \,, \tag{2.25d}$$

the equations above can be written in a closed form with

$$y_2 = \frac{\bar{\eta}_v c}{\bar{T}_M} x_1 - x_2 + \frac{\hat{\eta}_v c}{\bar{T}_M} w_1 + \frac{c\hat{T}_M}{\bar{T}_M} w_4 \tag{2.26a}$$
$$z_4 = -\frac{\bar{\eta}_v}{\bar{T}_M} x_1 - \frac{\hat{\eta}_v}{\bar{T}_M} w_1 - \frac{\hat{T}_M}{\bar{T}_M} w_4 \,. \tag{2.26b}$$

Therefore the model of the intake manifold can be represented as

$$\begin{bmatrix} \dot{x} \\ z \\ y \end{bmatrix} = \mathcal{F}_u(M_M, \Delta_M) \begin{bmatrix} x \\ w \\ u \end{bmatrix} \tag{2.27}$$

with the coefficient matrix

$$M_M = \left[\begin{array}{cc|cc|cc|cc}
-\bar{\eta}_v a & 0 & -\hat{\eta}_v a & 0 & b\hat{T}_M & 0 & b\bar{T}_M & b\bar{T}_M \\
0 & -\bar{\eta}_v a & 0 & \hat{\eta}_v a & 0 & 0 & 0 & -\bar{\eta}_v a \\
\hline
1 & 0 & 0 & 0 & 0 & 0 & 0 & 0 \\
0 & 1 & 0 & 0 & 0 & 0 & 0 & -1 \\
\hline
0 & 0 & 0 & 0 & 0 & 0 & 1 & 1 \\
-\frac{\bar{\eta}_v}{\bar{T}_M} & 0 & -\frac{\hat{\eta}_v}{\bar{T}_M} & 0 & 0 & -\frac{\hat{T}_M}{\bar{T}_M} & 0 & 0 \\
\hline
1 & 0 & 0 & 0 & 0 & 0 & 0 & 0 \\
\frac{\bar{\eta}_v c}{\bar{T}_M} & -1 & \frac{\hat{\eta}_v c}{\bar{T}_M} & 0 & 0 & \frac{c\hat{T}_M}{\bar{T}_M} & 0 & 0
\end{array}\right] . \tag{2.28}$$

A separate step is required to extend M_M in order to account for the variations in the sample time h, before Equation (2.27) on the preceding page can be written for the input vector $\left[\begin{smallmatrix} \dot{m}_{ATH} \\ \dot{m}_{\mathrm{EGR}} \end{smallmatrix}\right]$ and with Δ_M from the set

$$\{\Delta_M | \, \Delta_M = \operatorname{diag}(\delta\eta_v I_2, \delta T_M I_2, \delta h I_2) \, , \; |\delta i| \leq 1 \, , \delta i \in \mathbb{R} \, , \quad i = \eta_v, T_M, h\} \, . \tag{2.29}$$

Finally, the system is discretised using the bilinear transformation with a sample period of $\Delta\varphi$ deg, so that the structure of the parameter dependencies is preserved. The parameter variations may be constant or time-varying. In its present form the model can be updated at each sampling instant with the current values of η_v, T_M, and h, for example from the look-up tables in Figure 2.10 on page 30 and Figure 2.11 on page 31.

2.2.5 Fuel Injection

The process of fuel injection, until the fuel reaches the cylinder, is very complex and influenced by many design parameters, such as the location and the spray characteristics of the fuel injectors, the pressure regulation in the fuel rail and the injection timing. In particular, the dynamic behaviour of fuel in an intake port is influenced by all these parameters, not to mention the port geometry and its thermal properties, and it is very difficult, indeed, to resolve the effects of individual parameters.

Phenomenological Model

In the present engine configuration, all of these parameters are fixed, so we use a simple phenomenological model, *cf.* [2]:

$$\begin{bmatrix} \dot{m}_P \\ m_{F\,cyl} \end{bmatrix} = \left[\begin{array}{c|c} -\zeta & \chi \\ \hline \zeta & 1-\chi \end{array}\right] \begin{bmatrix} m_P \\ m_{F\,inj} \end{bmatrix} . \tag{2.30}$$

The parameter ζ can be related to a combined diffusive and convective process [50], but in practice the model parameters are obtained from system identification experiments [6, 11]. There are many other parameterisations, see *e.g.* [52]. In view of the derivation to come, a simple model is chosen, as it is yet to be established that more complex models represent the dynamics of fuel injection more adequately.

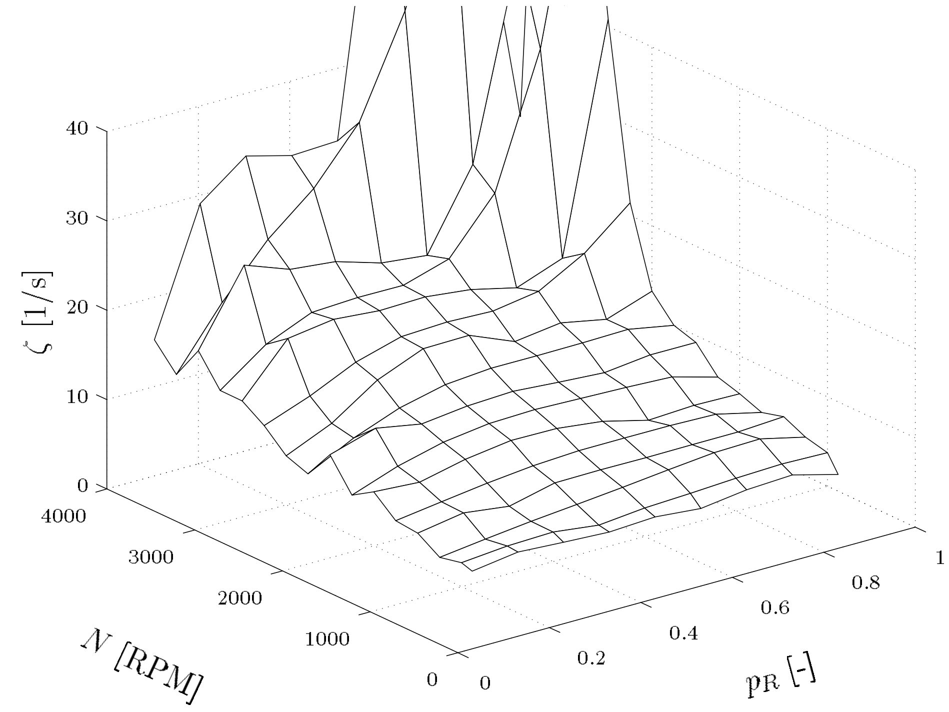

Figure 2.12: Fuel Evaporation Rate

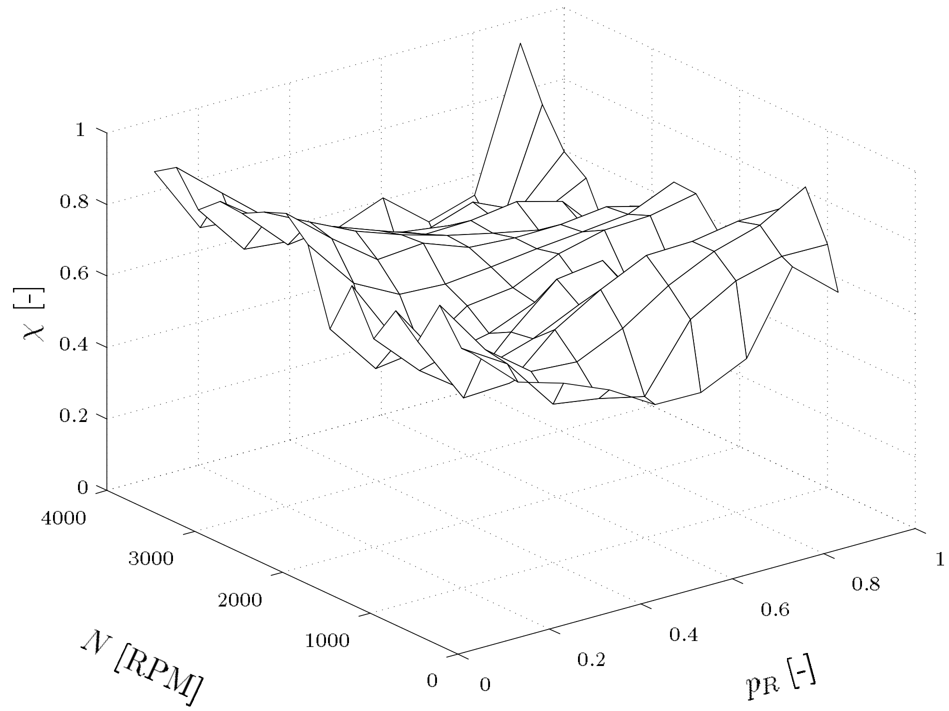

Figure 2.13: Fuel Fraction

For the purpose of system identification, the dynamics of the engine are excited by superimposing PRBS signals either on the fuel injection time or the throttle plate angle, or both. Typically, least squares system identification techniques are used to determine the parameters over a set of operating points [4]. Some results are shown in Figure 2.12 and Figure 2.13 on the facing page.

The model parameters can be given the following interpretation. A fraction χ of the amount of fuel that is injected $m_{F\,inj}$ is deposited on the walls of the intake port, while the remainder enters directly into the cylinder. Of the deposits in the intake port m_P, a certain amount re-entrains into the air stream and subsequently enters into the cylinder, as characterised by the rate of evaporation ζ.

In the sequel, we extend the model for a single intake port to a sequential fuel injection system for a four-cylinder engine. The aim is to separate the effects of the parameter variations from the effects of sampling.

LFT Formulation

In order to include the parameter variations in the system representation, Equation (2.30) on page 33 is re-written as a linear fractional transformation

$$\begin{bmatrix} \dot{m}_P \\ m_{F\,cyl} \end{bmatrix} = \mathcal{F}_\ell(M_F, \Delta_F) \begin{bmatrix} m_P \\ m_{F\,inj} \end{bmatrix}, \tag{2.31}$$

with the coefficient matrix

$$M_F = \left[\begin{array}{c|c:c:c} -\bar{\zeta} & \bar{\chi} & -\hat{\zeta} & \hat{\chi} \\ \hline \bar{\zeta} & 1-\bar{\chi} & \hat{\zeta} & -\hat{\chi} \\ \hdashline 1 & 0 & 0 & 0 \\ \hdashline 0 & 1 & 0 & 0 \end{array}\right] \tag{2.32}$$

and Δ_F from the set

$$\{\Delta_F |\, \Delta_F = \mathrm{diag}(\delta\zeta, \delta\chi),\ |\delta i| \leq 1, \delta i \in \mathbb{R}, \quad i = \zeta, \chi\}. \tag{2.33}$$

Note that for fixed perturbations, Equation (2.31) on this page is equivalent to the linear time-invariant case. Strictly speaking, the air-fuel ratio is only meaningful on a cycle-to-cycle basis. Therefore we consider the process of fuel injection as discrete and event-based. If the uncertainty set above is extended to include variations of the sample time:

$$\{\Delta_F |\, \Delta_F = \mathrm{diag}(\delta\zeta, \delta\chi, \delta h),\ |\delta i| \leq 1, \delta i \in \mathbb{R}, \quad i = \zeta, \chi, h\}, \tag{2.34}$$

a discrete event-based version of Equation (2.31) involves

$$
M_F = \left[\begin{array}{c|c:}
(1+\frac{\bar h}{2}\bar\zeta)^{-1}(1-\frac{\bar h}{2}\bar\zeta) & (1+\frac{\bar h}{2}\bar\zeta)^{-1}\bar\chi \\ \hline
\bar h\bar\zeta(1+\frac{\bar h}{2}\bar\zeta)^{-1} & 1-(1+\frac{\bar h}{2}\bar\zeta)^{-1}\bar\chi \\ \hdashline
\bar h(1+\frac{\bar h}{2}\bar\zeta)^{-1} & \frac{\bar h}{2}(1+\frac{\bar h}{2}\bar\zeta)^{-1}\bar\chi \\
0 & 1 \\
(1+\frac{\bar h}{2}\bar\zeta)^{-1} & \frac{1}{2}(1+\frac{\bar h}{2}\bar\zeta)^{-1}\bar\chi
\end{array}\right. \cdots
$$

$$
\cdots \left.\begin{array}{:ccc}
-\hat\zeta(1+\frac{\bar h}{2}\bar\zeta)^{-1} & (1+\frac{\bar h}{2}\bar\zeta)^{-1}\hat\chi & -\hat h\bar\zeta(1+\frac{\bar h}{2}\bar\zeta)^{-1} \\ \hline
\hat\zeta(1+\frac{\bar h}{2}\bar\zeta)^{-1} & -(1+\frac{\bar h}{2}\bar\zeta)^{-1}\hat\chi & \hat h\bar\zeta(1+\frac{\bar h}{2}\bar\zeta)^{-1} \\ \hdashline
-\frac{\bar h}{2}\hat\zeta(1+\frac{\bar h}{2}\bar\zeta)^{-1} & \frac{\bar h}{2}(1+\frac{\bar h}{2}\bar\zeta)^{-1}\hat\chi & \hat h(1+\frac{\bar h}{2}\bar\zeta)^{-1} \\
0 & 0 & 0 \\
-\frac{1}{2}\hat\zeta(1+\frac{\bar h}{2}\bar\zeta)^{-1} & \frac{1}{2}(1+\frac{\bar h}{2}\bar\zeta)^{-1}\hat\chi & -\frac{\hat h}{2}\bar\zeta(1+\frac{\bar h}{2}\bar\zeta)^{-1}
\end{array}\right], \qquad (2.35)
$$

according to the bilinear transformation in Appendix B. The fact that the parametric uncertainty may be time-varying is not especially emphasised in the notation. For easy reference, the coefficient matrix is partitioned as

$$
M_F = \left[\begin{array}{c|c:c}
A & B_1 & B_2 \\ \hline
C_1 & D_{11} & D_{12} \\ \hdashline
C_2 & D_{21} & D_{22}
\end{array}\right]. \qquad (2.36)
$$

Then a possible realisation of the nominal model in the case of a four-cylinder engine is given by

$$
\begin{bmatrix} \dot m_{P\,i[k]} \\ \dot m_{P\,i[k+1]} \\ \dot m_{P\,i[k+2]} \\ \dot m_{P\,i[k+3]} \\ m_{F\,cyl\,i[k]} \end{bmatrix}
= \left[\begin{array}{cccc|c}
0 & 1 & 0 & 0 & 0 \\
0 & 0 & 1 & 0 & 0 \\
0 & 0 & 0 & 1 & 0 \\
A & 0 & 0 & 0 & B_1 \\ \hline
C_1 & 0 & 0 & 0 & D_{11}
\end{array}\right]
\begin{bmatrix} m_{P\,i[k]} \\ m_{P\,i[k+1]} \\ m_{P\,i[k+2]} \\ m_{P\,i[k+3]} \\ m_{F\,inj} \end{bmatrix}, \qquad (2.37)
$$

where

$$
i[k] = k - n_{cyl} \cdot (k \bmod n_{cyl}) + 1 \qquad (2.38)
$$

is the index of the current cylinder at sample instant k. While the subsystem in Equation (2.31) on the page before is periodic with a period of $n_{cyl} \times \Delta\varphi$, this system is periodic with a period of $\Delta\varphi$. Furthermore, the inputs to the individual cylinders are

$$
m_{F\,inj\,i[k]} = \begin{cases} m_{F\,inj}[k] & \text{if } (k-i) \bmod n_{cyl} = 0 \\ 0 & \text{otherwise} \end{cases} \qquad i = 1, \dots, n_{cyl}\,. \qquad (2.39)
$$

Note that the multiplexing is independent of the choice of model for the subsystem. In general, the size of the compound dynamic matrix is $n_{cyl} \times \dim(A)$. Finally, the compound system including the perturbations is described by

$$
M_F = \left[\begin{array}{cccc|c|ccc}
0 & 1 & 0 & 0 & 0 & 0 & 0 & 0 \\
0 & 0 & 1 & 0 & 0 & 0 & 0 & 0 \\
0 & 0 & 0 & 1 & 0 & 0 & 0 & 0 \\
A & 0 & 0 & 0 & B_1 & B_{2\,\zeta} & B_{2\,\chi} & B_{2\,h} \\
\hline
C_1 & 0 & 0 & 0 & D_{11} & D_{12\,\zeta} & D_{12\,\chi} & D_{12\,h} \\
\hline
C_{2\,\zeta} & 0 & 0 & 0 & D_{21\,\zeta} & D_{22\,\zeta\zeta} & D_{22\,\zeta\chi} & D_{22\,\zeta h} \\
0 & 0 & 0 & 0 & D_{21\,\chi} & 0 & D_{22\,\chi\chi} & 0 \\
C_{2\,h} & 0 & 0 & 0 & D_{21\,h} & D_{22\,h\zeta} & D_{22\,h\chi} & D_{22\,hh}
\end{array} \right] . \tag{2.40}
$$

2.2.6 Exhaust Delays

The delays in the exhaust system are due to two separate effects.

Cycle Delay

After the induction stroke, as soon as the intake valves are closed, the mixture composition of the charge in the cylinder is completely determined. At this instant any mismatches between the quantities of air and fuel

$$
\delta\lambda = \frac{\delta m_A - (\mathrm{AFR})_s \delta m_F}{m_A} \tag{2.41}
$$

cannot be corrected any more and will appear later in the measurement of the air-fuel ratio in front of the catalyst. In fact, the delays can be considered to be part of the measurement process. After the intake valves are closed, the mixture remains in the cylinder, undergoing compression and combustion, until the exhaust valves open. This period takes about one half of the combustion cycle, or one engine revolution, and is approximated by a series of two unit delays

$$
G_{exh\,1} = z^{-2} . \tag{2.42}
$$

Transport Delay

Depending on the location of the catalyst in relation to the engine, the transport of the exhaust gas from the exhaust ports to the measurement location may constitute a major delay. If the catalyst is not closely coupled to the engine, the time delay must be considered as a function of the mean gas velocity, which depends on the operating condition. Therefore the exhaust transport delay

$$
G_{exh\,2} = e^{-s\tau_{exh}} \tag{2.43}
$$

was identified in steady-state experiments for a number of operating points. A first order hyperbolic regression of the experimental data is shown in Figure 2.14 on the following page.

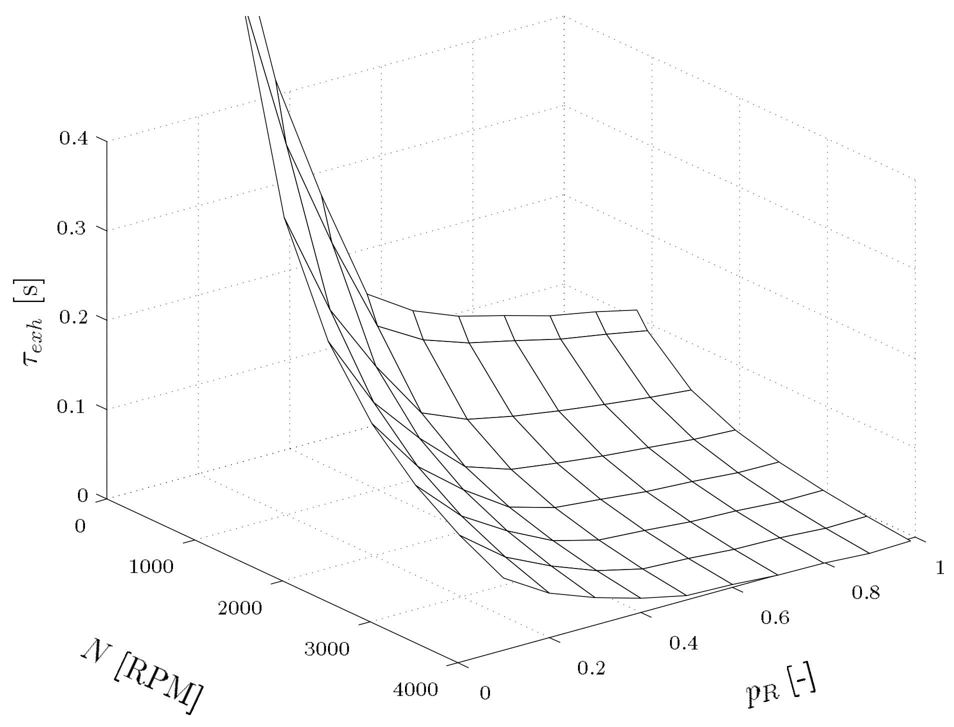

Figure 2.14: Exhaust Transport Delay

In order to include the variation of the time delay across the operating envelope, two different approaches are adopted. In the case of the linear time-invariant models in fixed operating points, the time delay is converted to crank angle and rounded to the closest integer multiple of the sample period, see Table 2.1. A corresponding number of unit delays is then included in each model.

	p_R [-]				
N [RPM]	0.20	0.35	0.50	0.65	0.80
870	14	8	5	4	4
1250	14	8	5	4	4
2000	11	6	4	3	2
2750	10	5	3	2	2
3500	8	4	1	1	1

Table 2.1: Exhaust Transport Delay in Units of Engine Events

For the construction of the parameter-dependent plant, the delay is approximated by a series of three first order Padé approximations

$$\left(\frac{6 - s\tau_{exh}}{6 + s\tau_{exh}}\right)^3 . \tag{2.44}$$

This rational transfer function is then interconnected with a polynomial representation of the data in Figure 2.14 to account for the parameter variations. The overall delay in the exhaust system is given by

$$G_{exh} = G_{exh\,2} G_{exh\,1} \,. \tag{2.45}$$

2.2.7 UEGO Sensor

The universal exhaust gas oxygen sensor is a linear measurement device that is used to characterise the exhaust gas composition. It is calibrated such that the mixture composition in terms of the air-fuel ratio can be inferred from the detected partial pressure of oxygen in the exhaust gas according to a linear relationship. A first order system was identified to represent the sensor dynamics, whose frequency response is depicted in Figure 2.15.

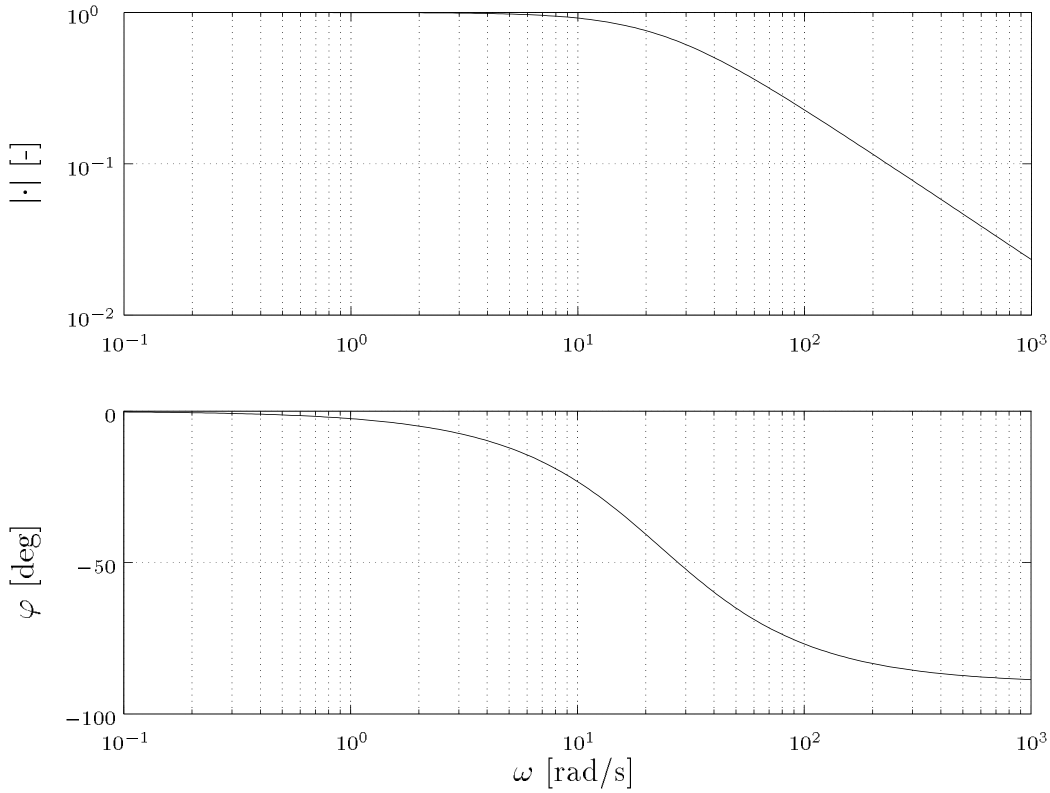

Figure 2.15: UEGO Sensor Dynamics

For a coherent system representation, the continuous dynamics are discretised, leaving the sample time as a free variable, just as in the case of the actuators.

2.3 Models in Fixed Operating Points

For the purpose of control design, the engine behaviour is captured with a set of models in fixed operating points over the operating envelope.

Operating Points

The operating envelope is covered with an equidistant grid in terms of engine speed N and the manifold pressure ratio p_R, as shown in Table 2.2.[5] Twenty-five linear time-invariant models were created by substituting the corresponding parameter values at the grid points in the parameter-dependent LFT representation.

	p_R [-]				
N [RPM]	0.20	0.35	0.50	0.65	0.80
870					
1250					
2000			G_{33}		
2750					
3500					

Table 2.2: Matrix of Operating Conditions

We refer to a single model as an element of the matrix in Table 2.2 by its row and column indices; for example, our nominal model is G_{33} at 2000 RPM and a manifold pressure ratio of 0.5. Each model

$$G_{ij}\,, \qquad i = 1, \ldots, I\,,\ j = 1, \ldots, J \tag{2.46}$$

has the following input-output behaviour:

$$\begin{bmatrix} \lambda_{cyl} \\ \alpha \\ \dot{m}_{\mathrm{EGR}} \\ p_M \\ \lambda_{exh} \end{bmatrix} = \begin{bmatrix} G_{11} & G_{12} & G_{13} & G_{14} \\ 1 & 0 & 0 & 0 \\ 0 & 1 & 0 & 0 \\ G_{41} & G_{42} & G_{43} & 0 \\ G_{51} & G_{52} & G_{53} & G_{54} \end{bmatrix} \begin{bmatrix} \alpha \\ \dot{m}_{\mathrm{EGR}} \\ i_{\mathrm{ABV}} \\ t_{inj} \end{bmatrix}. \tag{2.47}$$

The vector of inputs consists of the disturbances to the throttle plate angle α and the EGR mass flow $\dot{m}_{\mathrm{EGR}}$ as well as the controllable inputs: the current i_{ABV} which drives the air by-pass valve and the fuel injection time t_{inj}. Collected in the vector of outputs are the primary internal error signal, the air-fuel ratio in the cylinder λ_{cyl}, and the measurements that are available for feedforward and feedback. In addition to the

[5]We choose these coordinates to describe an operating point, although it is not sufficient to characterise the equilibrium of the engine in terms of engine speed and manifold pressure only. The engine may not be in equilibrium, if the position of the throttle plate or the EGR mass flow rate are not consistent. It would be unusual to characterise the equilibrium of a system in terms of exogenous variables, even though in the present case the disturbances are not zero mean and determine the trajectory of the system. For local analysis, we therefore assume that the off-sets of both the disturbance signals and the actuator settings are consistent with the engine states. This is in spite of the fact that the true engine behaviour may be quite different in realistic driving scenarios.

direct measurements of the input disturbances, the pressure in the intake manifold p_M and the exhaust air-fuel ratio λ_{exh} are available for feedback.

In this configuration the exhaust gas recirculation is commanded by a separate control system, which acts as a disturbance to the air-fuel ratio control loops. We treat the EGR controller in a modular approach as an unknown system and only make certain assumptions about the disturbance signal.

We also use a slightly different configuration including an EGR valve that is instrumented with a position sensor for active control of the exhaust gas recirculation. In that case, the measurement of the valve position y_{EGR} replaces the mass flow measurement, and the input disturbance becomes another control input: the current i_{EGR} to the EGR valve. We are more specific about the control configuration in Chapter 4. The internal structure of the model is principally the same in both cases and is shown in Figure 2.16.

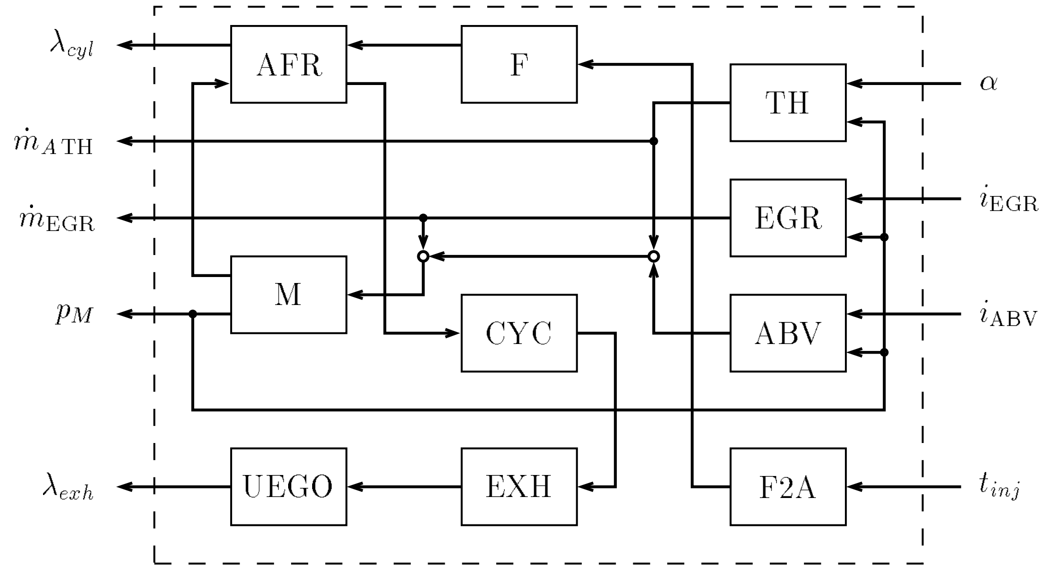

Figure 2.16: Open-loop Interconnection

The models evolve in discrete time with an event-based sample time corresponding to $\Delta\varphi = 180$ deg or half an engine revolution. Note that the transfer function matrix in Equation (2.47) on the preceding page is essentially lower triangular; the last output is a delayed measurement of the first output, which is an internal signal. The elements in the last row contain additional exhaust transport delays and the dynamics of the UEGO sensor. Further note that the state-space dimension of the model may be different in different operating points, as the exhaust transport delay is approximated with a different number of unit delays.

Nominal Model

From the set of models a nominal model was chosen for control design in a way as to cover the operating envelope in a ball of uncertainty around the model. The size of the uncertainty ball should not be unnecessarily large, as it would compromise the control behaviour to attempt to stabilise an unnecessarily large region. However, the nominal model should be an element of the set rather than the exact centre of a ball of minimal size, because, strictly speaking, the model data are only valid at the discrete points of the grid. The exact centre of the set would to a certain extent be arbitrary and difficult to compute. We discuss calculations in the gap metric in Chapter 4.

For a successful application of robust control techniques, the behaviour of the physical system must be contained in the set of models that is spanned by the nominal model and the uncertainty under all operating conditions. Yet, it is not clear how the changes in dynamics should be calculated on the basis of models in fixed operating points. For example, one approach would be to gain schedule between a number of models in order to cover the operating envelope in a less conservative way using interpolation, *cf.* Appendix D.1. In this sense the implementation of the initial control designs was intended to establish the validity of linear time-invariant models across the operating envelope.

2.4 Parameter-Dependent System Representation

For the analysis of the closed-loop system and advanced control system design, the engine behaviour across the operating envelope is represented by a single parameter-dependent system. For that purpose, the dependencies of the state-space matrices on different physical parameters are unified and normalised in terms of variations of engine speed δn, or, equivalently, the sample time $\delta h =: \delta_1$, and the manifold pressure ratio $\delta p_R =: \delta_2$.

This is achieved by approximating the nonlinear parameter functions, which are tabulated across the operating envelope, with two-dimensional polynomials. Since power series are readily represented as linear fractional transformations, the parameter-dependent subsystems and the parameter functions can be aggregated using LFT operations[6], to form a single parameter-dependent system. The result is a quasi-LPV system of the form shown in Figure 2.17. It is classified as quasi linear parameter-varying, because the state-space matrices do not only depend on exogenous variables δ_1, but also on the state of the system δ_2.

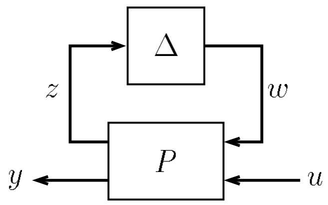

$$\begin{bmatrix} z \\ y \end{bmatrix} = \begin{bmatrix} P_{11} & P_{12} \\ P_{21} & P_{22} \end{bmatrix} \begin{bmatrix} w \\ u \end{bmatrix}$$

Figure 2.17: Generalised Plant

The parameter variations of compatible dimensions are from the set:

$$\{\Delta |\, \Delta = \operatorname{diag}(\delta_i I_{n_i})\,,\ |\delta_i| \leq 1\,, \delta_i \in \mathbb{R}\,, \quad i = 1, 2\}\,. \tag{2.48}$$

Note that the system is completely specified by the coefficient matrix P and a vector of parameter multiplicities, in general $\mathcal{N} = [n_1, n_2, \ldots, n_f]$ for f parameters.

[6] The interconnection of two LFT systems is again a linear fractional transformation.

Polynomial Approximations

We choose to approximate the variations of the model parameters, which were determined experimentally in the form of look-up tables, with two-dimensional polynomials of the form:

$$p(x, y) = \sum_{i,j} p_{ij} x^i y^j \,. \tag{2.49}$$

For a unified treatment of dynamic systems and such static nonlinear functions, both are represented as linear fractional transformations. An LFT realisation of two-dimensional power series is described in Appendix E. The polynomial coefficients in Equation (2.49) on the current page were calculated using a least squares optimisation algorithm to minimise the approximation error:

$$\min \sum_{i,j} \left(p(x_i, y_j) - z_{ij}\right)^2 \tag{2.50}$$

over a rectangular grid of data points (x_i, y_j, z_{ij}) for $i = 1, \ldots, I$ and $j = 1, \ldots, J$, or, equally, over any number of data points (x, y, z). The polynomial order was chosen individually for each model parameter with a view to keeping the approximation error small, without inflating the parameter multiplicity unnecessarily. While the functions can be approximated to any degree on the interior, the match on the outside may be arbitrarily poor. A reasonable compromise must be found.

Parameter Multiplicities

Table 2.3 on the following page lists the state-space dimensions of the individual subsystems and at the bottom the dimensions of the compound system. The columns are from left to right the number of states, the number of outputs, the number of inputs, and the parameter multiplicities respectively.

In the construction of the model, each copy of a model parameter is replaced by a polynomial approximant. Depending on how many times a parameter appears in the model, this can increase the state-space dimensions considerably. The volumetric efficiency, for example, appears twice in the differential equations which describe the intake manifold. Its polynomial approximation is of third order with respect to δ_1 and of first order with respect to δ_2, resulting in the parameter multiplicities 6 and 2 respectively. The generalised plant P can be used for complex μ or mixed μ analysis and is suited especially for the synthesis of parameter-dependent controllers according to the approach in [45], which is described in the next chapter.

	Dimensions				
System	n_x	n_y	n_u	n_1	n_2
TH	0	1	1	0	0
ABV	2	1	1	2	0
EGR	1	1	1	1	0
M	2	2	2	2	0
η_v	0	2	2	6	2
T_M	0	2	2	6	6
F2A	2	1	1	0	0
F	4	1	1	1	0
ζ	0	1	1	1	0
χ	0	1	1	3	3
AFR	0	1	1	0	0
m_A^{-1}	0	1	1	1	2
CYC	2	1	1	0	0
Padé	3	1	1	3	0
EXH	0	3	3	3	6
UEGO	1	1	1	1	0
P	17	5	4	30	19

Table 2.3: State-space Dimensions of Subsystems

3. ROBUST CONTROL THEORY

Even if the physical world could, in principle, be described completely, it would not be practical to do so in engineering. In reality, the information about physical processes is always incomplete. We do not only refer to imperfect process measurements but, more generally, to the limited knowledge about a system. On the one hand certain kinds of information may not be available, on the other hand certain phenomena may not be deterministic but, for example, chaotic, or uncertain for that matter. That is to say, uncertainty is not only the result of a lack of knowledge at a certain time but can be a genuine feature that is inherent in complex systems. When furthermore simplifying assumptions are made in order to derive a mathematical description of a process, uncertainty also occurs on a mathematical level in the form of approximation errors or numerical inaccuracies.

Robust control is an approach to the analysis of and the controller synthesis for uncertain systems. The notion of robustness refers to the ability of a system to maintain its characteristics in the presence of uncertainty. For instance, a system is called robust, if its stability and performance properties can be tolerated with respect to certain types of uncertainty. Such an approach naturally involves a mathematical model of the nominal process behaviour as well as the associated uncertainty.

Typically, uncertainty arises in different locations, and on different levels, of a system. Several generic types of uncertainty, additive, multiplicative, and linear fractional uncertainty, were introduced in Chapter 1 in Figure 1.1 on page 4. Uncertainty may be real- or complex-valued, constant or time-varying, dynamic or even nonlinear. Depending on the type, or class, of uncertainty, different classes of systems can be defined, such as the classes of linear time-invariant, parameter-dependent, or parameter-varying systems.

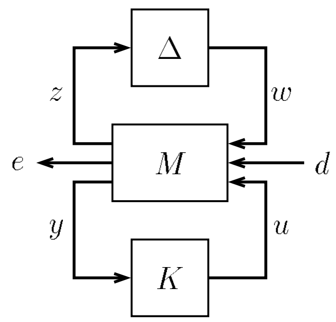

Figure 3.1: Generic Feedback Configuration

In all these cases, the systems can be represented as in Figure 3.1, where a linear system M is controlled by a controller K in the presence of perturbations Δ and disturbances d. Both the controller and the block of uncertainty are interconnected with the nominal plant in a linear fractional manner (See Section 3.1.3). The performance of the system is measured in terms of the error e induced by the disturbances and the perturbations. The measurements that are available for feedback are denoted y, u is the vector of control inputs. The specification of the signal spaces, finally, completes the set-up.

The prime motivation for feedback is to reduce the effect of uncertainty on the system's performance. More specifically, in terms of the block diagram, the control objective is to stabilise the system for all perturbations Δ and disturbances d and to minimise their effect on the system's performance, as measured by the error signals e. If the model were exact or the effect of uncertainty negligible, no feedback would be required. The dynamics of the plant could simply be inverted and substituted by feedforward to achieve the desired performance. Yet, this assumption is not realistic, and generally the effect of uncertainty must be accounted for in control system design.

The formulation of control problems in an $\mathcal{H}_\infty$ framework relies on worst-case optimisation. The induced norm of a system, which corresponds to the worst-case gain, is used to characterise the control objectives. Most often, the control problem is posed as a minimisation problem, to minimise the size of a combination of closed-loop transfer functions over a set of stabilising controllers. A great variety of control problems can be accommodated in the configuration in Figure 3.1. In this chapter, we only intend to highlight a number of control theoretic concepts that are relevant to the present application. For a comprehensive treatment of robust and optimal control the interested reader is referred to [59, 18]. Most of the software tools that were used in robust control design are available from the μ-Analysis and Synthesis Toolbox [5], which could serve as a more practical introduction to robust control.

3.1 Fundamentals

3.1.1 State-Space Systems

In this thesis, we always deal with systems in state-space form. For the most part, we consider finite-dimensional linear time-invariant systems described by the vector differential equation:

$$\begin{bmatrix} \dot{x} \\ y \end{bmatrix} = \begin{bmatrix} A & B \\ C & D \end{bmatrix} \begin{bmatrix} x \\ u \end{bmatrix}, \tag{3.1}$$

where $x \in \mathbb{R}^{n_x}$ is called the system state, $u \in \mathbb{R}^{n_u}$ is called the system input, and $y \in \mathbb{R}^{n_y}$ is called the system output. The matrices A, B, C, and D are real-valued and of appropriate dimensions. A dynamic system with a single input ($n_u = 1$) and a single output ($n_y = 1$) is called a SISO system, otherwise it is called a MIMO (multiple-input-multiple-output) system. The corresponding transfer function matrix is defined as

$$\left[\begin{array}{c|c} A & B \\ \hline C & D \end{array}\right] := C(sI - A)^{-1}B + D\,. \tag{3.2}$$

We do not distinguish discrete-time systems from continuous-time systems in our notation, so the above representation in terms of a block matrix may as well stand for a discrete-time system. Whether a particular system is in continuous or discrete time, will be clear from the context. The notation in Equation (3.2) on the current page is to indicate that the transfer function matrix can be calculated via a linear fractional transformation operating $\frac{1}{s}$ on the state-space data $\left[\begin{smallmatrix} A & B \\ C & D \end{smallmatrix}\right]$.

Generalised Systems

We rely extensively on system representations, where the input and output vectors are partitioned:

$$\begin{bmatrix} \dot{x} \\ z \\ \hdashline y \end{bmatrix} = \left[\begin{array}{c|c:c} A & B_1 & B_2 \\ \hline C_1 & D_{11} & D_{12} \\ \hdashline C_2 & D_{21} & D_{22} \end{array}\right] \begin{bmatrix} x \\ w \\ \hdashline u \end{bmatrix}, \tag{3.3}$$

to distinguish, for example, disturbances from control inputs, or control objectives from measurements. Note that this is of the same form as (3.1). On the other hand we refer to more general classes of systems, where the state-space data are a function of several, possibly time-varying, parameters, so that there is a significant difference in the interpretation of the partitioning of the input and output vectors, *cf.* Section 3.3.4.

Balanced Realisations

For the purpose of controller order reduction by means of balanced truncation, see Section 3.3.2, we require a balanced realisation of the controller, which is defined as follows.

Definition 3.1 ([38, pp. 83–4]) *Let* $\left[\begin{array}{c|c} A & B \\ \hline C & D \end{array}\right]$ *be a minimal realisation of an asymptotically stable system* $G(s) \in \mathcal{RH}_\infty$*, then this realisation is called balanced, if for*

$$P = \int_0^\infty e^{tA} B B^* e^{tA^*} dt$$
$$Q = \int_0^\infty e^{tA^*} C^* C e^{tA} dt\,,$$

we have $P = Q = \Sigma := \mathrm{diag}(\sigma_1, \sigma_2, \ldots, \sigma_n)$*.* Σ *is called the Gramian of the system. The decreasingly ordered, positive numbers,* $\sigma_1 \geq \sigma_2 \geq \cdots \geq \sigma_n > 0$*, are called the Hankel singular values.*

3.1.2 Frequency-Domain Spaces

To be precise about the set-up in Figure 3.1 on page 45, we define the underlying function spaces and induced norms for signals and systems. For the sake of brevity, the definitions are given in the frequency domain only.

Definition 3.2 ([38, p. 11]) *The* $\mathcal{L}_2/\mathcal{H}_2$ *norm of* $G(s)$ *is given by*

$$\|G\|_2 = \sqrt{\frac{1}{2\pi}\int_{-\infty}^{\infty} \mathrm{Trace}\left(G^*(j\omega)G(j\omega)\right) d\omega}\,. \tag{3.4}$$

$\mathcal{L}_2(j\mathbb{R})$*, or simply* $\mathcal{L}_2$*, is a Hilbert space of matrix-valued functions on* $j\mathbb{R}$ *with finite* $\mathcal{L}_2$ *norm.* $\mathcal{H}_2$ *is a subspace of* $\mathcal{L}_2(j\mathbb{R})$ *with matrix functions* $G(s)$ *analytic in* $\Re(s) > 0$*.*

Definition 3.3 *The $\mathcal{L}_\infty/\mathcal{H}_\infty$ norm of $G(s)$ is given by*

$$\|G\|_\infty = \operatorname*{ess\,sup}_{\omega\in\mathbb{R}} \bar{\sigma}\left(G(j\omega)\right) . \tag{3.5}$$

$\mathcal{L}_\infty(j\mathbb{R})$, or simply $\mathcal{L}_\infty$, is a Banach space of matrix-valued functions that are essentially bounded on $j\mathbb{R}$. $\mathcal{H}_\infty$ is a subspace of $\mathcal{L}_\infty$ with functions that are analytic and bounded in the open right half plane. The prefix $\mathcal{R}$ restricts the function spaces to consist of real-rational transfer function matrices only. The subspace $\mathcal{RH}_\infty$, for example, consists of all proper and real-rational stable transfer function matrices.

We only consider signals in $\mathcal{H}_2$ and measure the size of transfer function matrices using the $\mathcal{H}_\infty$ norm to characterise performance objectives. Even though the model in the previous chapter and the controller implementation in Chapter 5 are discrete and event-based, the control design is carried out in an equivalent continuous frequency domain, mainly for the convenience of using the synthesis procedures for continuous-time systems (See Appendix C). Note that for the problem at hand intersample behaviour is not an issue.

3.1.3 Linear Fractional Transformations

The types of interconnection in Figure 3.3 on page 50 are called linear fractional transformations. There are lower and upper forms, for which the closed-loop transfer function matrices are defined as follows:

$$\mathcal{F}_\ell(P,K) = P_{11} + P_{12}K\left(I - P_{22}K\right)^{-1}P_{21} \tag{3.6}$$

$$\mathcal{F}_u(T,\Delta) = T_{22} + T_{21}\Delta\left(I - T_{11}\Delta\right)^{-1}T_{12} . \tag{3.7}$$

The matrix functions are well-defined, if $(I - P_{22}K)$ and $(I - T_{11}\Delta)$ are invertible. More practically, the interconnection in Figure 3.3(a) can be interpreted as a nominal plant P that is controlled by a controller K, while in Figure 3.3(b) a closed-loop system T is perturbed by some Δ.

Linear fractional transformations can be applied to constant matrices, dynamic systems, or, more generally, to matrices that are varying with time or frequency, see the data formats of the μ-Analysis and Synthesis Toolbox [5] for more details. In addition to feedback interconnections of systems, many systems themselves admit representations via linear fractional transformations, for example, multi-dimensional polynomial or rational functions, state-space realisations of parameter-dependent or uncertain systems, *etc.* Since the interconnection of two LFT systems is again a linear fractional transformation, we can now be more precise about the image of an engine control system in Figure 1.3 on page 5. It can be expressed by the so-called star product:

$$\mathcal{S}(P,K) = \begin{bmatrix} \mathcal{F}_\ell(P,K_{11}) & P_{12}(I-K_{11}P_{22})^{-1}K_{12} \\ K_{21}(I-P_{22}K_{11})^{-1}P_{21} & \mathcal{F}_u(K,P_{22}) \end{bmatrix} . \tag{3.8}$$

3.1.4 Coprime Factorisations

Commonly, the input-output behaviour of a linear SISO system is described in the Laplace domain by a transfer function whose numerator and denominator are polynomials in the Laplace variable with real-valued coefficients. This concept of a fractional system representation is extended to the multi-variable case using coprime factorisations. As the notion of coprime factors is generalised to transfer function matrices, left, respectively right, coprime factor plant descriptions can be introduced. We confine our introduction to left coprime factorisations, since all results with respect to right coprime factorisations follow by the principle of duality. If M and N are left coprime over $\mathcal{RH}_\infty$, then

$$G = M^{-1}N \tag{3.9}$$

is called a left coprime factorisation of G. If in addition the following property

$$\begin{bmatrix} N & M \end{bmatrix} \begin{bmatrix} N^* \\ M^* \end{bmatrix} = I \tag{3.10}$$

holds for all frequencies ω on the imaginary axis, the factorisation is called normalised. The idea of $\mathcal{H}_\infty$ loop shaping is based on the stabilisation of a perturbed coprime factor plant description as in Figure 3.2, *cf.* Section 3.2.2.

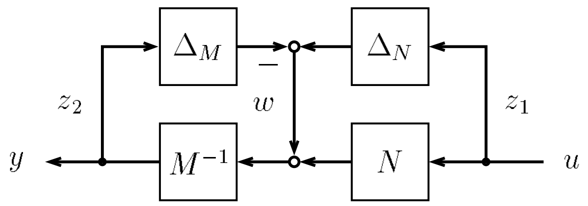

Figure 3.2: Coprime Factor Plant Description including Perturbations

The fact that the underlying coprime factorisation is normalised allows for an explicit solution of the robust stabilisation problem for

$$G = (M + \Delta_M)^{-1}(N + \Delta_N) \tag{3.11}$$

with

$$\{\begin{bmatrix} \Delta_N & \Delta_M \end{bmatrix} \mid \left\| \begin{bmatrix} \Delta_N & \Delta_M \end{bmatrix} \right\|_\infty < \varepsilon\}\,. \tag{3.12}$$

3.1.5 Stability Results

It is not sufficient to check the stability of a closed-loop system in terms of the sensitivity function only. First of all, the feedback arrangement in Figure 3.4 on page 52 must be well-posed, *i.e.* $(I - G(\infty)K(\infty))$ must be invertible for a unique solution of the loop equations to exist and be proper. Then the internal stability of a closed-loop system can be characterised according to the following lemma.

Lemma 3.4 ([59, p. 122]) *The pair (G, K) in the feedback arrangement in Figure 3.4 is stable*[7] *if and only if the transfer function matrix*

$$\begin{bmatrix} K(I-GK)^{-1}G & K(I-GK)^{-1} \\ (I-GK)^{-1}G & (I-GK)^{-1} \end{bmatrix} \tag{3.13}$$

from $\left[\begin{smallmatrix} w_1 \\ w_2 \end{smallmatrix}\right]$ *to* $\left[\begin{smallmatrix} z_1 \\ z_2 \end{smallmatrix}\right]$ *belongs to* $\mathcal{RH}_\infty$.

[7] This is also referred to as the internal stability of the feedback system.

In order to derive conditions for robust stability with respect to unstructured perturbations, a perturbed closed-loop system can be re-arranged to be again of the form in Figure 3.4, so that one block contains the nominal part of the system while the other block contains the perturbations. A condition for robust stability is then derived by applying the small gain theorem.

Theorem 3.5 (Small Gain Theorem, [59, p. 218]) *Suppose $K \in \mathcal{RH}_\infty$ and let $\gamma > 0$. Then the interconnected system shown in Figure 3.4 is well-posed and internally stable for all $G(s) \in \mathcal{RH}_\infty$ with*

a) $\|G\|_\infty \leq 1/\gamma$ *if and only if* $\|K(s)\|_\infty < \gamma$;

b) $\|G\|_\infty < 1/\gamma$ *if and only if* $\|K(s)\|_\infty \leq \gamma$.

3.2 Controller Synthesis

3.2.1 Standard $\mathcal{H}_\infty$ Problem

With reference to the set-up in Figure 3.3(a) optimal and sub-optimal control problems can be posed. In the optimal case, the objective is to find all admissible controllers $K(s)$ for a nominal plant P such that the $\mathcal{H}_\infty$ norm of the closed-loop transfer function T_{zw} is minimised:

$$\min_{K \text{ stblz}} \|\mathcal{F}_\ell(P, K)\|_\infty \,. \tag{3.14}$$

Alternatively, it can be of interest to find all sub-optimal controllers $K(s)$ such that

$$\|\mathcal{F}_\ell(P, K)\|_\infty < \gamma \,, \tag{3.15}$$

where $\gamma > 0$ is a pre-specified performance level. The synthesis of such controllers is based on the solution of two Riccati equations, which are solved iteratively in the general case in a γ iteration [19, 24].

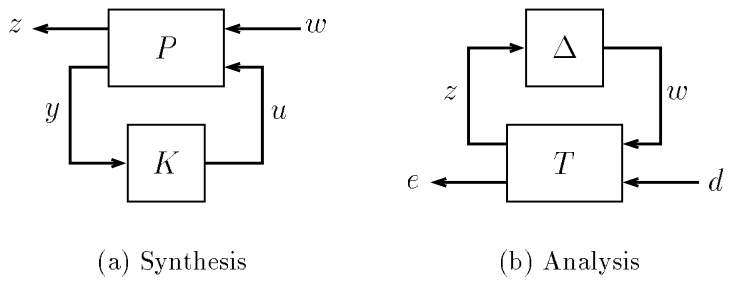

Figure 3.3: $\mathcal{H}_\infty$ Framework

From an analysis point of view a given controller can be considered in connection with a generalised plant in order to evaluate various robustness and performance measures in terms of the $\mathcal{H}_\infty$ norm, see Figure 3.3(b).

3.2.2 $\mathcal{H}_\infty$ Loop Shaping

$\mathcal{H}_\infty$ loop shaping is a simple and efficient control design methodology that originated from a particular control problem, the so-called robust stabilisation problem on the basis of a coprime factor plant description [38, 25]. More specifically, the design objective

$$\min_{K \text{ stblz}} \left\| \begin{bmatrix} K \\ I \end{bmatrix} (I - GK)^{-1} M^{-1} \right\|_\infty = \varepsilon_{\max}^{-1} \tag{3.16}$$

can be interpreted as to maximise the robust stability radius with respect to the coprime factor perturbations in Equation (3.12) on page 49. It is straightforward to calculate the expression in Equation (3.16) on this page as the closed-loop transfer function T_{zw}, when the perturbed plant in Figure 3.2 on page 49 is connected with a controller. Then the robust stability condition is derived by applying the small gain theorem.

The approach combines the robustness of $\mathcal{H}_\infty$ controllers with a performance specification via loop shaping. The performance requirements are incorporated into the design by shaping the open-loop singular values of the plant with pre- and post-compensators as in Figure 4.1 on page 59 and solving the robust stabilisation problem for the weighted plant

$$G_W = W_2 G W_1 \,. \tag{3.17}$$

All the classical guidelines for loop shaping apply. The controller for the original problem is recovered by re-arranging the weighting functions in the loop.

This kind of problem formulation is appealing for several reasons. The loop shaping design procedure results in a controller structure that is useful for implementation. If the coprime factorisation of the plant is normalised, the problem can be solved explicitly; no γ iteration is required. Moreover, the performance level ε^{-1} can be calculated *a priori*. The stability margin ε is also indicative of the compatibility of the loop shape with the desired robustness properties. As a rule of thumb, a value of 0.3 or above indicates good compatibility. Finally, the problem formulation is balanced with regard to the closed-loop characteristics at the input and output of the plant, as we shall see in the relationship to the four-block problem. This implies a frequency weighting in the design objective that is compatible with the plant characteristics.

The foundation of $\mathcal{H}_\infty$ loop shaping has been greatly enhanced with the introduction of the gap metric. Indeed, the set of plants which is stabilised by a loop-shaping controller can be characterised precisely in terms of the gap metric, *cf.* Theorem 3.7.

3.2.3 Four-Block Problem

The four-block problem, for which the set-up is shown in Figure 3.4 on the next page, is closely related to the robust stabilisation problem of the previous section.

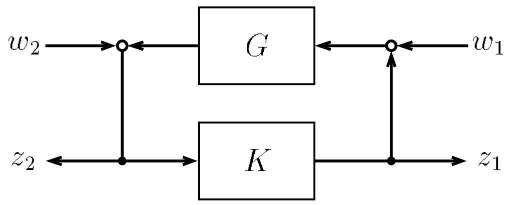

Figure 3.4: Standard Feedback Configuration

In fact, post-multiplying the expression in Equation (3.16) on the preceding page with $[\,N\ M\,]$ yields the corresponding transfer function matrix from w to z:

$$\begin{bmatrix} z_1 \\ z_2 \end{bmatrix} = \begin{bmatrix} K \\ I \end{bmatrix} (I - GK)^{-1} \begin{bmatrix} G & I \end{bmatrix} \begin{bmatrix} w_1 \\ w_2 \end{bmatrix}, \tag{3.18}$$

which consists of four blocks. Any controller that solves the one problem also solves the other. Note that the set-up for control design in Chapter 4 in Figure 4.1 on page 59 exhibits the same structure in the lower part of the diagram as in Figure 3.4. The definition of the generalised stability margin

$$b(G,K) := \begin{cases} \left\| \begin{bmatrix} K \\ I \end{bmatrix} (I - GK)^{-1} \begin{bmatrix} G & I \end{bmatrix} \right\|_\infty^{-1} & \text{if } (G,K) \text{ is stable} \\ 0 & \text{otherwise.} \end{cases} \tag{3.19}$$

is also with respect to this feedback configuration. The generalised stability margin and the gap metric are the key concepts in the robust stability analysis in Chapter 4.

3.3 Advanced Concepts

3.3.1 Gap Metric

A number of measures are available to measure the robustness of feedback systems. In particular, the two metrics δ_g and δ_ν provide a measure of the distance between two plants in the standard feedback configuration [23, 56]. For our purposes, it is sufficient to introduce the δ_ν metric in terms of its frequency-domain interpretation only rather than in its full generality, what would be mathematically more involved.

Definition 3.6 ([56, pp. 24, 62]) *First, define the pointwise distance between the frequency responses of two systems G_1 and G_2 as*

$$\kappa\left(G_1(j\omega), G_2(j\omega)\right) = \bar{\sigma}\left((I + G_1G_1^*)^{-1/2}(G_2 - G_1)(I + G_2^*G_2)^{-1/2}\right)(j\omega)\,. \tag{3.20}$$

Then, the δ_ν metric, can be written as

$$\delta_\nu\left(G_1, G_2\right) = \begin{cases} \max_w \kappa\left(G_1(j\omega), G_2(j\omega)\right) & \textit{if}\ \mathrm{wno}\ \det(G_1^*G_2) = 0 \\ 1 & \textit{otherwise,} \end{cases} \tag{3.21}$$

where wno(G) *denotes the winding number of $G(s)$ about the origin, as the Laplace variable s follows the standard Nyquist D-contour.*

In this thesis, we sometimes also refer to the δ_ν metric simply as the gap metric, although, strictly speaking, there are subtle technical differences between the two. The strong relationship of the gap metric with the generalised stability margin is expressed in the following robust stability theorem.

Theorem 3.7 ([56, p. 29])

i) Given a nominal plant G_1, a controller K, and numbers $\beta \leq \alpha < b_{opt}(G_1)$, where $b_{opt}(G) := \max_K b(G,K)$, then: $\arcsin b(G_2, K) > \arcsin \alpha - \arcsin \beta$ for all G_2 satisfying $\delta_\nu(G_1, G_2) \leq \beta$ if, and only if, $b(G_1, K) > \alpha$.

ii) Given a nominal plant G_1, a perturbed plant G_2 and numbers $\beta \leq \alpha < b_{opt}(G_1)$, then: $\arcsin b(G_2, K) > \arcsin \alpha - \arcsin \beta$ for all K satisfying $b(G_1, K) > \alpha$ if, and only if, $\delta_\nu(G_1, G_2) \leq \beta$.

Note that both quantities are normalised:

$$0 \leq b(G,K) \leq 1\,, \qquad 0 \leq \delta_\nu(G,K) \leq 1\,. \tag{3.22}$$

3.3.2 Model Reduction by Balanced Truncation

For the sake of completeness, a result on model reduction by balanced truncation is given in this section. This technique is employed in Chapter 4 to facilitate the implementation of $\mathcal{H}_\infty$ controllers. It was found to be sufficient in practice to consider the following case of unweighted model reduction with respect to additive approximation errors.

Theorem 3.8 ([59, pp. 158–9]) *Suppose $G(s) \in \mathcal{RH}_\infty$ and*

$$G(s) = \left[\begin{array}{cc|c} A_{11} & A_{12} & B_1 \\ A_{21} & A_{22} & B_2 \\ \hline C_1 & C_2 & D \end{array}\right] \tag{3.23}$$

is a balanced realisation with Gramian $\Sigma = \mathrm{diag}(\Sigma_1, \Sigma_2)$

$$\begin{aligned} \Sigma_1 &= \mathrm{diag}(\sigma_1 I_{s_1}, \sigma_2 I_{s_2}, \ldots, \sigma_r I_{s_r}) \\ \Sigma_2 &= \mathrm{diag}(\sigma_{r+1} I_{s_{r+1}}, \sigma_{r+2} I_{s_{r+2}}, \ldots, \sigma_N I_{s_N}) \end{aligned}$$

and

$$\sigma_1 > \sigma_2 > \cdots > \sigma_r > \sigma_{r+1} > \sigma_{r+2} > \cdots > \sigma_N\,,$$

where σ_i has multiplicity s_i, $i = 1, 2, \ldots, N$ and $s_1 + s_2 + \cdots + s_N = n$. Then the truncated system

$$\hat{G}_r(s) = \left[\begin{array}{c|c} A_{11} & B_1 \\ \hline C_1 & D \end{array}\right] \tag{3.24}$$

is balanced and asymptotically stable. Furthermore,

$$\left\| G(s) - \hat{G}_r(s) \right\|_\infty \leq 2(\sigma_{r+1} + \sigma_{r+2} + \cdots + \sigma_N) \tag{3.25}$$

and the bound is achieved, if $r = N - 1$, *i.e.,*

$$\left\| G(s) - \hat{G}_{N-1}(s) \right\|_\infty = 2\sigma_N \,. \tag{3.26}$$

Moreover, it turned out to be important to remove fast and slow modes of the controller before performing a further order reduction according to the above theorem in order to ensure a reliable approximation. While the approach is confined to stable systems as such, unstable systems can also be approximated via a coprime factorisation, when they are represented by two stable systems. More than that, model reduction based on coprime factorisations ties in with $\mathcal{H}_\infty$ loop shaping and robustness in the gap metric.

3.3.3 Structured Singular Value

So far we have only been dealing with unstructured uncertainty descriptions. However, quite often uncertainty arises in several locations of a system, so that the uncertainty description exhibits a particular structure on a macroscopic level. For example, a simple $\mathcal{H}_\infty$ set-up which combines a robust stability requirement with a performance objective can already be interpreted as to allow for two different types of uncertainty. The structured singular value μ [46] offers an integral framework for the treatment of systems with multiple sources of uncertainty, see Figure 3.5.

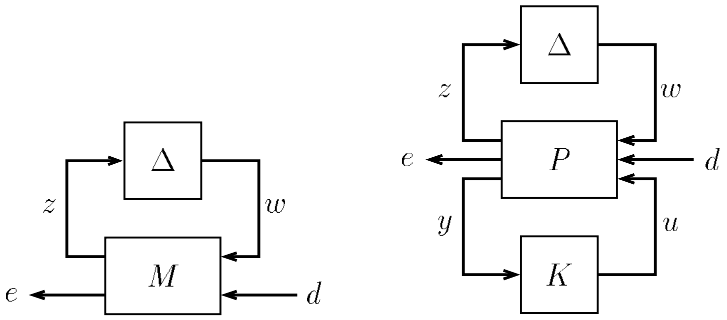

(a) Analysis (b) Synthesis

Figure 3.5: μ Framework

The matrix function $\mu(M)$ is defined with respect to an uncertainty structure

$$\mathbf{\Delta} = \{\operatorname{diag}(\delta_1 I_{r_1}, \ldots, \delta_S I_{r_S}, \Delta_1, \ldots, \Delta_F) \,|\, \delta_i \in \mathbb{C},\ \Delta_j \in \mathbb{C}^{m_j \times m_j}\} \subset \mathbb{C}^{n\times n}\,, \tag{3.27}$$

which consists of S repeated scalar blocks and F full blocks, where

$$\sum_{i=1}^{S} r_i + \sum_{j=1}^{F} m_j = n\,. \tag{3.28}$$

Definition 3.9 ([59, p. 278]) *For* $M \in \mathbb{C}^{n\times n}$, $\mu_{\mathbf{\Delta}}(M)$ *is defined as*

$$\mu_{\mathbf{\Delta}}(M) := \frac{1}{\min\{\bar\sigma(\Delta) \,|\, \Delta \in \mathbf{\Delta},\ \det(I - M\Delta) = 0\}}\,, \tag{3.29}$$

unless no $\Delta \in \mathbf{\Delta}$ *makes* $I - M\Delta$ *singular, in which case* $\mu_{\mathbf{\Delta}}(M) := 0$.

In this way the robustness of the system in Figure 3.5(a) on the facing page can be analysed with respect to norm-bounded structured perturbations $\|\Delta\|_\infty < 1$ by testing whether

$$\sup_{\omega\in\mathbb{R}} \mu_{\mathbf{\Delta}}(M(j\omega)) \leq 1\,. \tag{3.30}$$

If moreover the system representation combines several control objectives or the uncertainty structure is otherwise partitioned as

$$\mathbf{\Delta} = \{\begin{bmatrix}\Delta_1 & 0\\ 0 & \Delta_2\end{bmatrix} \,|\, \Delta_1 \in \mathbf{\Delta}_1,\ \Delta_2 \in \mathbf{\Delta}_2\}\,, \tag{3.31}$$

more detailed statements can be made about the stability and performance properties of the system according to the following theorem.

Theorem 3.10 (Main Loop Theorem, [59, p. 284]) *The following are equivalent:*

$$\mu_{\mathbf{\Delta}} \leq 1 \quad \iff \quad \begin{cases}\mu_2(M_{22}) \leq 1, \ \textit{and}\\ \max_{\Delta_2\in\mathbf{\Delta}} \mu_1(\mathcal{F}_\ell(M,\Delta_2)) \leq 1\,.\end{cases} \tag{3.32}$$

This method of analysis motivates a procedure to design controllers for systems with structured perturbations. A practical approach is to minimise the upper bound on μ

$$\min_{K} \inf_{D,\,D^{-1}\in\mathcal{H}_\infty} \left\|D\mathcal{F}_\ell(P,K)D^{-1}\right\|_\infty \tag{3.33}$$

iteratively over all stabilising controllers and a set of scaling matrices which commute with the uncertainty structure. In the so-called D-K iteration the robustness and performance channels z and w, respectively e and d, in the diagram in Figure 3.5(b) on the preceding page are scaled via convex optimisation alternately with the $\mathcal{H}_\infty$ controller synthesis. The problem formulation for the synthesis of parameter-dependent controllers in the next section is in the same spirit. We perform a complex μ analysis in Section 4.2.7 to assess the achievable performance in the presence of parametric uncertainty.

3.3.4 Parameter-Dependent Controller Synthesis

For a certain class of time-varying systems, parameter-dependent controllers can be designed by solving a generalised $\mathcal{H}_\infty$ problem based on a scaled version of the small gain theorem [45]. Consider a time-varying discrete system as in Figure 3.6 on the following page, also see Figure 1.3 on page 5, where the plant consists of a linear time-invariant part

$$\begin{bmatrix} z\\ e\\ y\end{bmatrix} = \begin{bmatrix}P_{11} & P_{12} & P_{13}\\ P_{21} & P_{22} & P_{23}\\ P_{31} & P_{32} & P_{33}\end{bmatrix}\begin{bmatrix} w\\ d\\ u\end{bmatrix} \tag{3.34}$$

which is perturbed by Δ_1. In particular, the perturbations are assumed to be from the set

$$\{\Delta_1 |\, \Delta_1 = \mathrm{diag}(\delta_i I_{n_i})\,,\ |\delta_i| \leq 1\,, \delta_i \in \mathbb{C}, \quad i = 1,\ldots,f\}\,. \tag{3.35}$$

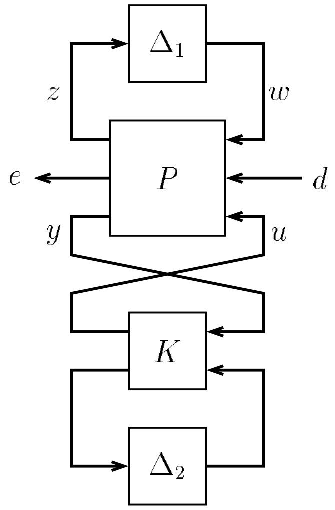

Figure 3.6: Time-Varying Closed-Loop System

Note that the plant is then completely specified by the coefficient matrix P and a vector of parameter multiplicities

$$\mathcal{N} = [n_1, n_2, \ldots, n_f] \; . \tag{3.36}$$

Furthermore, the problem set-up in Figure 3.6 assumes a controller of the same structure as the plant, which is defined similarly by a linear time-invariant part K and a vector of integers

$$\mathcal{R} = [r_1, r_2, \ldots, r_f] \tag{3.37}$$

to describe the uncertainty structure

$$\{\Delta_2 | \, \Delta_2 = \mathrm{diag}(\delta_i I_{r_i}) \, , \; |\delta_i| \leq 1 \, , \delta_i \in \mathbb{C} \, , \quad i = 1, \ldots, f\} \, . \tag{3.38}$$

As in the case of μ synthesis, the control objective involves a set of scalings which commute with the uncertainty structure:

$$\boldsymbol{J}(\mathcal{N}, \mathcal{R}) = \left\{ \begin{bmatrix} \mathrm{diag}(J_{11\,i}) & \mathrm{diag}(J_{12\,i}) \\ \mathrm{diag}(J_{21\,i}) & \mathrm{diag}(J_{22\,i}) \end{bmatrix} \middle| \begin{bmatrix} J_{11\,i} & J_{12\,i} \\ J_{21\,i} & J_{22\,i} \end{bmatrix} \in \mathbb{R}^{(n_i + r_i) \times (n_i + r_i)} \, , \right.$$
$$\left. \text{invertible}, i = 1, \ldots, f \right\} \, . \tag{3.39}$$

The synthesis problem for LFT parameter-dependent controllers can be stated as follows.

Definition 3.11 ([45, p. 83]) *The control synthesis problem associated with the open-loop data P and $\mathcal{N}$ consists in finding an f-tuple of nonnegative integers $\mathcal{R}$, a matrix $J \in \boldsymbol{J}(\mathcal{N}, \mathcal{R})$, and a stabilising, finite dimensional, linear time-invariant controller K, if they exist, such that*

$$\left\| \begin{bmatrix} J & 0 \\ 0 & I \end{bmatrix} \mathcal{F}_\ell(P_{\mathcal{R}}, K) \begin{bmatrix} J^{-1} & 0 \\ 0 & I \end{bmatrix} \right\|_\infty < 1 \, , \tag{3.40}$$

where

$$P_{\mathcal{R}} := \begin{bmatrix} P_{11} & 0 & P_{12} & P_{13} & 0 \\ 0 & 0_r & 0 & 0 & I_r \\ P_{21} & 0 & P_{22} & P_{23} & 0 \\ P_{31} & 0 & P_{32} & P_{33} & 0 \\ 0 & I_r & 0 & 0 & 0 \end{bmatrix} \tag{3.41}$$

for

$$r = \sum_{i=1}^{f} r_i \,. \tag{3.42}$$

The parameter-dependent model in Chapter 2 has been developed specifically towards this problem formulation. Although the control objective does not exploit the fact that the parameters δ_i, $i = 1, \ldots, f$, are real-valued, the structure of the controller lends itself to implementation (See Appendix D). Since the problem admits a representation in terms of linear matrix inequalities, it can be solved via convex optimisation using the LMI Control Toolbox [22, 10].

Alternatively, the stability and performance of linear parameter-varying systems have been studied in continuous time using quadratic Lyapunov functions [9, 8]. In this case, however, the problem is described by an infinite number of convex constraints and can only be solved by gridding the parameter space.

According to [58, 57], it is also possible to include the rates of change of the parameter variations in the control specification, but this results in a still more complex controller function. In view of the experimental results in Chapter 5, model reduction techniques for LFT systems, such as in [7], will be prerequisite for practical applications.

4. CONTROL DESIGN

The need for robust design in engine control applications has been motivated from a practical point of view in Chapter 1 and from a theoretical point of view in the previous chapter. In this chapter, we present two control designs based on the set of linear time-invariant models from Chapter 2. Although the models are genuinely discrete and event-based, it was found to be easier to carry out the design in a continuous frequency domain, see Appendix C.

We mostly deal with unstructured uncertainty descriptions and therefore employ the technique of $\mathcal{H}_\infty$ loop shaping. We also perform robustness and performance analyses using the gap metric δ_ν and the complex structured singular value μ. A special emphasis is on the integrated design of feedforward and feedback control.

Generalised Plant

The generic set-up for control design is shown in Figure 4.1. It is based on the four-block problem that was introduced in Section 3.2.3. The lay-out in the lower part of the diagram is the same as in Figure 3.4 on page 52. In the feedback part of the arrangement, the nominal plant G is augmented with the pre- and post-compensators W_1 and W_2. The generalised disturbances w_1 and w_2 act on the input and output of the weighted plant, z_1 is the output of the controller, and z_2 is the output of the plant disturbed by w_2.

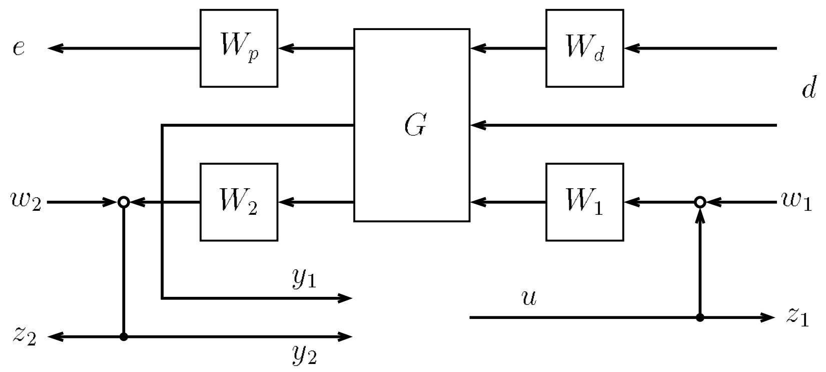

Figure 4.1: Set-up for Control Design

On top of the feedback part is the feedforward part of the arrangement. In the upper part of the diagram, the nominal plant is further augmented with the weighting functions W_p and W_d in the performance and disturbance channels. In addition to the input and output properties that are specified in the feedback part, the performance objectives are specified in terms of the closed-loop transfer characteristics from the physical disturbances d to the error signals e. The set-up allows for both weighted and unweighted error and disturbance signals. The dimensions of the systems involved in the interconnection determine the sizes of the vectors y_1 and d.

Finally, the vector y is partitioned in direct measurements y_1 for feedforward, and, possibly weighted, measurements y_2 for feedback; u is the control input. All signals may be vector-valued. The weighting functions are restricted to be square and diagonal. According to Figure 4.1, the generalised plant is therefore defined as

$$\begin{bmatrix} e \\ z \\ y \end{bmatrix} = P \begin{bmatrix} d \\ w \\ u \end{bmatrix} . \tag{4.1}$$

Furthermore, connecting the generalised plant with the controller

$$u = Ky , \tag{4.2}$$

yields the closed-loop control system

$$\begin{bmatrix} e \\ z \end{bmatrix} = \mathcal{F}_\ell(P, K) \begin{bmatrix} d \\ w \end{bmatrix} = T \begin{bmatrix} d \\ w \end{bmatrix} . \tag{4.3}$$

Index Conventions

We refer to subsystems of the nominal plant, the generalised plant, and the closed-loop system by using row and column indices for the elements of the transfer function matrices. However, in selecting a nominal plant $G_{(0)}$ for control design from the set of models that was derived in Chapter 2, the indices denote a particular operating condition, *i.e.* G_{33} is then the nominal model at 2000 RPM and a manifold pressure ratio of 0.5. Whether we are referring to an element of the set of models or an element of a transfer function matrix, will be clear from the context.

In the case of the closed-loop system, we also refer to certain transfer functions by selecting the corresponding input and output signals as indices, *e.g.* T_{ed} for the performance objective. A single index, finally, is to denote the design stage to which a system belongs.

4.1 Active EGR Control

Exhaust gas recirculation is an important feature in modern combustion engines in order to reduce the formation of nitrogen oxides in the combustion process. The requirements for the EGR system, primarily the desired rates of recirculation, are determined by experimental or theoretical analysis of the combustion process under steady-state conditions. While the steady-state requirements are clear-cut, that is to say that the exhaust gas should constitute a certain fraction of the cylinder charge depending on the operating condition, it is not so clear what the optimal requirements are under transient conditions.

In a multi-variable control framework, however, the EGR system can potentially also be used for transient air-fuel ratio control. Proper use of an electronic EGR valve would not only allow the desired EGR rates to be tracked, but could also assist in rejecting air mass flow disturbances in conjunction with the other actuators. For that purpose, we consider the following control configuration:

$$\begin{bmatrix} \lambda_{cyl} \\ \hline \dot{m}_{A\,\mathrm{TH}} \\ \hline \dot{m}_{\mathrm{EGR}} \\ \hline p_M \\ \lambda_{exh} \end{bmatrix} = \left[\begin{array}{c:c:cc} G_{11} & G_{12} & G_{13} & G_{14} \\ \hdashline 1 & 0 & 0 & 0 \\ \hdashline 0 & G_{32} & 0 & 0 \\ \hdashline G_{41} & G_{42} & G_{43} & 0 \\ G_{51} & G_{52} & G_{53} & G_{54} \end{array}\right] \begin{bmatrix} \dot{m}_{A\,\mathrm{TH}} \\ \hline i_{\mathrm{EGR}} \\ \hline i_{\mathrm{ABV}} \\ t_{inj} \end{bmatrix}. \tag{4.4}$$

It is slightly different to the configuration that was derived in Chapter 2, yet the model structure is the same, *cf.* Equation (2.47) on page 40. An additional actuator is available for EGR control, so the original input disturbance $\dot{m}_{\mathrm{EGR}}$ is replaced by the control input i_{EGR}. The dynamics of the actuator appear in the transfer function G_{32}.

Moreover, instead of perturbations to the position of the throttle plate, perturbations to the air mass flow into the intake manifold are considered as the primary input disturbance. The coupling of the EGR system with the air and fuel systems is represented by the elements $G_{\bullet 2}$ in the second column of the transfer function matrix. Note that the matrix is essentially lower triangular.

Input-Output Scaling

In order to normalise the transfer characteristics of the plant, the input and output channels are scaled with the factors from Table 4.1. The mass flows are effectively scaled from units in kg/s to g/s. Inputs to the air by-pass and EGR valves of size 0.25, on a normalised scale from zero to one, in this way correspond to a fuel injection time of 1 ms. The target for peak excursions of the air-fuel ratio is 5%.

	Signal						
	$\dot{m}_{A\,\mathrm{TH}}$	i_{EGR}	i_{ABV}	t_{inj}	$\dot{m}_{\mathrm{EGR}}$	p_M	λ
Unit	[kg/s]	[-]	[-]	[ms]	[kg/s]	[-]	[-]
Factor	5×10^{-3}	0.25	0.25	1	$1/10^{-3}$	1/0.1	1/0.05

Table 4.1: Input-Output Scale Factors[8]

The results that are presented in this chapter are all based on the scaled plant G. For the different designs, it is augmented with weighting functions to construct the generalised plant P, and the plants G_i, $i = 1, 2, 3$, respectively.

4.1.1 EGR Loop-Shaping Design

The EGR system is single-input-single-output and very simple as such. It consists of the first order valve dynamics and a nominal gain from the valve position to the EGR mass flow.[9] For the purpose of control design, the EGR system is therefore treated

[8]The scale factors are all multiplicative factors, both at the input and the output of the plant.

[9]The nonlinear flow characteristics were linearised by means of static inversion, see Appendix A, yielding a fairly constant gain across the operating envelope.

separately, in a modular approach, as to exploit the particular structure of the plant.

If suitable tracking properties for the EGR mass flow into the intake manifold can be ensured, the EGR controller will automatically serve the purpose of disturbance rejection for air-fuel ratio control, as perturbations to the mass flows of air and EGR affect the air-fuel ratio in the same way.

In principle, the control problem could be formulated to account for the minimisation of air-fuel ratio deviations in the presence of EGR explicitly, but the loop-shaping design is much simpler and equally effective. According to the set-up for multi-variable control design in Figure 4.1 on page 59, the EGR controller is calculated as follows. First, the generalised plant P is constructed by augmenting the nominal plant

$$\begin{bmatrix} e \\ y_3 \\ y_1 \\ y_2 \end{bmatrix} = G \begin{bmatrix} d \\ u_1 \\ u_2 \end{bmatrix} , \tag{4.5}$$

with several weighting functions that are discussed in the sequel. Then, certain elements of the weighted plant are extracted, which constitute the problem formulation for the control design of the subsystems, in the case of the EGR system:

$$y_1 = G_1 u_1 = P_{98} u_1 . \tag{4.6}$$

The output vector in Equation (4.5) on this page is partitioned according to the three stages of the control design, not to distinguish measurements for feedforward from measurements for feedback as in Figure 4.1. The state-space dimensions of the systems that are involved in the design process are summarised in Table 4.5 on page 74.

Weighting Function

The first element of the diagonal post-compensator W_2 is

$$\frac{5 \times 10^{-2}}{s + 3 \times 10^{-3}} \left(\frac{s}{7.5 \times 10^{-2}} + 1 \right) , \tag{4.7}$$

resulting in the loop shape in Figure 4.2 on the facing page. The loop gain is high but finite at low frequencies, because the pole at the origin was perturbed slightly giving a steady-state error of 6%. The location of the zero was adjusted to set the closed-loop bandwidth to 0.2 rad/s, which corresponds to a response time on the order of 20 events (Cf. Appendix C).

Robust Stabilisation

The controller synthesis based on a coprime factorisation of G_1 yields practically a unity feedback controller:

$$K_1 = -1 , \tag{4.8}$$

which is obvious from Figure 4.2. The achieved stability margin is more than sufficient ($\varepsilon = 0.76$) and only marginally lower for unity feedback ($\hat{\varepsilon} = b(G_1, K_1) = 0.71$).

Even though this is a good indication that the desired robustness and performance properties have been achieved, it is based on the assumption that the actuator nonlinearities are fully compensated. This assumption, however, turns out to be very critical, *cf.* Chapter 5. The EGR control loop is closed before the second design stage, *i.e.* the controller K_1 is absorbed into the generalised plant P.

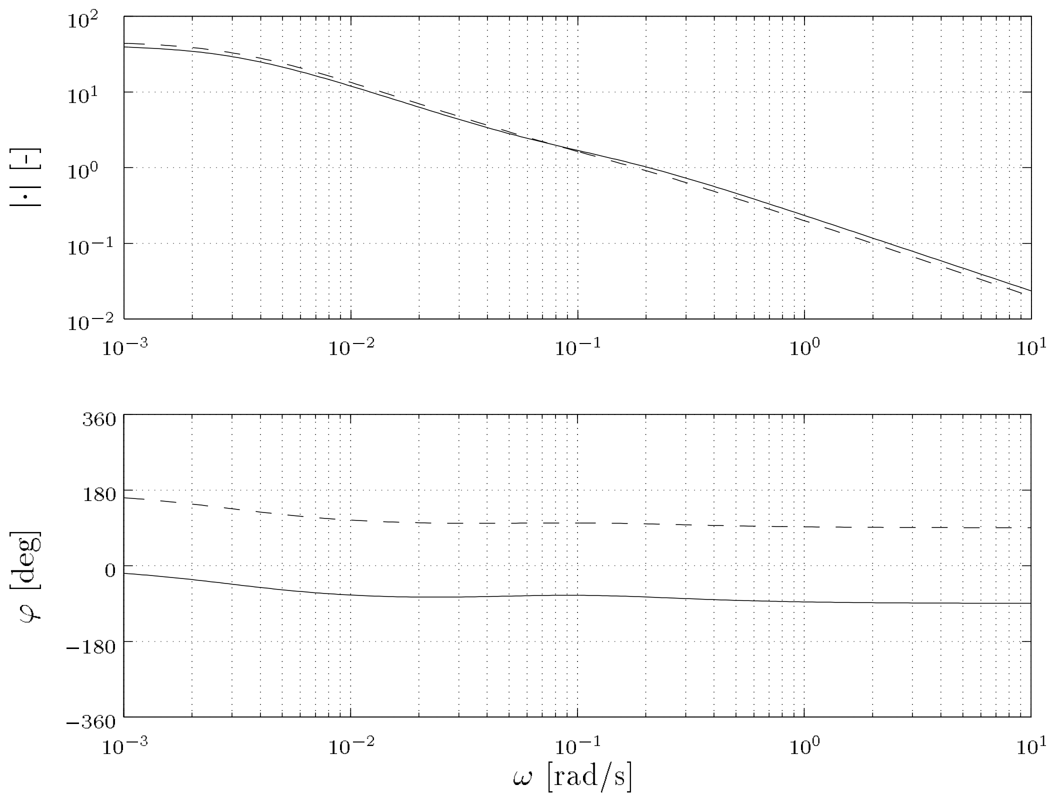

Figure 4.2: Loop Shape G_1K_1
Key: —— is G_1, – - is G_1K_1

4.1.2 AFR Loop-Shaping Design

In multi-variable control applications, it is often useful to break down the control problem into several smaller problems. Simple and modular controllers are often more desirable in practice than large and highly interconnected control schemes. In fact, simplicity and modularity are important design criteria to facilitate a transparent implementation, on- and off-line tests of the control algorithm as well as control system integrity and re-configureability.

Moreover, the trade-off between stability and performance becomes easier and the choice of the weighting functions more intuitive, the potential loop-holes of complicated problem formulations are avoided, and the design problem is generally more tractable.

Controller Structure

Based on practical considerations, we have thus far treated the EGR system separately and now divide the control problem further into feedback and feedforward control:

$$\begin{bmatrix} i_{\text{EGR}} \\ \hdashline i_{\text{ABV}} \\ t_{inj} \end{bmatrix} = \left[\begin{array}{c:c:c} 0 & K_1 & 0 \\ \hdashline K_3 & 0 & K_2 \end{array}\right] \begin{bmatrix} \dot{m}_{A\,\text{TH}} \\ \hdashline \dot{m}_{\text{EGR}} \\ \hdashline p_M \\ \lambda_{exh} \end{bmatrix}. \tag{4.9}$$

In the present control configuration, in which the input disturbance to the air system is measured directly, the separation into feedback and feedforward variables is fairly obvious. While the measurement of the air mass flow past the throttle is used as a feedforward variable, the measurements of the manifold pressure and the air-fuel ratio in the exhaust system are used for feedback. Alternatively, the manifold pressure signal could also be used in the feedforward part of the control scheme, since it is essentially only a filtered version of the input signal. Indeed, this approach turns out to be more appropriate and is adopted in Section 4.2.

The feedback controller should ensure a stable engine operation over a wide range of operating conditions as well as a zero steady-state error in the air-fuel ratio. These requirements are readily incorporated in a loop-shaping design for the weighted plant

$$y_2 = G_2 u_2 = \begin{bmatrix} P_{10\,9} & 0 \\ P_{11\,10} & P_{11\,10} \end{bmatrix} u_2 \tag{4.10}$$

that maximises the robust stability radius with respect to coprime factor uncertainty on one hand and achieves a suitably modified loop shape on the other hand.

Weighting Functions

The corresponding lower blocks of the pre- and post-compensators are given by:

$$W_{1\,22} = \begin{bmatrix} \frac{s}{s+10^{-2}} & 0 \\ 0 & 1 \end{bmatrix}, \qquad W_{2\,22} = \begin{bmatrix} 1 & 0 \\ 0 & \frac{2\times10^{-2}}{s}\left(\frac{s}{0.2}+1\right) \end{bmatrix}. \tag{4.11}$$

The post-compensator introduces integral action on the air-fuel ratio signal to ensure a zero steady-state error and sets the cross-over frequency to 0.2 rad/s. For the actuator setting of the air by-pass valve to return to its open-loop base value in steady state, the pre-compensator fades out the control effort at low frequencies.

Furthermore, for the choice of scale factors in Table 4.1 on page 61 and the weighting functions in Equation (4.11) on this page, the first singular value is dominant in the loop shape in Figure 4.3 on the next page. The second singular value is less than one for all frequencies and as such does not affect the transfer characteristics of the controller. While the measurement of the pressure in the intake manifold is valuable for feedforward, there is actually no requirement to control the pressure in steady state or during transients.

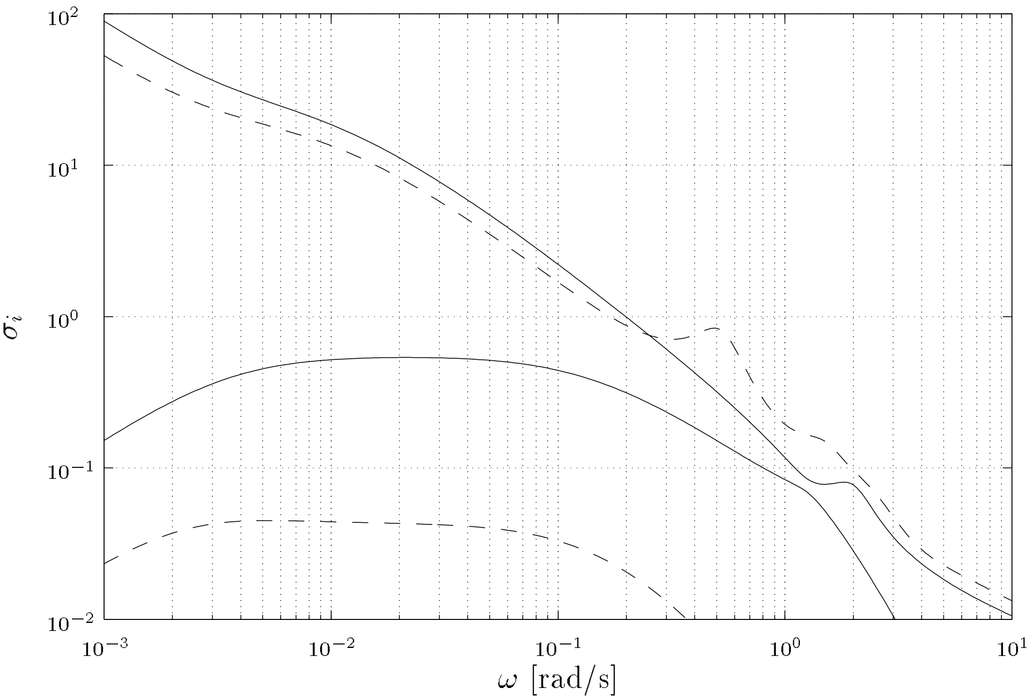

Figure 4.3: Loop Shape G_2K_2
Key: — is G_2, - - is G_2K_2

Robust Stabilisation

Both compensators have another important interpretation in the design process. Not only do they serve as the design parameters to specify the performance of the control system, but they are also selected on the basis of gap metric calculations to ensure sufficient robustness to model uncertainty. In their selection, the classical guidelines for loop shaping apply as much as the consideration to maximise the region of robust stability over the operating envelope.

As a result, all models in other operating points in Table 4.2 on page 67 are stabilised by the loop-shaping controller with a stability margin of $\varepsilon = 0.42$ for G_0 that are less than ε away from the nominal model. Possibly, this is also true for their linear combinations, provided the variations are smooth in the gap metric.

Even for the weighted plant, the plant characteristics change significantly over the operating envelope. For example, the model G_{51}, at 3500 RPM and a manifold pressure ratio of 0.2, which could be considered to be characteristic of a tip-out scenario, is as far away as $\delta_\nu(G_0, G_{51}) = 0.72$ and is not stabilised by the controller K_2. In any case, it is not realistic to stabilise the engine over the entire operating envelope with a single linear time-invariant controller. However, on the basis of the values in Table 4.2, stability can be guaranteed for quite a large neighbourhood of operating conditions.

Controller Order Reduction

To be consistent with the design procedure and the analysis in the gap metric, the controller order reduction is based on a coprime factorisation of the controller.

The optimal controller is reduced to eight states via balanced truncation:

$$K_2 = \hat{K}_\infty^8 \,. \tag{4.12}$$

In achieving the necessary simplification, it is important to retain the closed-loop properties as much as possible. Therefore the quality of the controller approximation in terms of the approximation error bounds is not as important as the deterioration of the loop shape in terms of the stability margin. In this measure, the reduced order controller is almost the same as the full order controller ($\hat{\varepsilon} = 0.41$). The frequency response of the reduced order controller, which is virtually overlaying the frequency response of the full order controller, is shown in Figure 4.4.

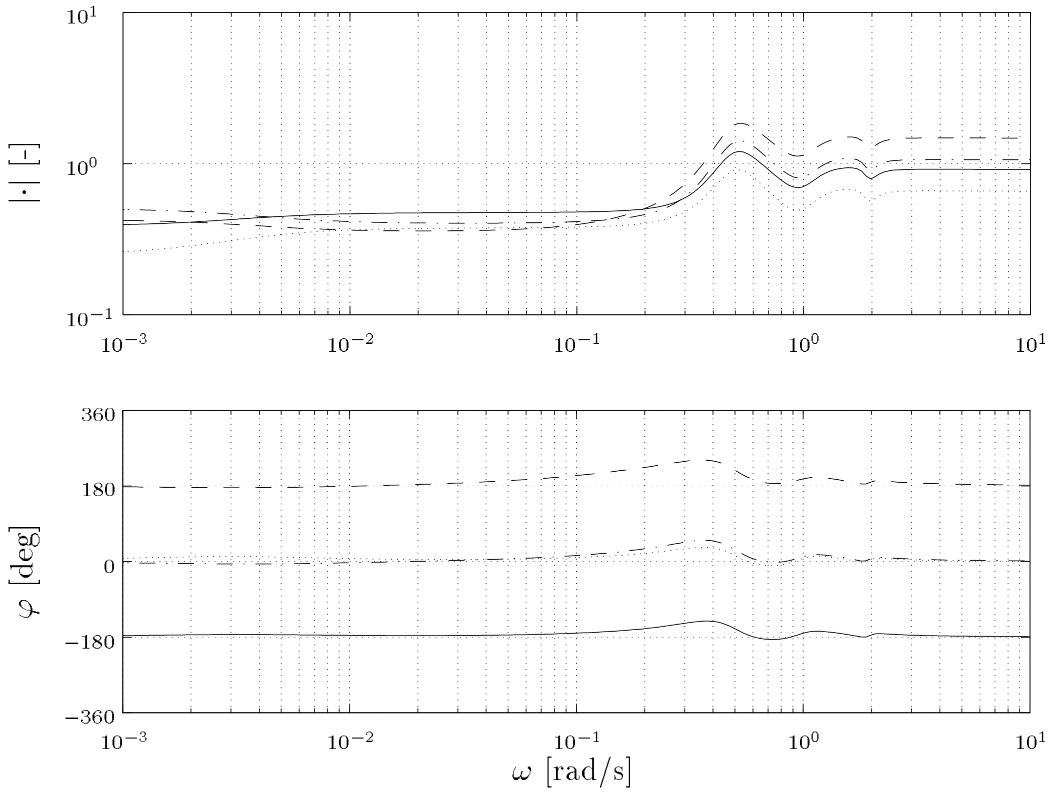

Figure 4.4: Frequency Response of Controller K_2
Key: —— is K_{11}, – - is K_{12}, ······ is K_{21}, · – is K_{22}

The effect of the pre-compensator is visible in the element K_{21}. Note that the resonant peaks, which are characteristic of the multiplexed dynamics of the fuel injection system, appear in the response due to the high bandwidth requirements. The shape of the phase of the controller is completely determined by the controller synthesis for the robust stabilisation problem.

Gap Metric Calculations

Because of the strong relationship between the generalised stability margin and the gap metric, we do not only use the stability margin as a design indicator, but also carry out a complementary analysis of the stability properties of the closed-loop system in the gap metric. As we are not only considering engine operation in a single operating point but over a wide range of operating conditions, we are particularly interested in predictions, how the closed-loop system should behave away from its nominal operating conditions, *i.e.* away from the design point.

	p_R [-]				
N [RPM]	0.20	0.35	0.50	0.65	0.80
870	0.61	0.49	0.51	0.47	0.47
1250	0.59	0.36	0.33	0.34	0.37
2000	0.61	0.23	0.00	0.16	0.25
2750	0.68	0.38	0.27	0.32	0.35
3500	0.72	0.49	0.43	0.44	0.44

Table 4.2: Distances in the Gap Metric $\delta_\nu(G_0, G_{ij})$

First of all, robust stability can be guaranteed on the basis of the values in Table 4.2 over a region where

$$\delta_\nu(G_0, G_{ij}) < \varepsilon \,, \tag{4.13}$$

as was discussed earlier. Although quite large perturbations to the nominal operating conditions are tolerated, it is not possible to stabilise the engine over its entire operating envelope with this linear time-invariant controller that is optimised at a central operating point. The region of robust stability could be extended to cover the entire operating envelope by combining several controllers that were designed at different operating points via gain scheduling, or by applying another form of parameter-dependent control. Such controllers were calculated by repeating the design over the set of operating points, *cf.* Section 4.1.6.

If it is a realistic objective to stabilise the chosen set of models, the average distances between the models[10] are an indication of the requirements for stability. From the numbers in Table 4.3 on the next page, it is evident that a single robust controller, even with a reasonable stability margin, is not sufficient for the task. Note that the models are more similar towards higher engine speed and higher manifold pressure than they are at low speed and low manifold pressure. These trends are quite consistent with the physical intuition that the models at lower speed and lower pressure are more difficult to stabilise due to larger time delays.

With a suitable choice of weighting functions the models could be made more similar but only to a limited extent without sacrificing the performance of the control system. For further alignment the weighting functions could be varied, as the models vary over the operating envelope, yet this would be less insightful for the analysis of a single design.

[10]For all gap metric calculations, the models are augmented with the pre- and post-compensators, and the gap is calculated for the square subsystem corresponding to the plant G_2. In this sense the notation that is used in the captions of the tables is only symbolic.

	p_R [-]				
N [RPM]	0.20	0.35	0.50	0.65	0.80
870	0.45	0.44	0.32	0.21	0.20
1250	0.45	0.41	0.30	0.26	0.24
2000	0.40	0.38	0.30	0.25	0.24
2750	0.33	0.29	0.23	0.20	0.17
3500	0.30	0.24	0.18	0.17	0.13

Table 4.3: Average Distances between Models
$\bar{\delta}_\nu(G_{ij}, G_{kl})$, $i-1 \leq k \leq i+1$, $j-1 \leq l \leq j+1$

The robustness of the design must be balanced with the desired performance. Clearly, the further away the engine is operated from the conditions that the controller was designed for, the worse the performance will be. Table 4.4 shows the performance degradation in terms of the stability margin, now used as a performance index.

	p_R [-]				
N [RPM]	0.20	0.35	0.50	0.65	0.80
870	0.09	0.21	0.25	0.27	0.30
1250	0.11	0.28	0.36	0.32	0.00
2000	0.10	0.28	0.41	0.36	0.36
2750	0.08	0.26	0.36	0.36	0.32
3500	0.10	0.28	0.34	0.35	0.33

Table 4.4: Stability Margin $b(G_{ij}, K)$

The control system is only marginally stable at a manifold pressure ratio of 0.2, so that the performance will not be satisfactory under this condition. The same trends that were observed in Table 4.3 are apparent in the data here. The performance of the control system should be a lot better towards higher engine speed and higher load than during idle operation and perhaps only slightly worse than in the nominal operating point.[11] Before continuing with the third design stage, the feedback control loop is closed by absorbing the controller K_2 into the generalised plant.

4.1.3 Feedforward Control Design

The limiting factors in feedback control design for transient air-fuel ratio control are the time delay in the exhaust system, because of the distant location of the UEGO sensor from the engine, and the time delay in the fuel injection system, due to the particular

[11] In conjunction with the model G_{25} the stability margin is zero, indicating an instability; however, this is not realistic, as this particular model is numerically ill-conditioned due to some irregularity in the model data.

engine operation. The delay in the air-fuel ratio feedback loop is on the order of ten events, depending on the operating condition, and as such a fundamental limitation to the response time of the closed-loop system. Similarly, the closed-loop gain from the manifold pressure to the fuel injection time is limited by several additional units of delay in the timing of the fuel injection. It is only possible to overcome these constraints of the system's response with feedforward action, which is relying on faster measurements and intervening earlier in the process to counteract the disturbances.

In the present control configuration, the disturbance to the air mass flow into the intake manifold is measured directly. There is also the possibility to modulate the air flow past the throttle by means of the air by-pass valve, which, even though designed for idle speed control, has significant authority for the most part of the operating envelope. For such a control effort, however, to have the desired effect, it must be precisely adjusted with the fuel injection. While quite a large amount of uncertainty can be tolerated in the feedback part of the model, high fidelity in the feedforward part is essential for precise air-fuel ratio control during transients. To what extent the achievable performance is limited by the inaccuracies of the model is indicated as part of the second control design in Section 4.2.7.

Nominal Performance

The division in feedback and feedforward control implies a division of the control objectives in robust stability and nominal performance. This division is motivated primarily by practical considerations in the attempt to account for the particular nature of the control problem.

The notion of robustness is genuinely based on a feedback configuration. Since the desired transient performance can only be achieved in the present case by means of feedforward control on the basis of a measurement of the input disturbance, robust performance is not a reasonable design objective for the design of the feedforward controller. Nevertheless, robust performance can certainly be assessed for the overall system. Consequently, we assume in the design of the feedforward controller for nominal performance that closed-loop stability and the robustness of stability are guaranteed by the feedback controller.

The feedforward control design is set up as an S/KS problem, involving a penalty on the sensitivity function T_{ed} as well as a penalty on the control effort, so that the problem is well-posed. In the pertaining subsystem of the generalised plant

$$\begin{bmatrix} e \\ z_1 \\ y_3 \end{bmatrix} = G_3 \begin{bmatrix} d \\ u \end{bmatrix} \tag{4.14}$$

the total control effort is penalised, *i.e.* the sum of the feedforward and feedback control activity.

Weighting Functions

In addition to the weighting functions in the feedback loop, the plant is further augmented in the performance and disturbance channels with

$$W_p = \frac{s+1}{s+0.1}, \qquad W_d = 1 \tag{4.15}$$

to specify the shape of the sensitivity function from the air mass flow disturbances to the air-fuel ratio in the cylinder. Information about the nature of the disturbance signals, *e.g.* their frequency contents, could be represented in the weighting function W_d but is not available. The low-pass filter W_p emphasises the disturbance rejection at frequencies below 0.1 rad/s roughly ten times higher than at frequencies above 1 rad/s. The frequency response of the closed-loop transfer function

$$\lambda_{cyl} = \begin{bmatrix} T_{11} & T_{12} \end{bmatrix} \begin{bmatrix} \dot{m}_{A\,\mathrm{TH}} \\ w_1 \end{bmatrix} \tag{4.16}$$

in Figure 4.6 on page 72 and the norm calculations in Table 4.7 on page 76, however, show that this specification was too tough to achieve.[12] The magnitude of the element T_{11} is greater than one for a range of frequencies above 1 rad/s and still greater than 0.1 for frequencies above 0.001 rad/s.[13]

Controller Order Reduction

There is no underlying structure to the S/KS problem, like a coprime factorisation of the plant, that would allow for an explicit solution, as in the case of the loop-shaping design. It is a standard $\mathcal{H}_\infty$ problem and solved in a γ iteration. Therefore the resulting controller exhibits no particular structure that could be exploited in the process of order reduction; yet, because of the desired feedforward properties, it exhibits several very fast and very slow modes.

For numerical conditioning, these modes are removed by decomposing the controller into an unstable and a stable part, sequentially on the left and right edges of the spectrum. In doing so, the DC gain of the controller is recovered with an extra feedthrough term. Finally, the controller is truncated further to four states in a balanced state-space form:

$$K_3 = \hat{K}_\infty^4 \,. \tag{4.17}$$

A suitable choice of the order of the approximation is not so much determined by the open-loop bounds of the approximation error or mismatches in the frequency response of the controller, see Figure 4.5 on the next page, than by the deterioration of the closed-loop norm that characterises the performance objective.

---

[12] The first component of w_1 in Figure 4.1 on page 59 is also considered for better comparison with the second control design.

[13] While the performance weight is included in the plant for controller synthesis, it is not included in the calculation of the frequency response or the norm calculations for better comparison with the second control design.

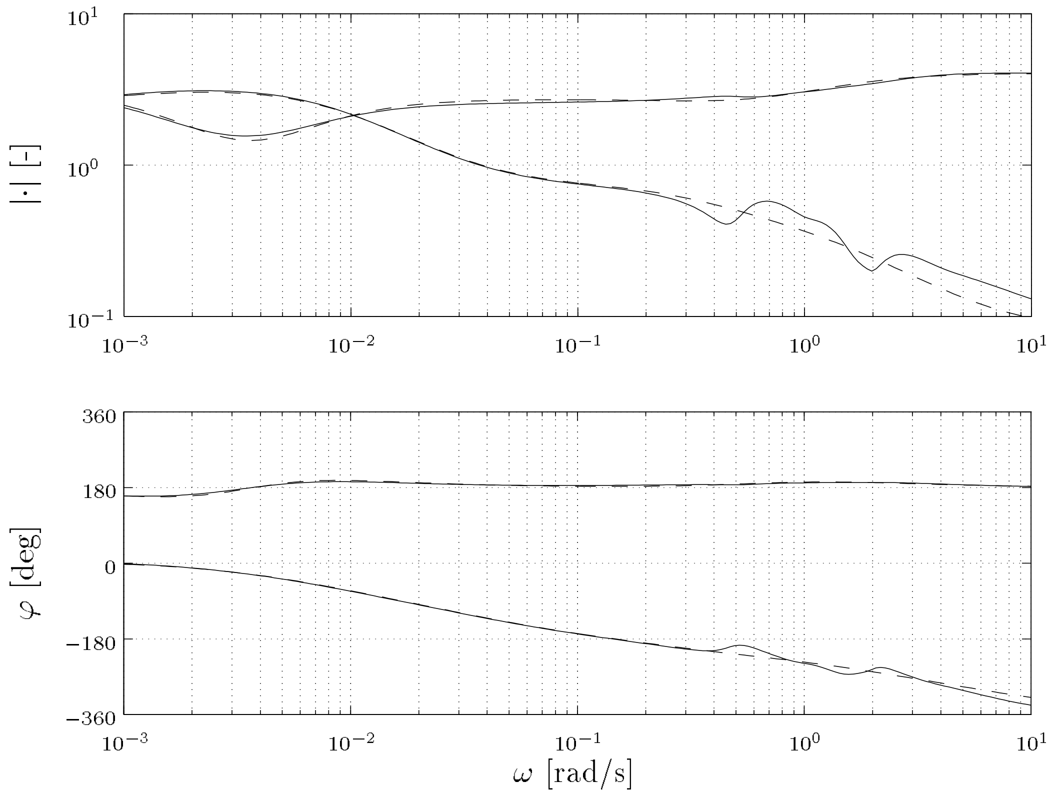

Figure 4.5: Frequency Response of Controller K_3
Key: —— is K_∞, – - is K_3

In Figure 4.5 the gain of the controller in the ABV channel is greater than one for all frequencies, the phase is shifted by 180 deg, as necessary. It would seem that the controller is overly active, as becomes obvious in linear simulations. The frequency responses of the sensitivity function and the actuator demand

$$\begin{bmatrix} i_{\mathrm{ABV}} \\ t_{inj} \end{bmatrix} = \begin{bmatrix} T_{31} & T_{32} \\ T_{41} & T_{42} \end{bmatrix} \begin{bmatrix} \dot{m}_{A\,\mathrm{TH}} \\ w_1 \end{bmatrix} \tag{4.18}$$

that were jointly minimised are shown in Figure 4.6 and Figure 4.7 on the next page.[14] If the system is excited in the frequency band where the sensitivity is greater than one, the peak excursion in the air-fuel ratio will be greater than 5% and in the worst case slightly greater than 10% ($\|T_{ed}\|_\infty = 2.16$). The actuator demand is dominated by the feedforward term.

[14]The first component of w_1 can be considered to act approximately like an EGR mass flow disturbance in comparison with the configuration of the second control design.

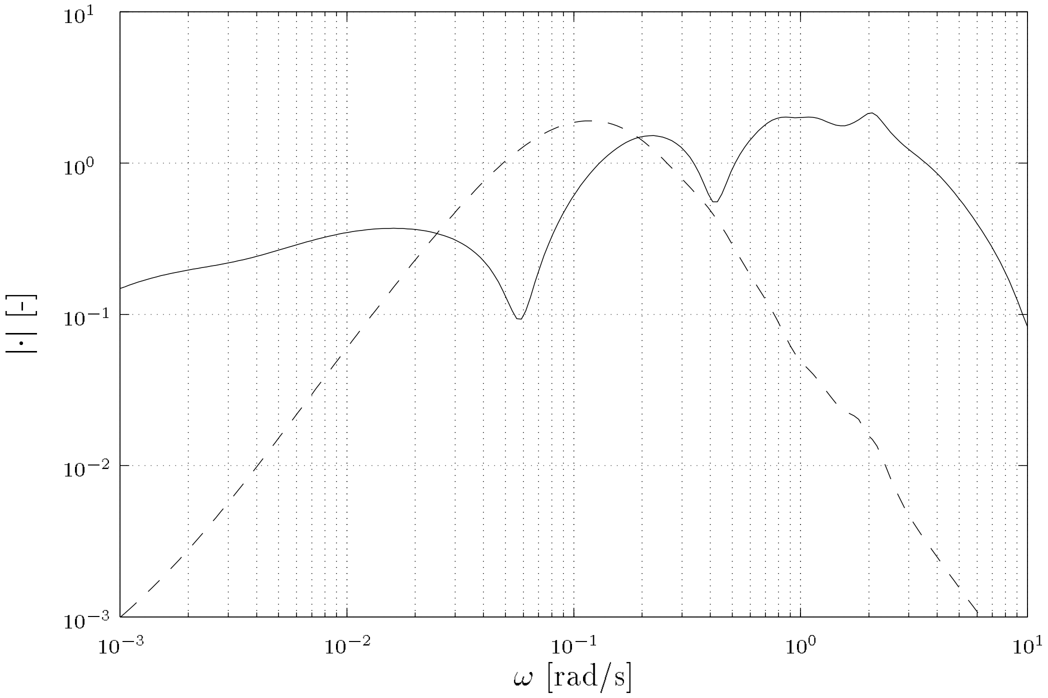

Figure 4.6: Sensitivity T_{ed}
Key: —— is T_{11}, – - is T_{12}

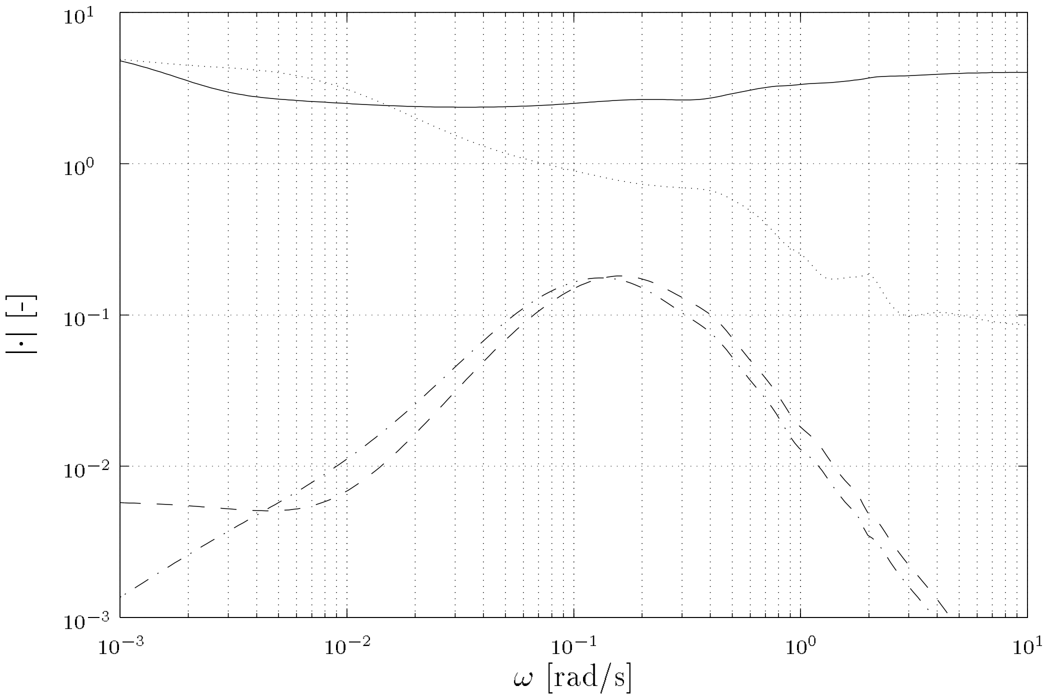

Figure 4.7: Actuator Demand $T_{z_1 d}$
Key: —— is T_{31}, – - is T_{32}, ······ is T_{41}, · – is T_{42}

4.1.4 Linear Simulation

The controller is tested in linear simulation before the implementation on the engine, to assess the performance that can be expected. The assessment is simply based on the response of the nominal closed-loop system to a unit step at the disturbance input, because the validation of a hybrid, nonlinear model is not yet complete. It would also be too difficult to keep the parameter trajectories and the system trajectories consistent in a linear parameter-dependent set-up in more complex driving scenarios. As the linear models are only local approximations, the assessment applies only locally in a neighbourhood of the nominal model. Nevertheless, linear simulations give a good insight into the principal interactions between the plant and the controller.

The generalised plant is re-constructed for simulation in a way that the internal signals z and w in the closed loop are unweighted. The weighting functions are re-arranged in the loop and combined with the controller. According to Table 4.1 on page 61, a unit step in the disturbance corresponds to a change of the air mass flow past the throttle of 5 g/s. Similarly, a unit on the vertical axis in Figure 4.8 corresponds to an excursion of 5% in the air-fuel ratio. The other signals are scaled in the same way. The disturbance reaches its final value in ten sample steps at a rate which should be representative of the fastest throttle transients.

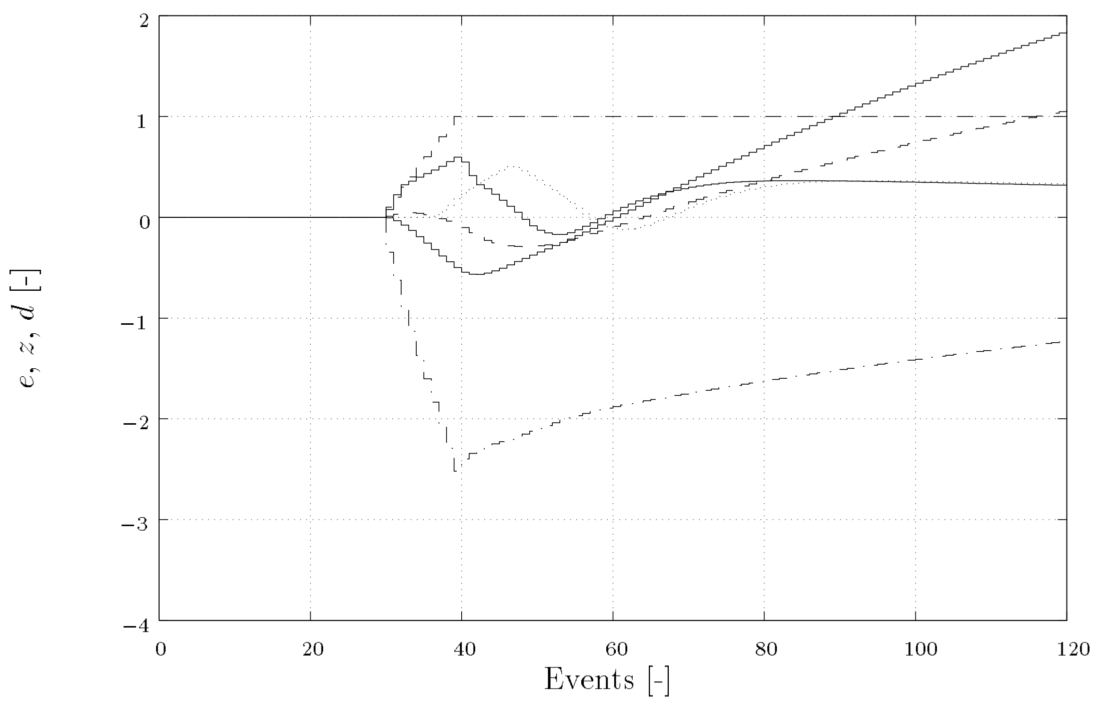

Figure 4.8: Closed-Loop Time Response
Key: —— is λ_{cyl}, – - is p_M, ······ is λ_{exh}, · – is i_{ABV}, —— is t_{inj}, – - is $\dot{m}_{A\,\mathrm{TH}}$

Two phases can be distinguished in the transient signals in Figure 4.8. During the initial phase the controller rejects the disturbance as much as possible using an increasingly large amount of the authority of the air by-pass valve. There is so much control activity that the manifold pressure is hardly increasing. The air-fuel ratio stays within a band of only 2.5% around the stoichiometric value, because the fuel injection time is decreased suitably in advance of the onsetting pressure drop that is brought about by the shutting air by-pass valve. In the second phase, from sample instance 40 onwards, the system recovers from the disturbance. It takes too long to reach a new equilibrium point, yet the disturbance is rejected effectively. Principally, the feedforward action exhibits the necessary features, but the overreaction of the controller prolongs the recovery phase unreasonably. It would be more appropriate, if the response of the controller to the step disturbance was more impulsive in the ABV channel.

4.1.5 Design Summary

The systems that were involved in the design process are listed in Table 4.5. Simple, diagonal weighting functions were used in the specification of the control problem. Central to the control design was the generalised plant P, serving as a starting point for the designs of the subsystems and their subsequent analysis.

		Dimensions		
System	Symbol	n_x	n_y	n_u
Nominal Plant	G	19	5	4
Pre-Compensator	W_1	1	3	3
Post-Compensator	W_2	2	3	3
Disturbance Weight	W_d	0	1	1
Performance Weight	W_p	1	1	1
Generalised Plant	P	23	11	10
Loop-Shaping Design	G_1	8	1	1
EGR Controller	K_1	0	1	1
Loop-Shaping Design	G_2	19	2	2
Feedback Controller	K_2	8	2	2
S/KS Design	G_3	29	4	3
Feedforward Controller	K_3	4	2	1
Closed Loop	T	34	7	7

Table 4.5: State-space Dimensions of Systems involved in the Design Process

After closing the control loops sequentially, the closed-loop system T was analysed by means of norm calculations and in simulation. The controllers of the individual subsystems can be arranged in a compound system, as in Equation (4.19), that fits in the generic feedback configuration in Figure 3.1 on page 45:

$$\left[\begin{array}{c} i_{\mathrm{EGR}} \\ \hdashline i_{\mathrm{ABV}} \\ t_{inj} \end{array}\right] = \left[\begin{array}{c:c:c} 0 & K_1 & 0 \\ \hdashline K_3 & 0 & K_2 \end{array}\right] \left[\begin{array}{c} \dot{m}_{A\,\mathrm{TH}} \\ \hdashline \dot{m}_{\mathrm{EGR}} \\ \hdashline p_M \\ \lambda_{exh} \end{array}\right]. \tag{4.19}$$

There is a slight ambiguity in the notation, because the vectors contain physical signals, while the elements K_i were defined for the weighted plants G_i. Yet, it is easy to imagine that, for the purpose of implementation, the weighting functions could be absorbed in the controller. The total number of states in the control system is fifteen. The implementational issues and the experimental results are discussed in the next chapter.

4.1.6 Design over a Set of Operating Points

The potential for gain scheduling was investigated in order to extend the functionality of the control scheme over the operating envelope, by repeating the design over a set of operating points. For simplicity, the same weighting functions were chosen for all operating conditions, and the controllers K_i, $i = 1, 2, 3$, were re-designed in each operating point to be of the same state-space dimensions. If the different controllers are conditioned appropriately, it is quite feasible to interpolate them, as described in Appendix D.1, depending on the operating condition.

	p_R [-]				
N [RPM]	0.20	0.35	0.50	0.65	0.80
870	0.28	0.35	0.41	0.46	0.48
1250	0.27	0.36	0.41	0.46	0.00
2000	0.24	0.35	0.41	0.47	0.50
2750	0.25	0.34	0.41	0.48	0.51
3500	0.28	0.38	0.44	0.48	0.52

Table 4.6: Stability Margin $1/\left\|T_{zw}\right\|_\infty$

The resulting behaviour of the control system is characterised in terms of the closed-loop norms in Table 4.6 and Table 4.7 on the next page.[15] Even though the approach to evaluate the stability and the performance of a gain-scheduled control scheme in fixed operating points is simplistic, it is naturally the next step before extensive simulation studies. Although the reserve in the stability margin is perhaps slightly too small at low and slightly too large at high manifold pressure, the stability properties are

[15]The notation in the captions of the tables is slightly abused, in that the transfer function T_{ed} also includes the channel from the first component of w_1 to the error e. Furthermore, the components of the signals z and w pertaining to the EGR feedback control loop are excluded from the transfer function T_{zw} to be consistent with other norm calculations.

altogether quite sufficient, according to Table 4.6 on the preceding page.[16] How the stability margin would deteriorate due to time-varying perturbations, as the operating conditions change, cannot be inferred from the values in the table, but, if the plant and controller data are smooth, the control system should behave well.

	p_R [-]				
N [RPM]	0.20	0.35	0.50	0.65	0.80
870	27.02	11.05	9.23	7.73	5.89
1250	13.34	7.58	5.79	4.60	0.00
2000	18.67	4.86	2.16	2.22	2.82
2750	27.51	3.00	3.44	3.18	2.96
3500	4.58	5.08	4.16	3.72	3.33

Table 4.7: Closed-Loop Norm $\|T_{ed}\|_\infty$

From Table 4.7, however, it must be concluded that the overall performance will not be satisfactory, especially not at low pressure. The performance index in the nominal operating point is not very indicative of the performance that is achievable in other operating points. Because of the significant differences in the model data over the operating envelope, a single design specification on the basis of a nominal operating point is not sufficient.

A possible solution is to choose the weighting functions for each operating point individually in order to trade off stability versus performance more effectively. The interpolation scheme would be more complicated and computationally demanding, because the weighting functions as well as the controllers would be varying with the operating condition. In any case, the design must be improved, before it could be used for gain scheduling.

4.2 Modular Feedforward Design

This design evolved out of the design that was discussed in the previous section after practical experience with the controller on the engine. For better performance, more emphasis is placed on the feedforward side of the control problem. In fact, the modular approach to the design of the feedforward part of the control scheme accounts better for the nature of the control problem. The problem of transient control on top of the optimal settings for steady-state operation becomes a lot easier by adapting the base values for the actuator settings, primarily for the fuel injection, quickly to the driving situation.

[16]The zero entry in the second row and the fifth column of the tables should be disregarded, as before, due to an irregularity in the model data of G_{25}.

History of Changes

While both designs are in three stages and apply the same techniques, there are a number of differences with regard to the model, the control configuration, and the controller structure. After the first series of engine tests with the initial controller new experiments were conducted to re-identify the model parameters ζ and χ, which parameterise the dynamics in the fuel injection system. The identification results, however, were so different, that only the latest versions of the parameters are documented in Chapter 2, because they are thought to be more accurate. Since the data were so different in quality, the resulting differences in the dynamics of the model were not analysed further.

Moreover, the model of the fuel injection system was affected by a change in the engine interface in refining the real-time communication software. This had the advantage that the delay in the timing of the fuel injection between the actuator demand and its realisation on the fuel injectors was reduced from three to two sample events.

In the evaluation of the control system in practice, it became evident that the EGR control problem was ill-defined for the given hardware configuration. In particular, the nonlinear flow characteristics of the valve were so severe, that the system was uncontrollable. Therefore the development of an active EGR control system as part of the control scheme for air-fuel ratio control had to be discontinued. In the present control configuration

$$\left[\begin{array}{c} \lambda_{cyl} \\ \hdashline \alpha \\ \dot{m}_{\mathrm{EGR}} \\ p_M \\ \hdashline \lambda_{exh} \end{array}\right] = \left[\begin{array}{cc;{2pt/2pt}cc} G_{11} & G_{12} & G_{13} & G_{14} \\ \hdashline 1 & 0 & 0 & 0 \\ 0 & 1 & 0 & 0 \\ G_{41} & G_{42} & G_{43} & 0 \\ \hdashline G_{51} & G_{52} & G_{53} & G_{54} \end{array}\right] \left[\begin{array}{c} \alpha \\ \dot{m}_{\mathrm{EGR}} \\ \hdashline i_{\mathrm{ABV}} \\ t_{inj} \end{array}\right] \tag{4.20}$$

the active components are removed from the EGR system. It is assumed that the control of the exhaust gas recirculation is performed by a separate, unknown control system, whose actions interfere with the control scheme for air-fuel ratio control in the form of EGR mass flow disturbances into the intake manifold. Except for the measurement of the disturbance $\dot{m}_{\mathrm{EGR}}$ we do not require any more information about the operation of the EGR system in order to deal with its effects by means of disturbance rejection.

Finally, instead of perturbations to the air mass flow into the intake manifold, perturbations to the position of the throttle plate are considered as the primary input disturbance, to be able to include in the model the effect of the manifold pressure in the nonlinear flow equation in terms of the local gain.

Input-Output Scaling

The transfer characteristics of the plant are normalised by scaling the input and output channels with the factors from Table 4.8 on the following page, so that any cross-coupling between the channels is equally undesirable. In scaled coordinates a unit of the throttle plate angle corresponds to 4 deg, and the EGR mass flow is measured in kg/s. Since the actuator demand for the air by-pass valve was too high in the previous design, the gain in the ABV channel is reduced relative to the gain of the fuel injection time. Now, an input to the air by-pass valve of size 0.1, on a normalised scale from zero to one, corresponds to a fuel injection time of 2 ms. All results in this section are based on the plant G scaled according to Table 4.8. The generalised plant P and the plants G_i, $i = 2, 3$, respectively, are constructed by augmenting the nominal plant with weighting functions.

	Signal					
	α	$\dot{m}_{\mathrm{EGR}}$	i_{ABV}	t_{inj}	p_M	λ
Unit	[deg]	[kg/s]	[-]	[ms]	[-]	[-]
Factor	4	2×10^{-3}	0.1	2	1/0.1	1/0.05

Table 4.8: Input-Output Scale Factors

4.2.1 Phase Advance of Fuel Injection

The limiting factors for transient air-fuel ratio control are the delays in the system, which we discussed in Section 4.1.3. The delay in the measurement of the air-fuel ratio in the exhaust system limits the use of this measurement for feedback. If the model of the engine were perfect, optimal air-fuel ratio control could be achieved via feedforward alone, and the measurement in the exhaust system would be obsolete.

From the structure of the model it becomes clear that the target variable is not the air-fuel ratio in the exhaust system but the air-fuel ratio in the cylinder. Hence, the delay in the timing of the fuel injection is more critical to the mixture composition than the delay in the exhaust system. In the way the engine is operated the fuel injection is based on past measurements and lags behind the corresponding induction event. That is to say, an actuator demand can be affected only after approximately two events. Consequently, this effect must be accounted for in the calculation of the fuel injection time.

Physical Approach

Since we parameterise the air charge in the cylinder in terms of the pressure in the intake manifold and engine speed, the corresponding base value of the fuel injection time is tabulated over a set of operating points in terms of these variables, see Figure 4.9 on the facing page.

A high-pass filtered measurement of the manifold pressure is used in the calculation of the base value for the fuel injection time in order to introduce the necessary phase advance to compensate the delay between the air and the fuel system. In this way, the fuel injection time is linked to the manifold pressure through a feedforward term. Expressed formally in terms of the inputs and outputs of the plant

$$\begin{bmatrix} e \\ y_3 \\ y_2 \end{bmatrix} = G \begin{bmatrix} d \\ u \end{bmatrix}, \tag{4.21}$$

the third component of the vector of feedforward variables p_M is connected to the second component of the vector of control inputs t_{inj} via a feedforward controller K_1.[17] Note that the manifold pressure is not controllable with the fuel injection time ($G_{44} = 0$), so there is no feedback involved.

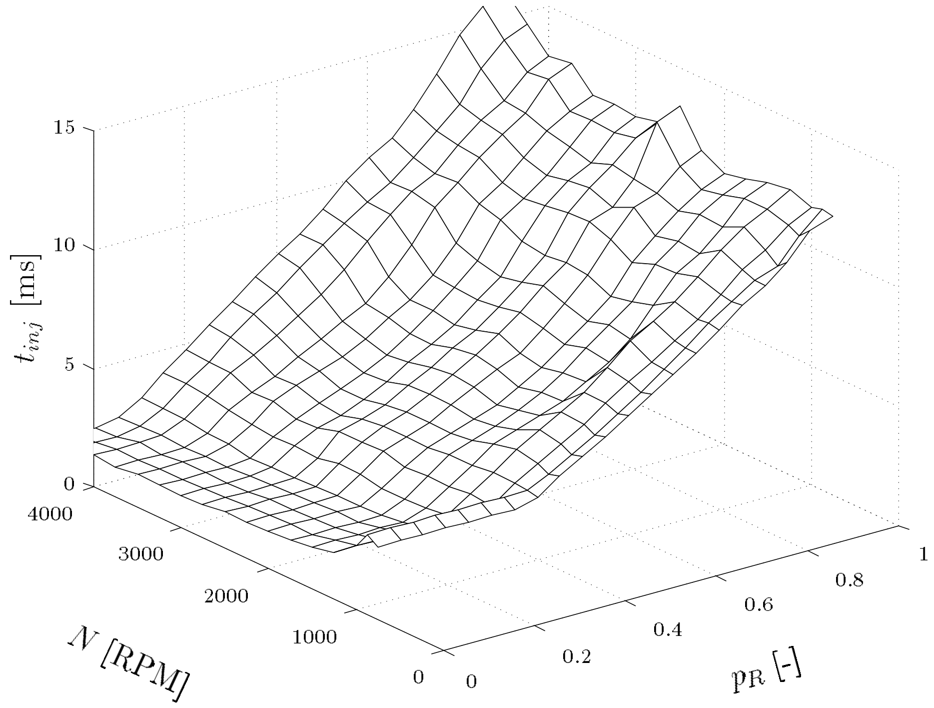

Figure 4.9: Base Fuel Injection Time

On-Line Tuning

A simple finite impulse response filter as a function of a single parameter was chosen to be tuned on-line in engine experiments:

$$K_1 = 1 + \gamma \left(1 - z^{-1}\right) , \qquad \gamma = 5 . \tag{4.22}$$

To compensate the two units of delay in the model, about 60 deg of phase advance are required. A value of 5 for the parameter γ was found to give the best results. The frequency response of the equivalent continuous-time system is shown in Figure 4.10 on the next page.

[17]The partitioning of the output vector in Equation (4.21) on the preceding page is to distinguish the measurements for feedforward from the measurements for feedback as in Figure 4.1 on page 59, only the index denotes the pertaining stage of the control design.

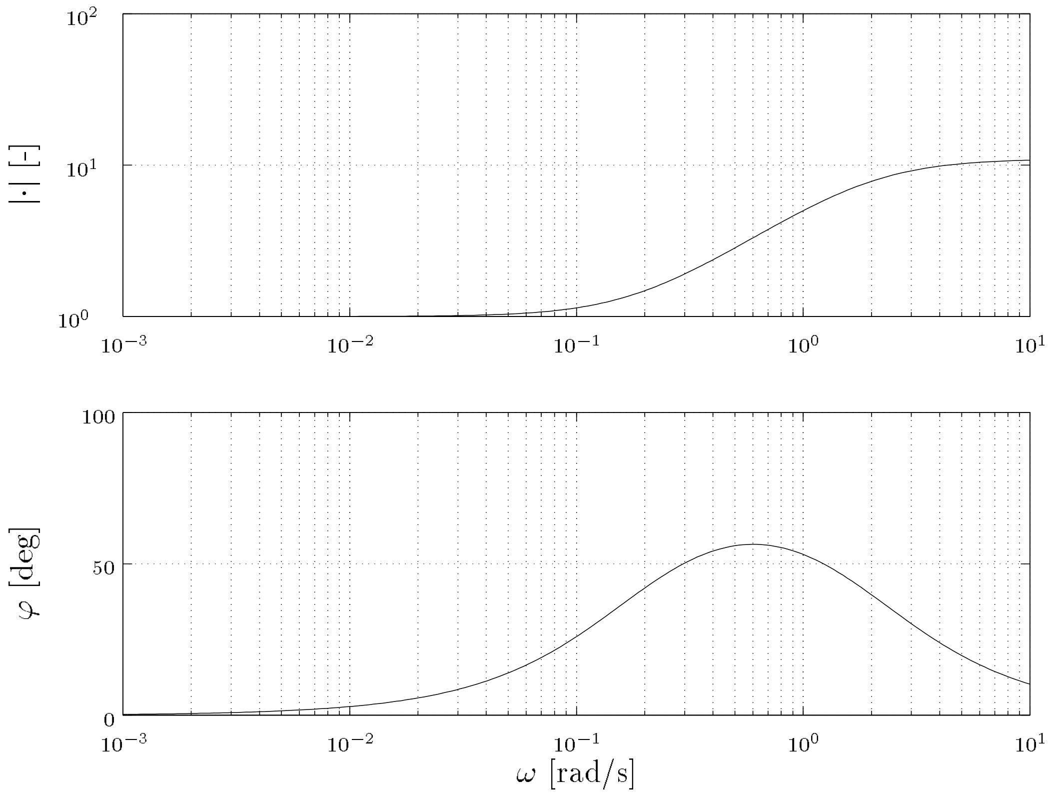

Figure 4.10: Frequency Response of Controller K_1

The phase advance is as expected, and the gain ten times larger at high frequencies than nominally. Therefore the noise in the pressure signal will be amplified to a certain extent but not critically for reasonable signal-to-noise ratios.

The controller K_1 is absorbed into the generalised plant P before the second design stage. The gradient of the data in Figure 4.9 on the preceding page with respect to pressure is obtained by numeric differentiation and included as part of the plant. For a summary of the systems that are involved in the design process see Table 4.12 on page 91.

4.2.2 Loop-Shaping Design

The set-up for control design via loop shaping implies that all outputs of the plant should be controlled to zero. It was already noted in Section 4.1.2 that, while the error in the air-fuel ratio should, indeed, be controlled to zero, there is no such requirement for the manifold pressure, neither during transients nor in steady state. This peculiarity was treated in the problem formulation in Section 4.1.2 by letting the corresponding singular value drop below one for all frequencies, instead of aligning the singular values as usual. As a result, the problem formulation was somewhat artificial, because the fact that a zero input to the plant should give zero output was still implied in the loop-shaping set-up. Therefore the control scheme was re-configured to account for the nature of the control problem more explicitly.

Controller Structure

Based on practical considerations, we have thus far included a predominant feedforward term in the plant and now divide the air-fuel ratio control problem further into feedback and feedforward control:

$$\begin{bmatrix} i_{\mathrm{ABV}} \\ t_{inj} \end{bmatrix} = \left[\left[\begin{array}{c:c:c} 0 & 0 & 0 \\ 0 & K_1 & 0 \end{array} \right] + \left[\begin{array}{c:c} K_3 & 0 \\ & K_2 \end{array} \right] \right] \left[\begin{array}{c} \alpha \\ \dot{m}_{\mathrm{EGR}} \\ \hdashline p_M \\ \hdashline \lambda_{exh} \end{array} \right] . \tag{4.23}$$

In the present control configuration, the input disturbances to the air system are measured directly, so a division into feedback and feedforward variables is fairly obvious. Considering the manifold pressure signal as a filtered version of the input signals, the first three measurements are used as feedforward variables, and only the measurement of the air-fuel ratio in the exhaust system is used for feedback.

In principle, nothing changes with regard to the requirements for feedback control in this configuration, *i.e.* to ensure a stable engine operation over a wide range of operating conditions as well as a zero steady-state error in the air-fuel ratio. The control problem is formulated according to the loop-shaping design procedure for the scalar plant:

$$y_2 = G_2 u_2 = P_{98} u_2 \,, \tag{4.24}$$

in order to maximise the robust stability radius with respect to coprime factor uncertainty and achieve good performance in terms of the loop shape.

Weighting Functions

The pre- and post-compensators in Figure 4.1 on page 59 are given by:

$$W_1 = \begin{bmatrix} \frac{5s}{s+5\times 10^{-2}} & 0 \\ 0 & \frac{0.65}{2s+1} \end{bmatrix} , \qquad W_2 = \begin{bmatrix} 1 & 0 \\ 0 & \frac{1.5\times 10^{-2}}{s}\left(\frac{s}{0.6}+1\right) \end{bmatrix} . \tag{4.25}$$

The post-compensator is slightly modified, *cf.* Equation (4.11) on page 64, to reduce the cross-over frequency of the loop shape to 0.1 rad/s. Furthermore, to attenuate the control activity of the air by-pass valve over a wider range of frequencies and emphasise the high frequency content, the cut-off frequency of the upper element in the pre-compensator is shifted from 10^{-2} to 5×10^{-2} rad/s. This requirement, albeit not relevant for the present feedback control design, is mentioned already at this point for comparison with the previous design; it is included in the problem formulation for the feedforward control design in the next section.

The lower element in the pre-compensator was introduced in the air-fuel ratio control loop, because the model was found to be inconsistent with the engine behaviour in experiments. To reveal the inconsistency, an instability was induced in the closed loop by a relay feedback arrangement, and the frequency of the induced oscillation was measured. In order to match the model at the point of instability, it was necessary to reduce the gain by 35% and add an extra 60 deg of phase lag, which is achieved by multiplying the nominal model with the pre-compensator in Equation (4.25) on the preceding page. The shaped frequency response is shown in the Bode diagram in Figure 4.11.

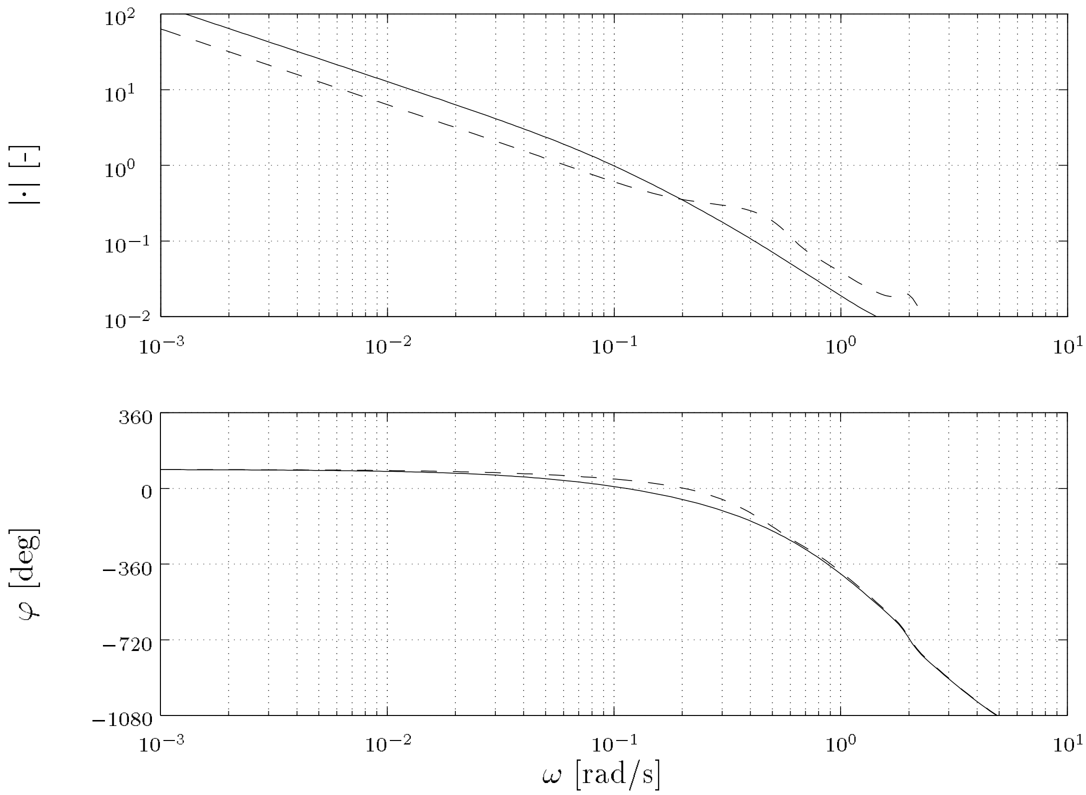

Figure 4.11: Loop Shape G_2K_2
Key: —— is G_2, – - is G_2K_2

The frequency response that is actually achieved with the reduced order controller K_2 is not very different from the desired shape: the magnitude is slightly smaller at low frequencies and slightly larger at high frequencies, the cross-over frequency lies slightly lower than specified at 6×10^{-2} rad/s. The controller advances the phase in the cross-over region to give a sufficient stability margin, $\varepsilon = 0.43$ in the optimal case.

Robust Stabilisation

Generally, it can be concluded that the reduced order controller K_2 robustly stabilises the plant G_2 for additive perturbations to its coprime factors maximally of size $1/\hat{\varepsilon}$, where $\hat{\varepsilon} = b(G_2, K_2)$. More precisely, we can measure the robustness of the feedback system in the gap metric by interpreting the stability margin in relation to the distance of the nominal model to models in other operating points across the operating envelope.

In particular, the models in other operating points in Table 4.9 on page 84 that are less than $\hat{\varepsilon} = 0.42$ away from the nominal model:

$$\delta_\nu(G_0, G_{ij}) < \hat{\varepsilon} \tag{4.26}$$

can be guaranteed to be stable in closed loop. After the experience with the previous design the priorities of the design objectives were re-arranged, in that the nominal performance of the system was rated above its robustness properties, with a view to assessing what performance is achievable. The aim was to achieve maximum performance in a small neighbourhood of the nominal model, before extending the control scheme over the operating envelope.

In this sense, the models in Table 4.9 on the next page are very similar in a small neighbourhood of the nominal model, while they are very dissimilar further away. Especially benign are the perturbations from the nominal model G_0 to the models G_{32}, G_{34}, and G_{43}. However, the controller which is optimised for the centre of the operating envelope may not perform well with the models in the first and last column of the table.

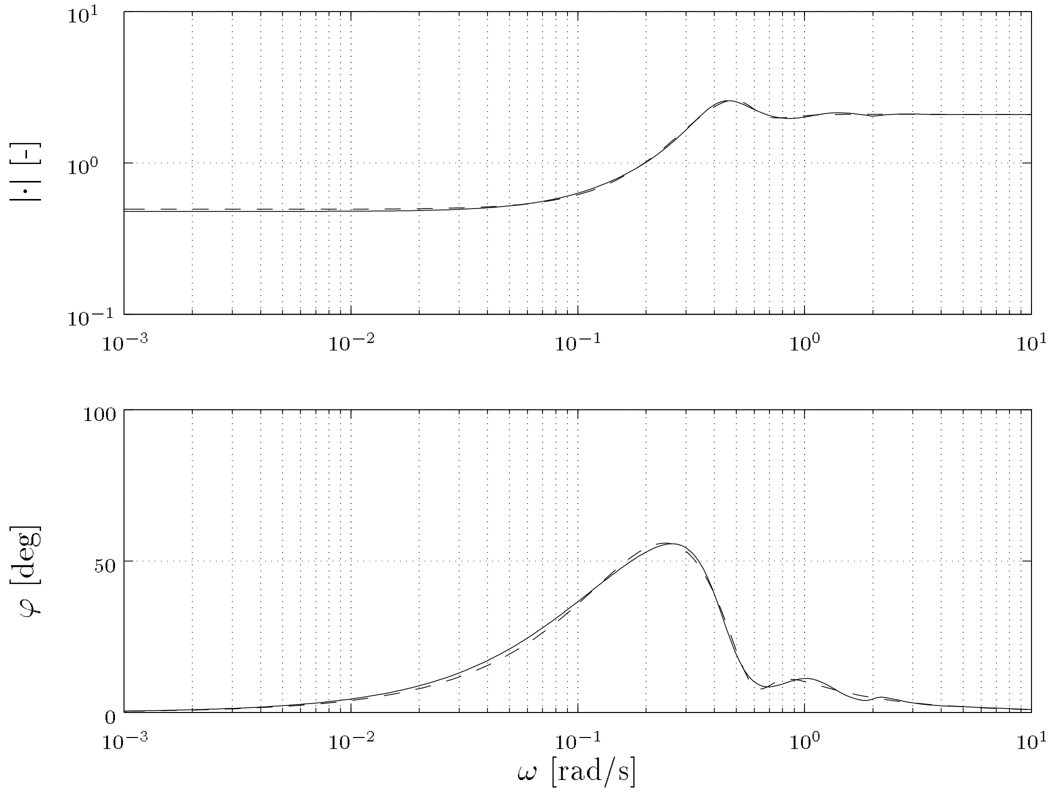

Figure 4.12: Frequency Response of Controller K_2
Key: —— is K_∞, - - is K_2

Controller Order Reduction

Consistent with the design procedure and the analysis in the gap metric, the controller order reduction is based on a coprime factorisation of the controller. Via balanced truncation the optimal controller is reduced to four states:

$$K_2 = \hat{K}_\infty^4 \,. \tag{4.27}$$

In terms of the stability margin, there is hardly any compromise in the order reduction ($\hat{\varepsilon} = 0.42$). Moreover, the frequency response of the reduced order controller is virtually overlaying the frequency response of the full order controller in Figure 4.12.

Gap Metric Calculations

The distances of the weighted models across the operating envelope with respect to the design point are shown in Table 4.9 and respectively the average distances from any operating point to the models surrounding it in Table 4.10.[18] Note that in comparison with the previous design both the models and the weighting functions are different. While the models that are surrounding the design point are somewhat better aligned than previously, the amount of scatter and the distribution in general are very similar.

	p_R [-]				
N [RPM]	0.20	0.35	0.50	0.65	0.80
870	0.78	0.48	0.46	0.43	0.43
1250	0.73	0.36	0.26	0.25	0.28
2000	0.57	0.17	0.00	0.15	0.37
2750	0.52	0.20	0.18	0.28	0.52
3500	0.51	0.25	0.30	0.40	0.59

Table 4.9: Distances in the Gap Metric $\delta_\nu(G_0, G_{ij})$

The data in Table 4.9 appears to be more irregular and less balanced by the weighting functions, yet, because much of the information is aggregated in the gap metric, one can hardly be more specific about the physical causes.

	p_R [-]				
N [RPM]	0.20	0.35	0.50	0.65	0.80
870	0.50	0.44	0.29	0.28	0.25
1250	0.49	0.38	0.26	0.28	0.32
2000	0.41	0.34	0.23	0.25	0.27
2750	0.43	0.27	0.18	0.20	0.23
3500	0.38	0.29	0.18	0.18	0.23

Table 4.10: Average Distances between Models
$\bar{\delta}_\nu(G_{ij}, G_{kl})$, $i-1 \leq k \leq i+1$, $j-1 \leq l \leq j+1$

The general impressions about the possible scope of a linear control design and the requirements for robust stability over the operating envelope are reinforced. As before, the potential difficulties at low engine speed and low manifold pressure are very apparent. Whether the large differences at high speed and high pressure, for example $\delta_\nu(G_0, G_{45}) = 0.52$, reflect practical difficulties or whether they are artificial, remains to be seen.

[18] The gap between the models is calculated only for the feedback part of the system, which includes the pressure feedback loop to be consistent with the previous calculations in Section 4.1.2 on page 67.

From the stability margins of the controller with the other models in Table 4.11 it can be seen that the design is much more focused at the central operating point.[19] The nominal performance is recovered only in a small neighbourhood and degrades significantly more than 750 RPM and 0.15 units of pressure away from the design point. In fact, the closed loop is unstable at a manifold pressure ratio of 0.2. Recall that the robustness of stability was deliberately sacrificed in the trade-off between the design objectives to achieve maximum performance. For the continuation of third design stage, the feedback control loop is closed by absorbing the controller K_2 into the generalised plant P.

	p_R [-]				
N [RPM]	0.20	0.35	0.50	0.65	0.80
870	0.00	0.13	0.26	0.24	0.25
1250	0.00	0.19	0.31	0.22	0.18
2000	0.05	0.27	0.34	0.21	0.13
2750	0.09	0.25	0.31	0.20	0.11
3500	0.06	0.25	0.29	0.15	0.22

Table 4.11: Stability Margin $b(G_{ij}, K)$

4.2.3 Feedforward Control Design

In the event-based engine model in Chapter 2, the time delays were approximated in discrete time with a series of unit delays, as the experimental accuracy of the delay parameter seemed not sufficient for an exact discretisation to be worthwhile. More significant than the errors which are involved in such an approximation are perhaps the variations of the time delay with the operating condition. Under these circumstances an attempt to compensate the delays exactly is unlikely to be successful.

Instead, we have dealt with the delays in the system by sequentially closing the loop on the manifold pressure and the air-fuel ratio in the exhaust system. In the present case, this approach is straightforward and not introducing any undesired cross-coupling because of the lower triangular structure of the plant. On the contrary, the cross-coupling that is introduced with the feedforward controller K_1 between the manifold pressure and the fuel injection time is, in fact, necessary. The resulting control system is robust with respect to uncertainty in the time delay in the exhaust system to the extent that the feedback controller K_2 can tolerate phase uncertainty. The phase margin is approximately 50 deg.

The modular structure of the controller in Equation (4.23) on page 81 might suggest that the design of the feedforward controller K_3 is independent of the other subsystems, but this is not the case. For the feedforward control to be effective, it relies on the

[19]The calculation of the stability margin includes the pressure feedback loop, as it was the case with the gap metric calculations. Therefore the corresponding elements of the feedforward controller K_3 are included in the feedback controller in this instance. This is why the stability margin with the nominal model is $b(G_0, K) = 0.34$ and not 0.42.

features that have been modified in the plant characteristics with the controllers K_1 and K_2. In order to allow for the necessary co-ordination of the controller K_3 with the other controllers, they are integrated in the problem formulation by closing the corresponding loops in the set-up in Figure 4.1 on page 59.

In the present control configuration, the position of the throttle plate and the EGR mass flow into the intake manifold are measured directly. To refine the adjustment of the fuel injection time to the manifold pressure, which is so critical for transient air-fuel ratio control, it seems best to design K_3 as an incremental controller that acts on top of the base fuel injection time and the feedback control signal. By means of the air by-pass valve the controller is in a position to moderate the pressure transients simultaneously.

Nominal Performance

In principle, the same argument applies as in Section 4.1.3 on page 68. Several noise terms are added to the problem formulation to account for the sensitivity of the system's performance to model uncertainty, *cf.* Section 4.2.7. More specifically, the set-up for the design of the feedforward controller is extended on the basis of the S/KS problem to include the effect of measurement noise on the feedforward variables at a level of 10%.

The extra emphasis on the closed-loop characteristics at the plant output, in addition to the penalty on the sensitivity function T_{ed}, must be balanced with the input characteristics, *i.e.* the penalty on the control effort. For the problem to be well-posed, not only the total control effort z_1 is penalised in the pertaining subsystem of the generalised plant

$$\begin{bmatrix} e \\ u_2 \\ z_1 \\ y_3 \end{bmatrix} = G_3 \begin{bmatrix} d \\ w_2 \\ u \end{bmatrix} \tag{4.28}$$

but also the feedforward component of the second control input u_2.

Weighting Functions

Further to the specification of the feedback properties in terms of the pre- and post-compensators, the plant is augmented in the performance and disturbance channels with the weighting functions

$$W_p = \frac{s + 0.1}{s + 10^{-3}}\,, \qquad W_d = I_2 \tag{4.29}$$

to specify the shape of the sensitivity function from the throttle plate and EGR mass flow disturbances to the air-fuel ratio in the cylinder

$$\lambda_{cyl} = \begin{bmatrix} T_{11} & T_{12} \end{bmatrix} \begin{bmatrix} \alpha \\ \dot{m}_{\mathrm{EGR}} \end{bmatrix} . \tag{4.30}$$

There are no further assumptions about the nature of the disturbance signals, which is why the identity matrix was chosen for the disturbance weight. The low-pass filter W_p

emphasises the disturbance rejection at frequencies below 10^{-3} rad/s roughly a hundred times higher than at frequencies above 0.1 rad/s.

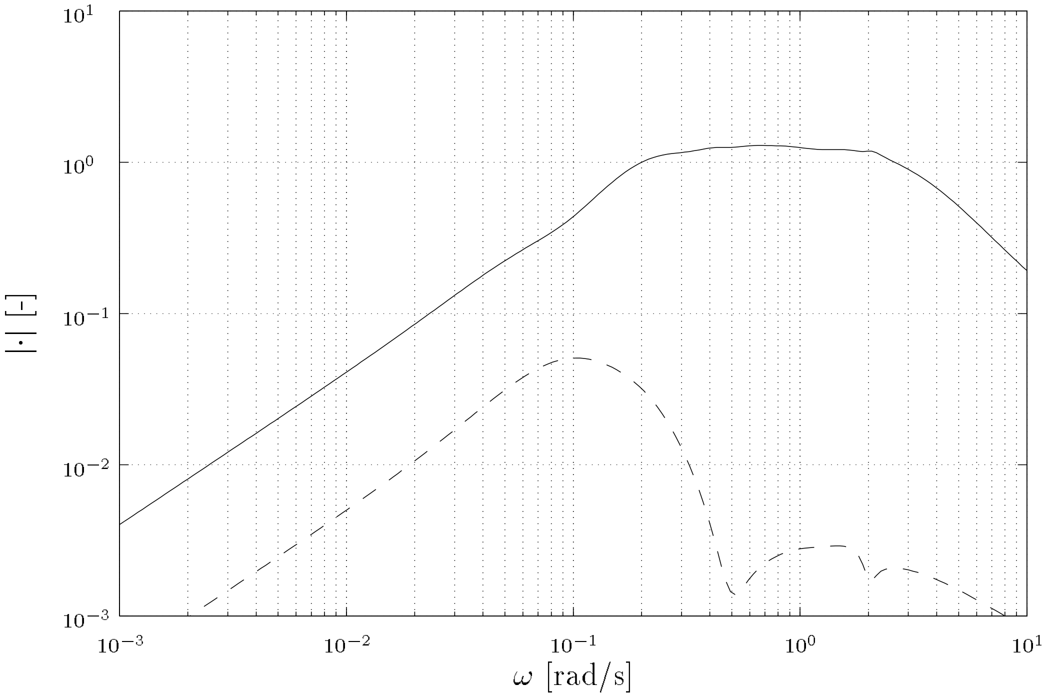

Figure 4.13: Sensitivity T_{ed}
Key: — is T_{11}, - - is T_{12}

According to Figure 4.13, the specification is almost met, only above 0.1 rad/s the frequency response of the sensitivity function is larger than one for a range of frequencies ($\|T_{ed}\|_\infty = 1.29$).[20] Note that the performance specification is less stringent at high frequencies, as the cut-off frequency is shifted to the left by a decade. The overall actuator demand resulting from the disturbances

$$\begin{bmatrix} i_{\text{ABV}} \\ t_{inj} \end{bmatrix} = \begin{bmatrix} T_{21} & T_{22} \\ T_{31} & T_{32} \end{bmatrix} \begin{bmatrix} \alpha \\ \dot{m}_{\text{EGR}} \end{bmatrix} \tag{4.31}$$

is shown in Figure 4.14 on the next page. It can be seen that the disturbances to the position of the throttle plate are dominating the controller's response and that the primary actuator for their rejection is the air by-pass valve. In comparison with Figure 4.7 on page 72, the control activity is reduced in both channels. With regard to the EGR mass flow disturbances the control action is quite similar, although the signals w_1 and $\dot{m}_{\text{EGR}}$ enter at different points in the loop.

[20]While the performance weight is included in the plant for controller synthesis, it is not included in the calculation of the frequency response or the norm calculations for comparison with the previous design.

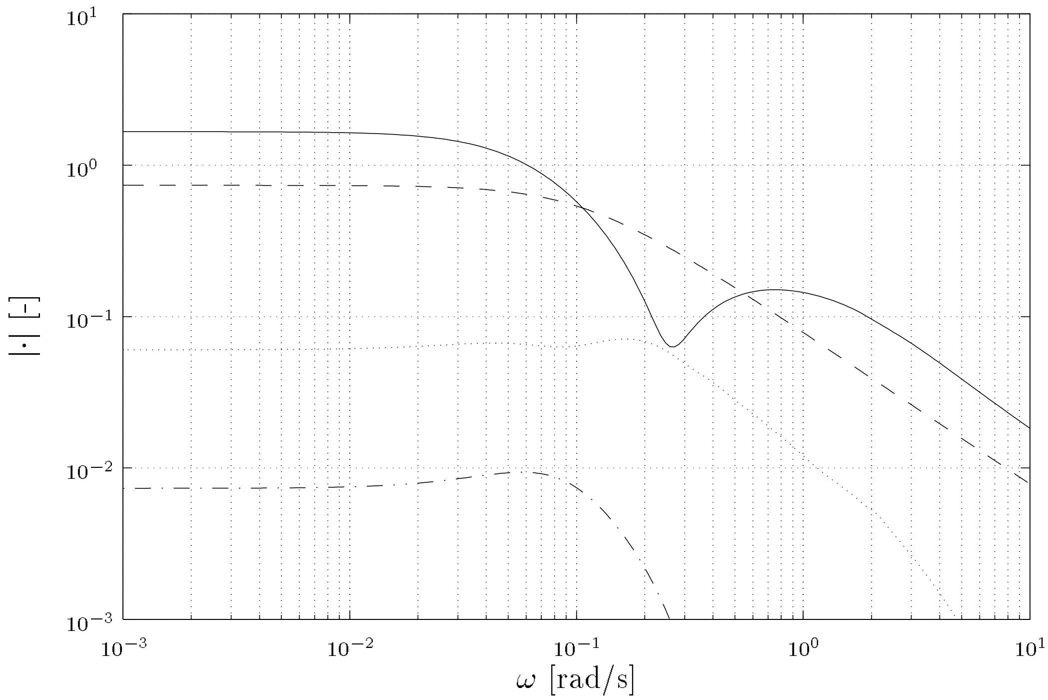

Figure 4.14: Actuator Demand $T_{z_1 d}$
Key: —— is T_{21}, – - is T_{22}, ······ is T_{31}, · – is T_{32}

Controller Order Reduction

The solution to the standard $\mathcal{H}_\infty$ problem for the generalised plant G_3 exhibits no particular structure that could be exploited in the process of order reduction. However, by the nature of feedforward design, several very fast and very slow modes appear in the controller, which are removed in order to improve the numerical properties for the order reduction and the controller implementation. The procedure is the same as detailed on page 70. Finally, the controller is truncated to ten states in a balanced state-space form:

$$K_3 = \hat{K}_\infty^{10}\,. \tag{4.32}$$

The order of the approximation is relatively high because of the complex transfer characteristics of the controller, which are shown in Figure 4.15 on the facing page. The frequency response of the reduced order controller is shown for the ABV channel in Figure 4.15(a) with respect to the throttle plate angle, the EGR mass flow, and the manifold pressure, and respectively for the fuel injection time in Figure 4.15(b).

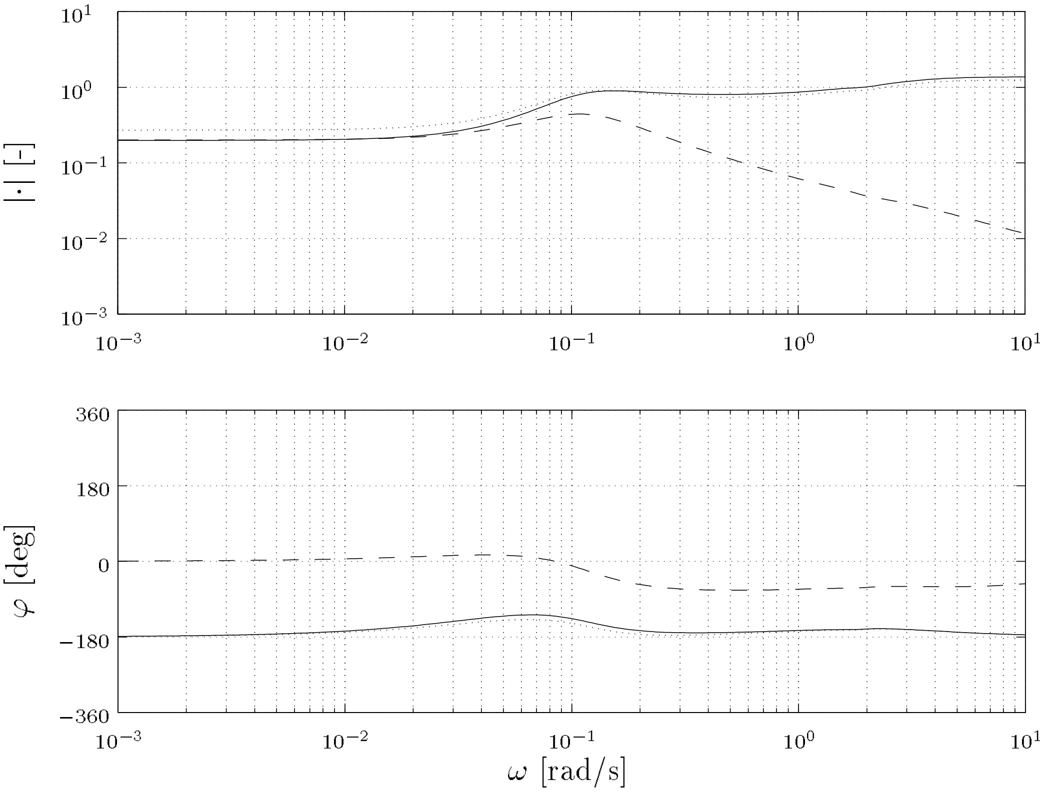

(a) $K_{1\bullet}$

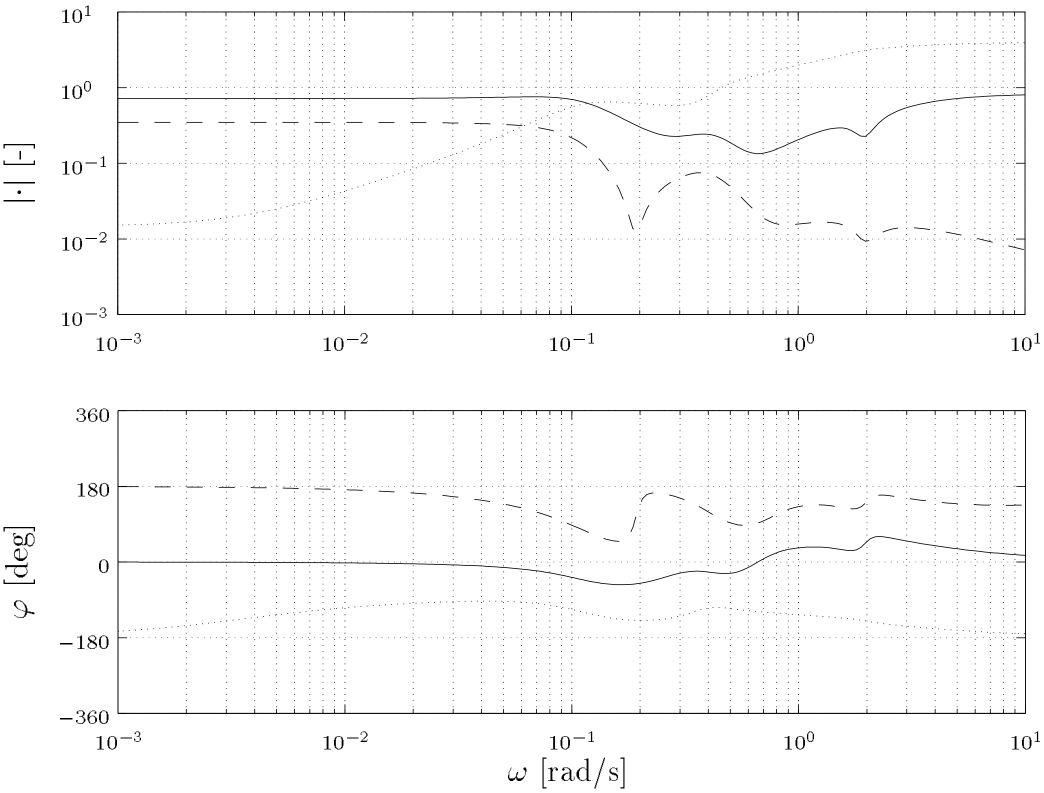

(b) $K_{2\bullet}$

Figure 4.15: Frequency Response of Controller K_3
Key: —— is $K_{\bullet 1}$, – - is $K_{\bullet 2}$, ······ is $K_{\bullet 3}$

4.2.4 Linear Simulation

Before the implementation on the engine, the controller is tested in linear simulation to assess control system's performance in the time domain. The simulation is in discrete time to emulate the event-based engine operation. Since the design was carried out compatibly with this way of operation, the performance is not affected by the sampling.

For the purpose of simulation, the nominal model is connected with the final, multivariable controller in Equation (4.33) on page 92 according to Figure 4.1 on page 59. Because we are interested in the unweighted, physical signals at the input and output of the plant, the weighting functions in the feedback loop are absorbed in the controller.

A step disturbance with the same profile as in Figure 4.8 on page 73 is applied to the closed-loop system in the first disturbance channel. According to Table 4.8 on page 78, the size of the step corresponds to a change of the throttle plate position of 4 deg. The signal reaches its final value in ten samples, which is equivalent to a rate of change of 37.5 ms/deg.

Furthermore, a unit on the vertical axis in Figure 4.16 corresponds to a deviation of 5% in the air-fuel ratio, to an increment of 0.1 in the setting of the air by-pass valve, or an increment of 2 ms in the fuel injection time.

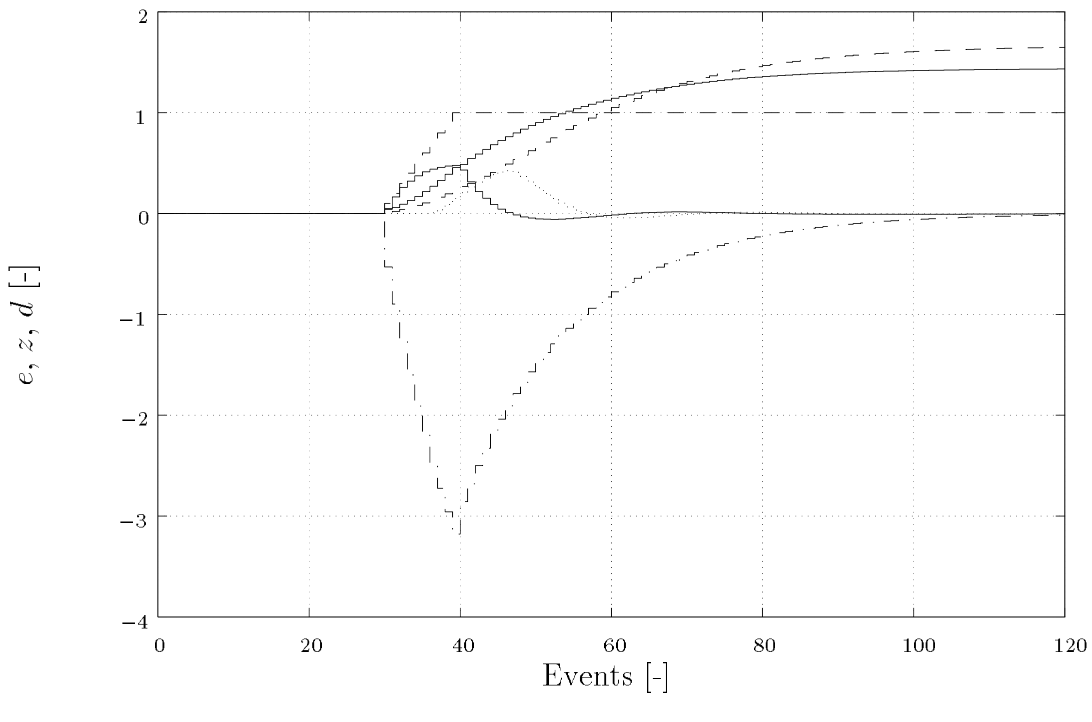

Figure 4.16: Closed-Loop Time Response

Key: —— is λ_{cyl}, – - is p_M, ······ is λ_{exh}, · – is i_{ABV}, —— is t_{inj}, – - is α

Two phases can be distinguished in the time response in Figure 4.16. During the initial phase of the transient, the first ten samples, the controller rejects the disturbance as much as possible using an increasing amount of the authority of the air by-pass valve. Simultaneously, it advances the fuel injection time before the rise in the manifold pressure. As a result, the air-fuel ratio stays clearly within a band of 2.5% around the stoichiometric value in the presence of the disturbance, and its nominal value is recovered only after twenty samples. In the second phase, from sample instance 40 onwards, the system recovers from the disturbance. The effect of the disturbance on the air-fuel ratio is not apparent beyond sample instance 60, *i.e.* after thirty samples, and a new equilibrium point is reached about a hundred samples, after the disturbance occurred. The good performance is due to the proper timing of the control action.

4.2.5 Design Summary

In summary, the systems that were involved in the design process are listed in Table 4.12. In this case, the nominal plant G had only 17 states, as opposed to 19 states in Table 4.5 on page 74, because the EGR valve component was excluded and the delay in the timing of the fuel injection was reduced from three to two unit delays.

Unmodelled dynamics that were identified in analysing engine test data were included in the pre-compensator W_1 for the control design but not for implementation. A phase lead element was used to change the plant characteristics in a way as to improve the timing of the fuel injection with the induction process. The control specification and the analysis in the gap metric was then in terms of the generalised plant P.

		Dimensions		
System	Symbol	n_x	n_y	n_u
Nominal Plant	G	17	5	4
Pre-Compensator	W_1	2	2	2
Post-Compensator	W_2	1	2	2
Disturbance Weight	W_d	0	2	2
Performance Weight	W_p	1	1	1
Phase Lead	K_1	1	1	1
Generalised Plant	P	22	9	8
Loop-shaping Design	G_2	19	1	1
Feedback Controller	K_2	4	1	1
S/KS Design	G_3	26	7	7
Feedforward Controller	K_3	10	2	3
Closed Loop	T	35	5	6

Table 4.12: State-space Dimensions of Systems involved in the Design Process

Finally, the closed-loop system T was analysed in the frequency domain, by means of norm calculations, and in simulation.

The final, multi-variable controller K fits in the generic feedback configuration in Figure 3.1 on page 45 and exhibits the following structure:

$$\begin{bmatrix} i_{\text{ABV}} \\ t_{inj} \end{bmatrix} = \left[\begin{bmatrix} 0 & 0 & 0 \\ 0 & K_1 & 0 \end{bmatrix} + \begin{bmatrix} K_3 & & 0 \\ & & K_2 \end{bmatrix} \right] \begin{bmatrix} \alpha \\ \dot{m}_{\text{EGR}} \\ \hline p_M \\ \hline \lambda_{exh} \end{bmatrix} . \tag{4.33}$$

We can imagine that the weighting functions belong either to plant or the controller, in which case the total number of states in the control system is seventeen. The implementational issues and the experimental results are discussed in the next chapter.

4.2.6 Design over a Set of Operating Points

In order to assess what level of performance is achievable across the operating envelope, the design was repeated over a set of operating points. Analogously to the approach in Section 4.1.6, the same weighting functions were chosen for all operating conditions, and the controllers K_i, $i = 2, 3$, were re-designed in each operating point to be of the same state-space dimensions. Since the delay in the timing of the fuel injection is independent of the operating condition, the controller K_1 can be used for all operating conditions.

It makes only sense to interpolate between the design points, if, first of all, the local performance is satisfactory and both the stability and the performance properties are consistent over the operating envelope.

	p_R [-]				
N [RPM]	0.20	0.35	0.50	0.65	0.80
870	0.07	0.14	0.18	0.22	0.33
1250	0.11	0.23	0.27	0.33	0.39
2000	0.17	0.29	0.34	0.38	0.45
2750	0.18	0.31	0.37	0.41	0.45
3500	0.24	0.32	0.40	0.40	0.45

Table 4.13: Stability Margin $1/\left\|T_{zw}\right\|_\infty$

The behaviour of the control system is characterised in terms of the closed-loop norms in Table 4.13 and Table 4.14 on the next page in fixed operating points only. It would be substantially more complicated to analyse a gain-scheduled control scheme as a linear parameter-varying system, and the conditions for robust stability and robust performance would only be sufficient in this framework, so that practically one often resorts to nonlinear simulation studies. Yet, the simple numbers $1/\left\|T_{zw}\right\|_\infty$ and $\left\|T_{ed}\right\|_\infty$ already give a good indication of the control system behaviour.

The system exhibits good stability properties over a wide range of operating conditions, at low manifold pressure, however, and especially during idle operation, the stability is compromised.

Apart from the principal difficulties to control the engine at low load, the experience with the models at such operating conditions suggests that either the dynamics of the model or at least the techniques of system identification that were used are not wholly appropriate. At present, the asymmetric engine behaviour in tip-in and tip-out scenarios is not accounted for, neither in the structure of the model, the model parameters, nor the control design.

According to Table 4.14, the performance across the operating envelope is fairly good and quite consistent. Indeed, in this case, the performance index in the nominal operating point is indicative of the performance that is achievable in the other operating points.

	p_R [-]				
N [RPM]	0.20	0.35	0.50	0.65	0.80
870	4.46	0.72	1.21	1.39	1.07
1250	0.94	1.56	1.51	1.41	1.16
2000	0.78	1.19	1.29	1.36	1.43
2750	0.85	1.43	1.51	1.55	1.64
3500	0.84	1.29	1.50	1.79	1.60

Table 4.14: Closed-Loop Norm $\|T_{ed}\|_\infty$

Recall that a norm of one approximately corresponds to a peak excursion of 5% in the air-fuel ratio. Idle operation is certainly a special case that could perhaps be improved by a special choice of weighting functions.

4.2.7 Complex μ Analysis

We conclude our assessment of the control system's performance before the implementation on the engine by studying the sensitivity of the system's performance to certain perturbations, using the structured singular value μ. It has already been emphasised, that the accuracy of the feedforward part of the model is very important for precise air-fuel ratio control.

In order to indicate what level of accuracy is required, the robustness of the control system's performance is calculated in a parameter study with respect to several perturbations of different sizes. More specifically, the calculation assumes that the nominal transfer function T_{ed} is perturbed by output multiplicative uncertainty in each of the feedforward variables and input multiplicative uncertainty in the ABV channel. Thus the structured singular value μ_{RP} is calculated with respect to the following uncertainty structure:

$$\begin{aligned}\{\Delta_{RP} \,|\, \Delta_{RP} = \operatorname{diag}(\delta\alpha, \delta\dot{m}_{\mathrm{EGR}}, \delta p_M, \delta i_{\mathrm{ABV}}, \Delta_p)\,, \\ |\delta i| \le 1\,, \delta i \in \mathbb{C},\ \ i = \alpha, \dot{m}_{\mathrm{EGR}}, p_M, i_{\mathrm{ABV}}\,,\ \ \Delta_p \in \mathbb{C}^{2\times 1}\}\,. \quad (4.34)\end{aligned}$$

The resulting performance degradation is shown in Figure 4.17 on the next page as a function of the size of the complex perturbations. Note that the sizes of the perturbations are not varied individually but all in the same way from 0 to 10%. While the effect of the parametric uncertainty is negligible with regard to the stability properties, it is critical for the control system's performance in the frequency range from 0.05 rad/s to 0.5 rad/s. In this frequency range the closed-loop norm deteriorates by 50% at 0.2 rad/s and more over the range of perturbations.

Since the ultimate objective for transient air-fuel ratio control is to reduce the peak excursions of about 10% down to 5% or less, *i.e.* at least by a factor of two, the task may be ill-founded on the basis of a model that is only accurate to within 10% in certain places.

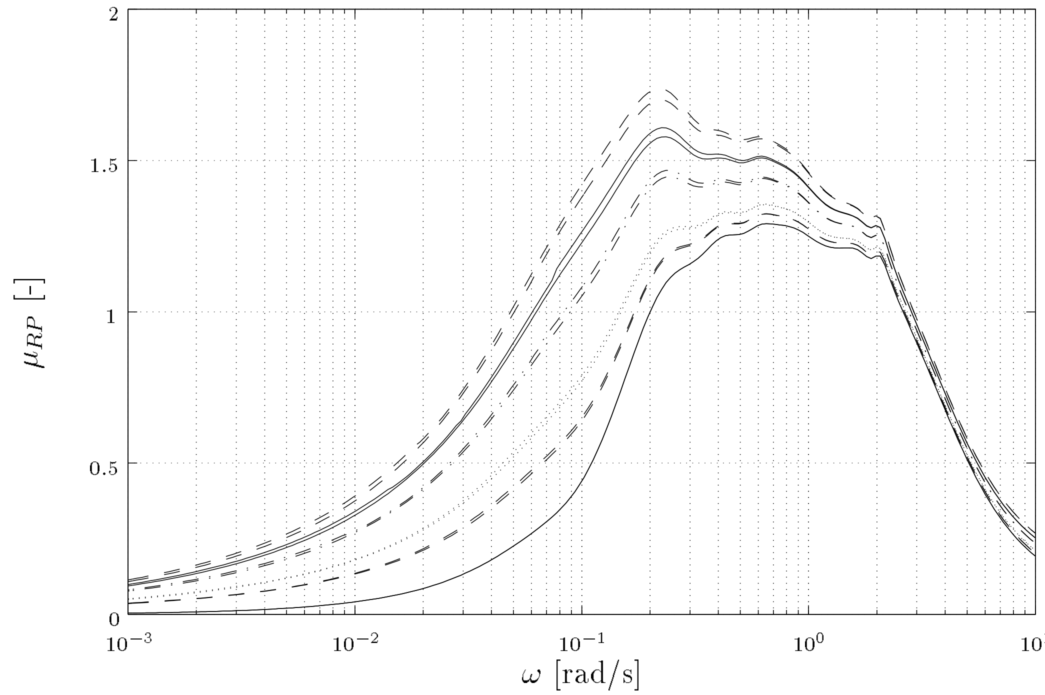

Figure 4.17: Robust Performance Test
Key: —— is 0%, – - is 1%, ····· is 2%, · – is 5%, —— is 7.5%, – - is 10%
Size of Perturbations

In the worst case, the performance advantages that are gained in the design for the nominal system could be lost completely due to the intolerable discrepancies between the model and the physical system. Typically, mean value engine models may be accurate to within 2 or 3% in steady state, but the accuracy in dynamics may only be 10% [29]. With such demanding requirements for control it is in any case questionable, whether state-of-the-art engine models are sufficiently accurate for the task.

In the design process, the closed-loop behaviour was also sensitive to the order reduction of the feedforward controller, and special care was taken to eliminate such effects. The principal difficulty, however, is not so much the complexity of the model than the accuracy and sensitivity with respect to the model parameters. With this in mind, the experimental results are discussed in the next chapter.

5. EXPERIMENTAL RESULTS

5.1 Experimental Set-Up

The two control schemes from the previous chapter were implemented on a 1.8l Ford Zetec engine in a vehicle installation.[21] All experimental work was conducted exclusively at Ford research and development facilities. In addition, the Ford Motor Company provided the environment for rapid prototyping and test support. The experimental set-up in the test cell is shown in Figure 5.1 on the following page.

While the air-fuel ratio control strategy was implemented on a digital signal processor using a rapid prototyping system, a conventional engine control unit was operated simultaneously to provide all other functionality for engine control, *cf.* Figure 1.4 on page 8. An implementation in floating point arithmetic was chosen to be able to experiment freely without computational constraints.

For the implementation on the engine, the control scheme was specified in a block-oriented language, as in Figure 5.2 on page 98 and Figure 5.3 on page 99, using XMATH and SYSTEMBUILD on a workstation. The controller block diagram was then translated into C language and converted to DSP code using an auto code facility, to be downloaded onto the digital signal processor, which was hosted by a personal computer, via a computer network.

To a certain extent software had to be custom-made in order to interface with the signal processing boards, in particular for the generation of pulse-width-modulated signals to drive the fuel injectors. However, the lower layers of the implementation, such as the hard- and software interface, as well as the technical details of the instrumentation, the signal conditioning, and the driver circuits, are not described here, as they are proprietary to the Ford Motor Company. Ideally, the controller implementation should be independent of the underlying hard- and software architecture.

The engine tests that are to be presented are throttle transients at a constant engine speed, passing through the operating point for which the controller was designed. A robot driver was used in the vehicle installation in order to ensure the repeatability of the tests. For that purpose, the throttle transients were programmed on a DSP board as a command to the dynamometer control computers. The tests were performed for an engine under warm operating conditions.

5.2 Implementation

As can be seen from the block diagrams in Figure 5.2 on page 98 and Figure 5.3 on page 99, the implementation is simple and fully transparent. In principle, all signals and controller parameters can be accessed, modified, and monitored on-line. The flexibility of the computing environment allows for sophisticated experimentation, be it for the

[21]The control scheme including active EGR control was implemented in December 1995, and the modular feedforward control configuration was tested in May 1996.

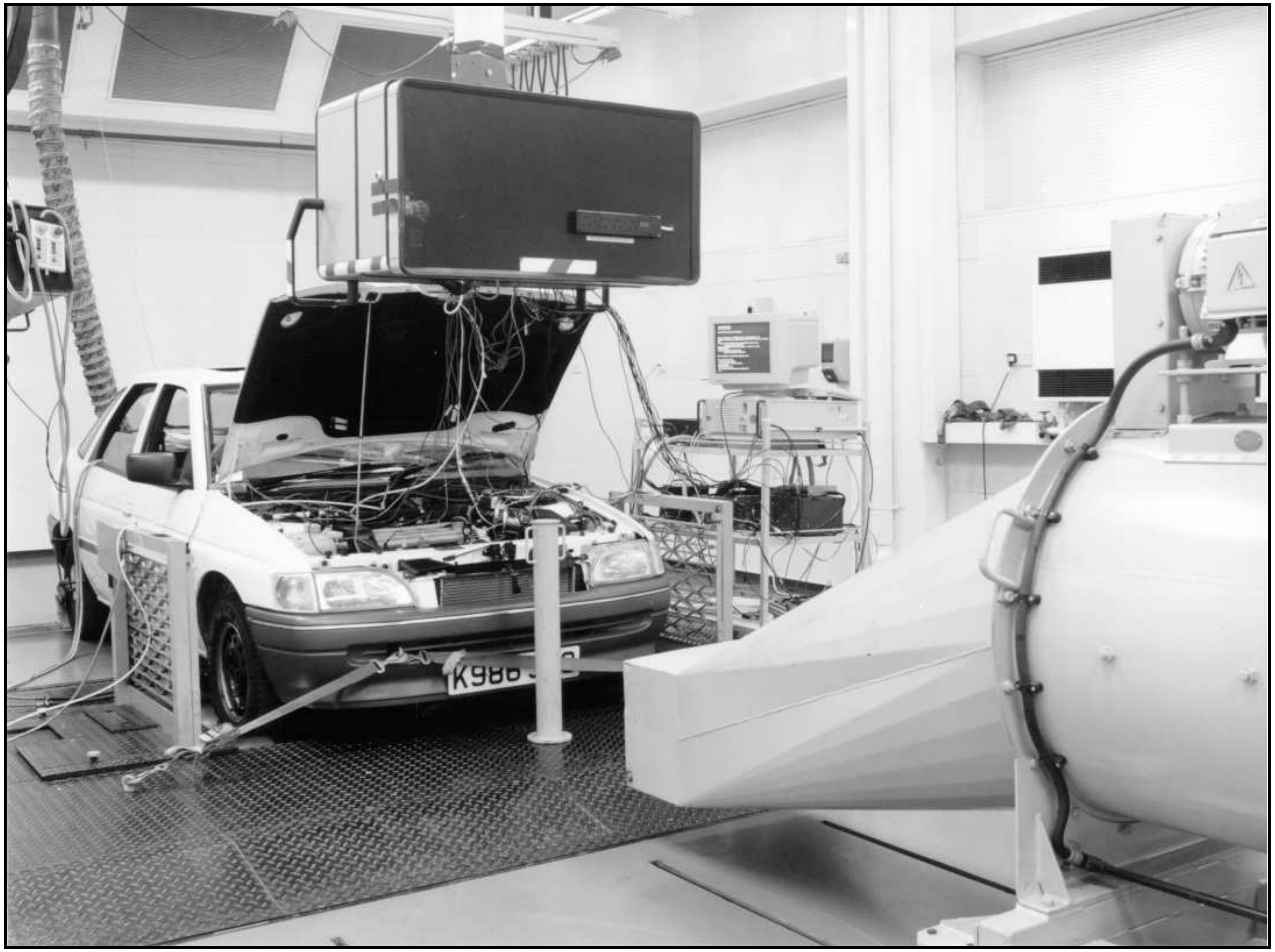

Figure 5.1: Chassis Roll Dynamometer at Ford European Electronics Operations

evaluation of the control system's performance or for closed-loop system identification, as in the case of the stability analysis that was described on page 81. Since the control scheme is re-configured simply by block diagram manipulations and the control design process is automated for the most part, it is also possible to revise a controller in the test cell on a notebook computer within a couple of hours.

We now describe the implementation in more detail by the example of the modular feedforward design. In the earlier case of active EGR control the block diagrams were very similar and are therefore omitted. Figure 5.2 on the next page shows the control scheme in which the air-fuel ratio controller is embedded. It consists of several look-up tables for the calculation of the error signals and the open-loop settings of the actuators. In this way the transient deviations are separated from the static nonlinear behaviour of the engine.

The engine was calibrated in a number of operating points (n_i, p_j), $i = 1, \ldots, I$, $j = 1, \ldots, J$ such that the position of the throttle plate, the EGR mass flow into the intake manifold, and the open-loop settings of the actuators were consistent with engine speed and the pressure in the intake manifold in steady state.

The position of the throttle plate, for example, is tabulated in terms of engine speed and manifold pressure. In order not to counteract the control action, the open-loop setting of the air by-pass valve was made a function of the throttle plate angle rather than the manifold pressure. Also note that the feedforward controller K_1 is used to calculate the open-loop setting of the fuel injection time. While the active range of the air by-pass valve is fixed, the maximum length of fuel injection is dependent on engine speed.

The EGR mass flow signal was taken from the engine control unit. During the tests the base values were fixed corresponding to the nominal operating conditions at 2000 RPM and a manifold pressure ratio of 0.5. A static compensation of the nonlinear flow characteristics of the air by-pass valve was not necessary in this instance. The target value λ_r was set to one for stoichiometric engine operation.

The controller modules K_2 and K_3 and the weighting functions $W_{1\,11}$ and $W_{2\,22}$ were implemented according to Figure 5.3 on page 99. For a summary of the state-space dimensions of these systems see Table 4.12 on page 91. The controller structure is reflected in the block diagram, where the matrix operations have been broken down into smaller units for greater efficiency. The input-output scale factors are implemented separately in order to enable or disable certain signal paths easily.

5.3 Test Data

5.3.1 Active EGR Control

Figure 5.4 on page 102 shows the air-fuel ratio during throttle steps between 8 and 12 deg of throttle plate angle at a rate of change of approximately 12.5 ms/deg. Engine speed is practically constant throughout the test at 2000 RPM. Note that this disturbance is about three times faster than the throttle ramp which was used in simulation. In Section 4.1.4 the input disturbance to the nominal closed-loop system was a throttle ramp at a rate of change of 37.5 ms/deg. As a result, the engine load changes in terms of the manifold pressure ratio between 0.45 and 0.60.

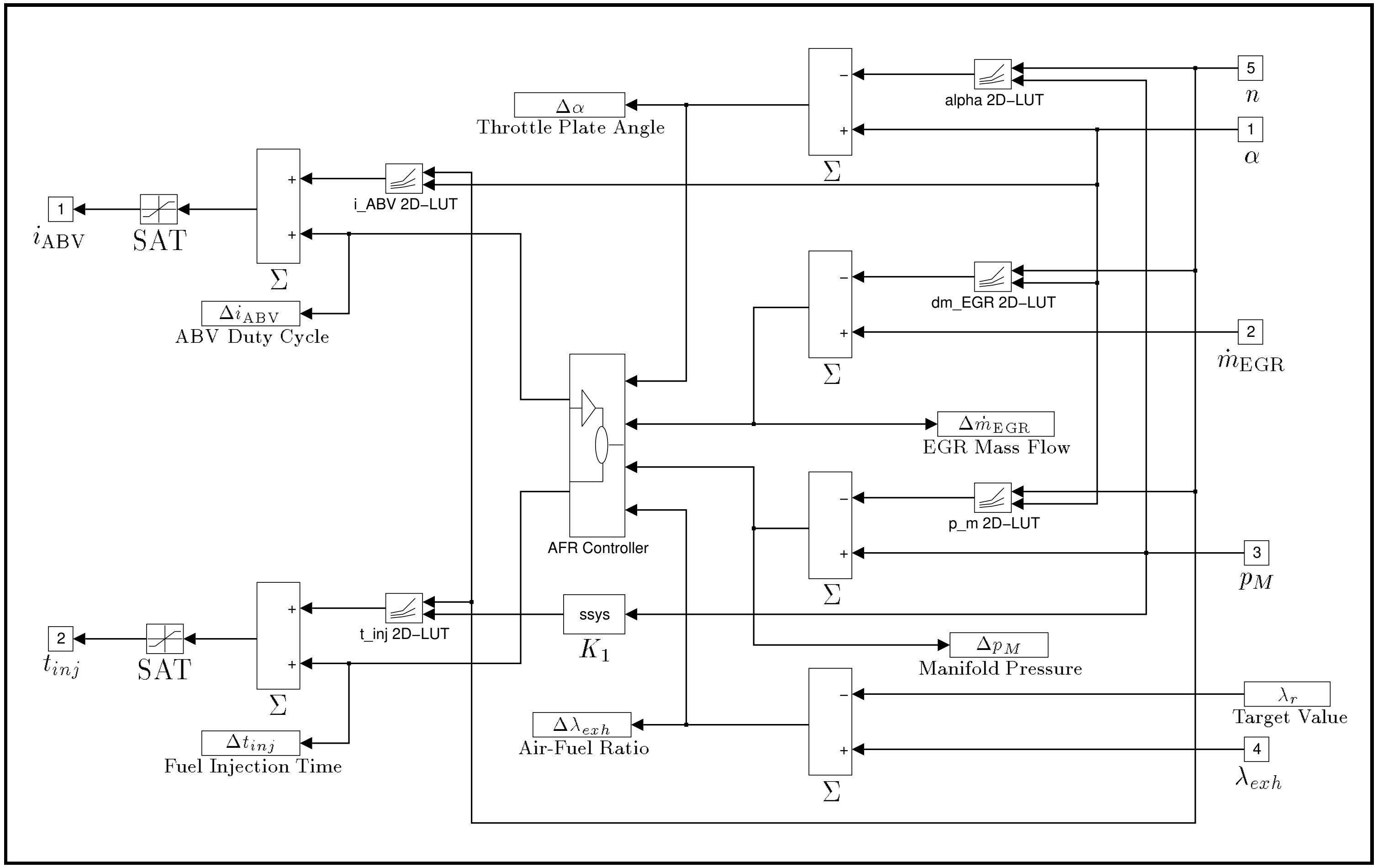

Figure 5.2: Control Scheme

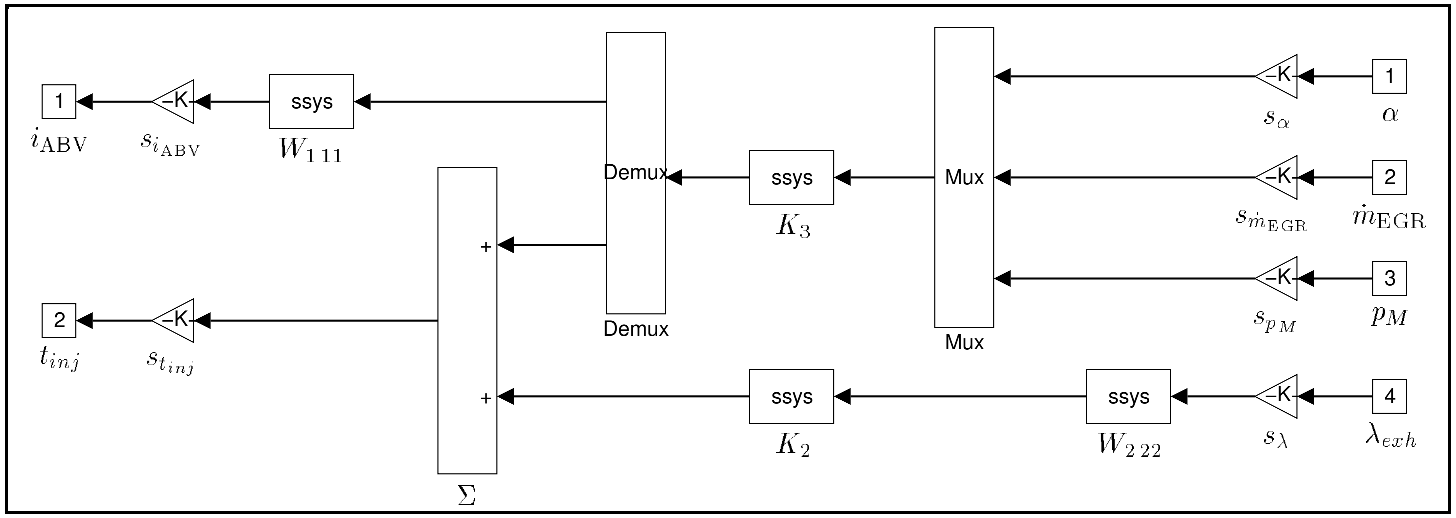

Figure 5.3: Controller Implementation

$$\begin{bmatrix} i_{\mathrm{ABV}} \\ t_{inj} \end{bmatrix} = \begin{bmatrix} s_{i_{\mathrm{ABV}}} & 0 \\ 0 & s_{t_{inj}} \end{bmatrix} \begin{bmatrix} W_{1\,11} & 0 \\ 0 & 1 \end{bmatrix} \left[\begin{array}{c:c} K_3 & \begin{matrix} 0 \\ K_2 \end{matrix} \end{array}\right] \begin{bmatrix} I_3 & 0 \\ 0 & W_{2\,22} \end{bmatrix} \begin{bmatrix} s_\alpha & 0 & 0 & 0 \\ 0 & s_{\dot m_{\mathrm{EGR}}} & 0 & 0 \\ 0 & 0 & s_{p_M} & 0 \\ 0 & 0 & 0 & s_\lambda \end{bmatrix} \left[\begin{array}{c} \alpha \\ \dot m_{\mathrm{EGR}} \\ p_M \\ \hdashline \lambda_{exh} \end{array}\right]$$

The deviations in the air-fuel ratio from the stoichiometric value are characterised by a peak excursion of 6% and a duration of about 1.2 s, which corresponds to 80 events at 2000 RPM.

In both the tip-in and tip-out scenarios, the initial excursion is minute, as the disturbance to the air mass flow is overcompensated by the air by-pass valve. In the first case, the air by-pass valve even shuts temporarily, and the reaction to compensate for the rich excursion is quite visible in the fuel injection, see Figure 5.5 on page 103.

One would think that it should be possible to improve the control system's performance further with a more precise adjustment of the control action of the air by-pass valve with the fuel injection. However, it must be pointed out, how different the dynamics of the engine are during acceleration and deceleration, as can be seen from the asymmetry of the air-fuel ratio trace.

The EGR system is self-contained and adapts itself to a new operating condition within about a second. Yet, the highly nonlinear gain of the EGR system is critical. Already little changes in the actuator setting result in large changes in the EGR mass flow and the manifold pressure. Therefore the EGR valve is shut during the transient at 12.5 s to minimise the air flow disturbance.

5.3.2 Modular Feedforward Design

In the test shown in Figure 5.6 on page 104 the position of the throttle plate was perturbed ± 2 deg around a nominal value of 9 deg at a rate of change of approximately 75 ms/deg. As before, the engine speed was kept constant during the test. In comparison to the simulation in Section 4.2.4, the rate of change of the disturbance was smaller by a factor of two.

Initially, the engine load is significantly below its nominal level of 0.50 at 0.33 and then increases sequentially to values of 0.45 and 0.58.

The effect of the air by-pass valve is visible in smoothing the pressure transients. In particular, the control action in Figure 5.7 on page 105 is less abrupt but more sustained. There is also less overshoot in the fuel injection. At times it becomes apparent in the trace of the fuel injection time that the noise content in the measurement of the manifold pressure is amplified slightly by the controller K_1.

The conventional EGR system is only designed for steady-state control. At 4 and 17.2 s respectively a threshold value is reached below which no EGR is commanded.

The peak excursions in the air-fuel ratio do not exceed 5% except in the last case for the tip-out to low load. According to Table 4.9 on page 84, the behaviour of the engine at this operating point is 0.17 units away from the behaviour at the nominal operating point in the gap metric. Indeed, it is stabilised by the controller albeit with slight difficulty, also *cf.* Table 4.11 on page 85. The duration of the transients is on average 1.6 s, which corresponds roughly to 105 events.

In order to achieve this level of performance, it was necessary to modify the nominal model by reducing the gain by 35% and adding an extra phase of 60 deg in the transfer function from the fuel injection time to the air-fuel ratio, as it was explained on page 81. It is quite clear that model inaccuracies to such an extent are critical to the achievable performance, especially in the attempt to adjust feedforward and feedback control precisely given the sensitivities in Figure 4.17 on page 94.

5.4 Interpretation

It is a challenging task to develop new control strategies with a view to complying with future emissions standards. Some progress has been made to this end with the application of robust control techniques, as is evident from the experimental results in this chapter.

A single multi-variable controller can be optimised to give a high level of performance over a restricted operating region that is superior to the performance of current engine management systems. With such a controller the air-fuel ratio can be maintained within a sufficiently narrow band around the stoichiometric value in the presence of moderate throttle plate disturbances. Moreover, the duration of the excursions is reduced significantly in comparison to the excursions incurred with current engine management strategies.

However, the control system's performance must be improved further in fixed operating points, before the control scheme can be extended across the operating envelope. A greater effort must be made especially in the refinement of the engine data to improve the accuracy of the models.

5.5 Outlook

The gain scheduling schemes described in Appendix D were tested on-line to assess the computational requirements for realistic problem sizes on the basis of their run-time behaviour. For that purpose, four controllers were taken from Table 4.13 on page 92 and implemented according to Figure 5.3 on page 99 by replacing the blocks for the time-invariant state-space systems K_2 and K_3 with their gain-scheduled counterparts. Recall that the weighting functions were not varied across the operating envelope. For the given hardware configuration this was perfectly feasible.

The execution of the second control scheme, however, failed already for modest problem sizes, where $\dim(M_{33}) > 2$. Either the computing power must be increased significantly, or, what is more likely, the complexity of the controller must be reduced suitably before the implementation, *cf.* final remark in Section 3.3.4.

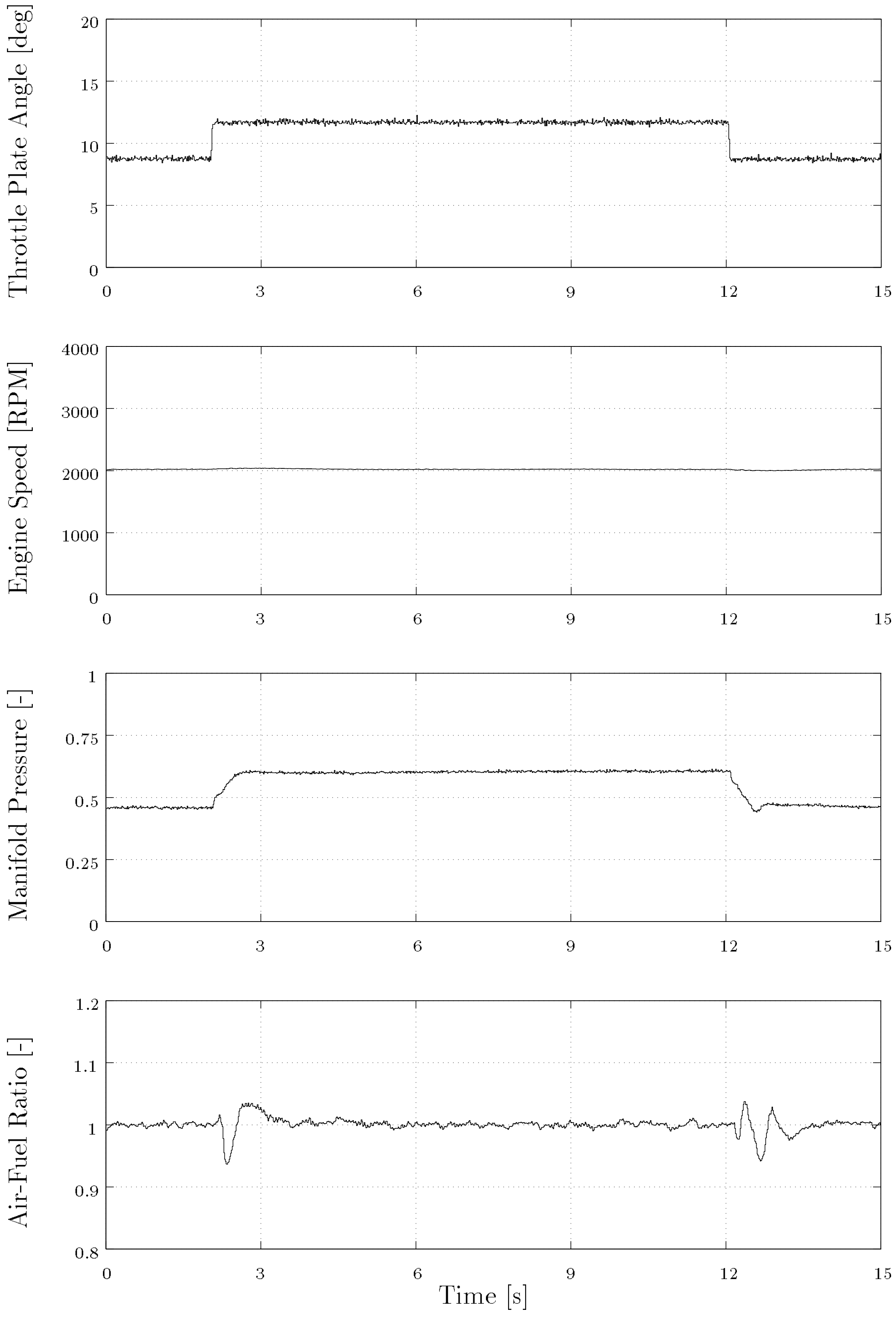

Figure 5.4: Active EGR Control, Measurements

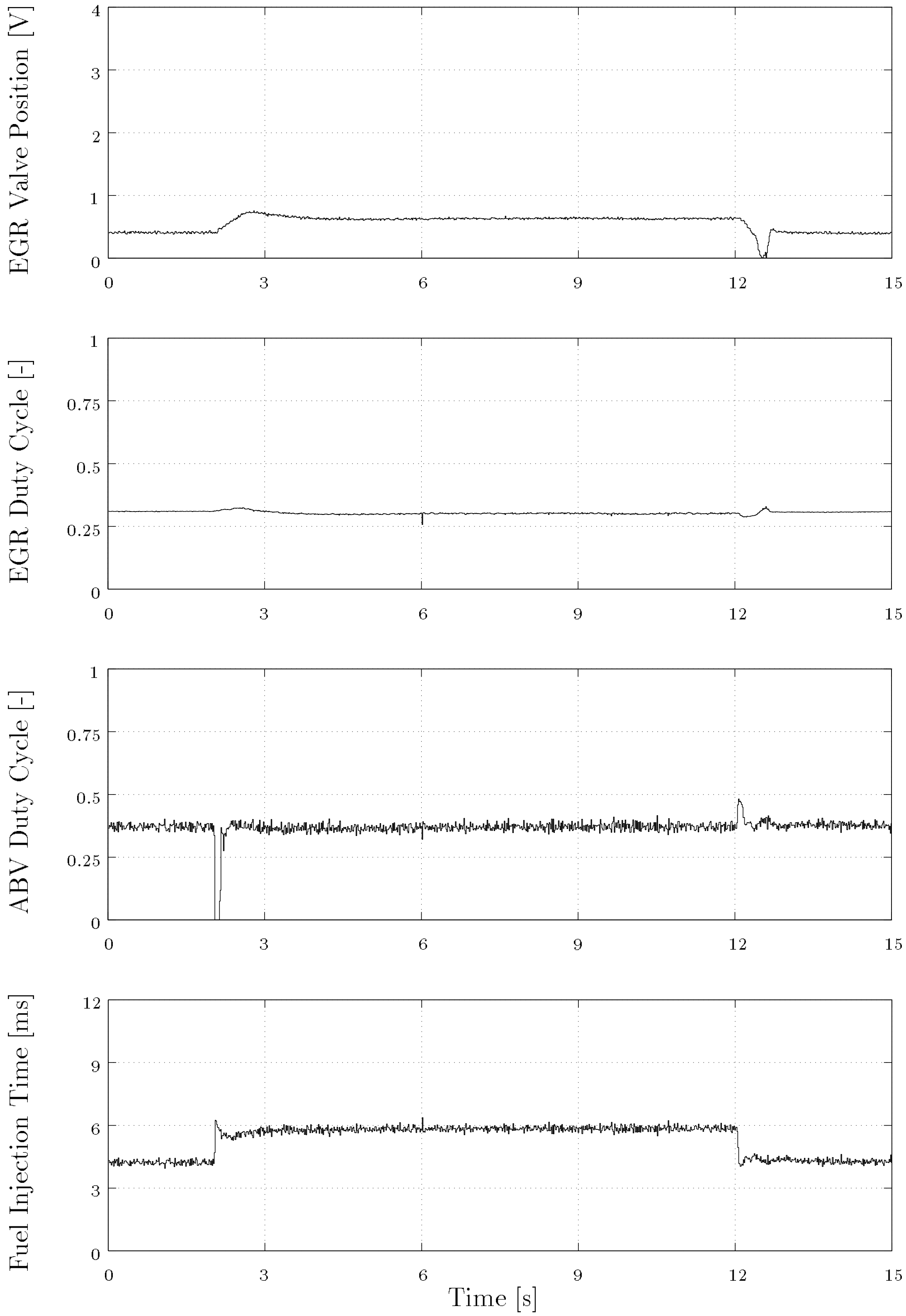

Figure 5.5: Active EGR Control, Control Signals

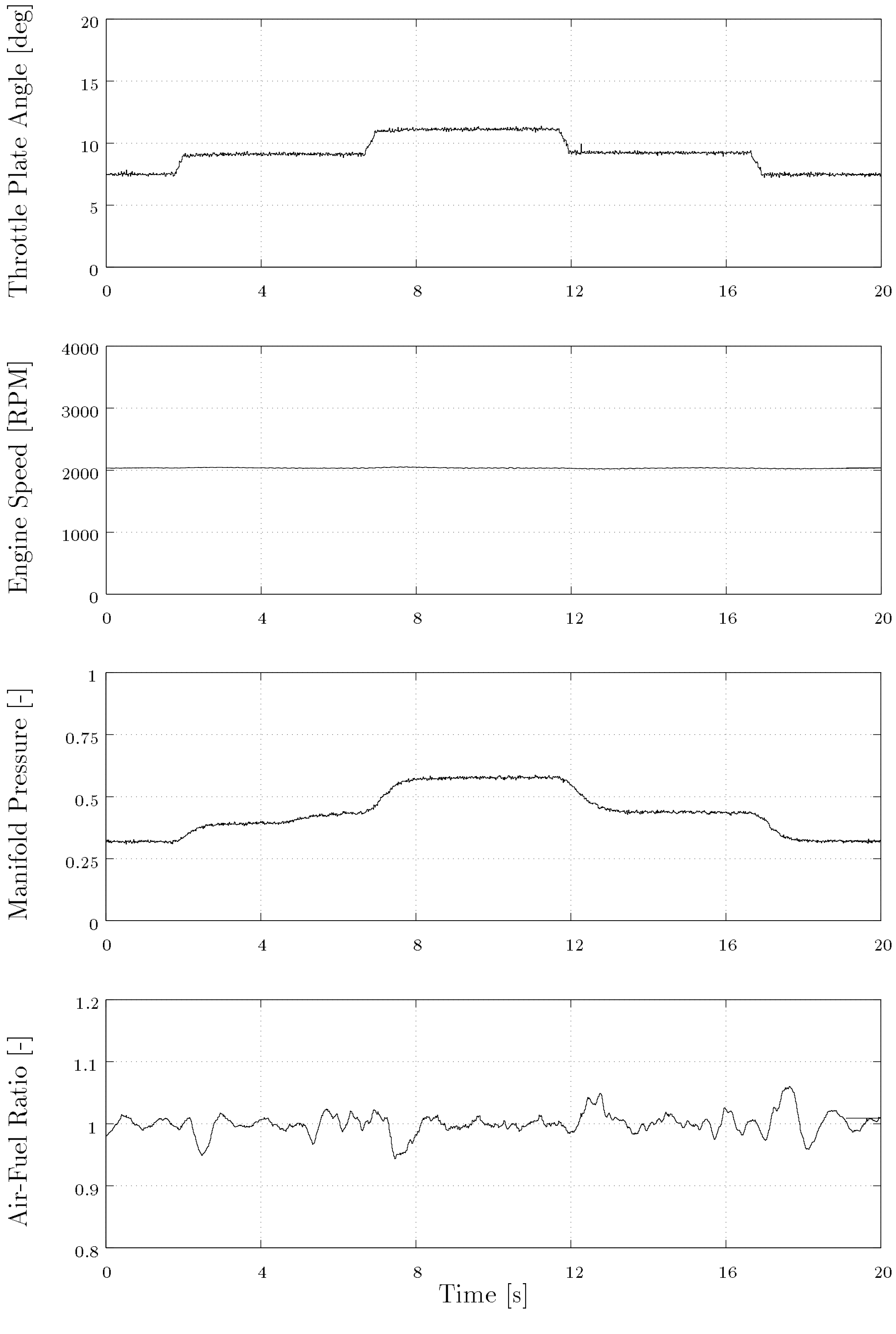

Figure 5.6: Modular Feedforward Design, Measurements

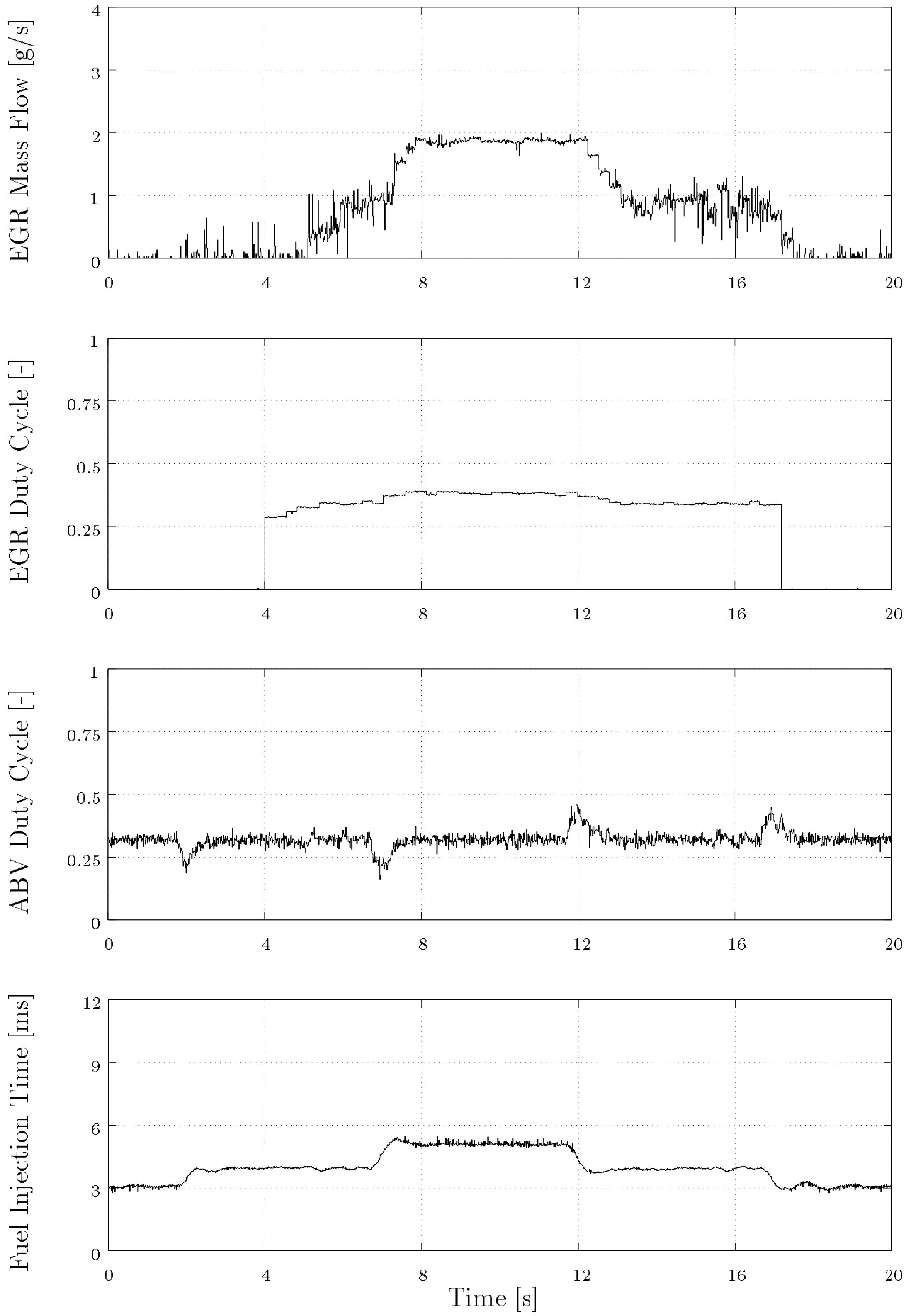

Figure 5.7: Modular Feedforward Design, Control Signals

6. CONCLUSIONS

6.1 Summary

In this thesis, the problem of transient air-fuel ratio control has been studied in a robust control framework. On the one hand the approach was based on a sophisticated theory of uncertain systems, on the other hand it had to be pragmatic, to cope with the practical requirements and the implementational issues. The design process was driven primarily by the experimental results and the experience gained in engine tests with a rapid prototyping system. At all design stages simple systematic procedures, such as the stability analysis in the gap metric, model matching, or the performance assessment via μ analysis, were applied to reveal the nature of problems as they occurred. In these applications, the suite of robust control techniques has proven to be a set of elegant, versatile, and effective tools.

6.2 Contribution

The problem of air-fuel ratio control has been studied in a robust control framework. The suitability of robust control techniques and their effectiveness for this application were demonstrated in a number of ways during control system design.

A uniformly discrete event-based representation of the engine processes was derived for robust control. In particular, the periodicity inherent in the engine operation was exploited in the derivation. Furthermore, the parameter dependencies in the model were incorporated in the system representation by assuming an underlying LFT model structure. In this way, the structure of the parameter dependencies in the component models was preserved, and the different effects of sampling and the variations of the physical parameters on the engine dynamics were explicitly accounted for. Different uncertainty descriptions were developed together with the model to capture the different sources of uncertainty.

The model development was geared particularly towards the design of parameter-dependent controllers and gain scheduling via linear fractional transformations. However, a complex μ analysis showed that the accuracy of the model should be improved by an order of magnitude above today's standards before such techniques could be used reliably.

Without additional devices such as electronic throttle or secondary air injection, usually no attempt is made at modulating the air flow through the engine in response to the driver's demand. Our approach has been to use an already existing component, the air by-pass valve, in a new way for air-fuel ratio control. Yet, its original functionality for idle speed control remains unaffected. The use of the air by-pass valve is especially effective, when it is co-ordinated with the fuel injection in a multi-variable control scheme.

The mechanism of exhaust gas recirculation was also integrated in the air-fuel ratio control scheme. We have dealt with the effects of exhaust gas recirculation in different control configurations and demonstrated the modularity and flexibility of our approach to control system design. The problem of exhaust gas recirculation should not be considered separately from the problem of air-fuel ratio control because beyond the merely static requirements for the EGR control system, there are opportunities to influence the mixture composition during transients by introducing EGR. The modular design serves as an example of how to treat interactive control systems without the need for switching between different modes of operation.

Recent advances in robust control theory were applied in the design of multi-variable controllers for transient air-fuel ratio control. The robustness and performance requirements were incorporated systematically in the problem formulation and the choice of weighting functions in an iterative design process. Both the stability and the sensitivity of the closed-loop system were analysed in a quantitative way to provide *a priori* predictions of its robustness and performance properties.

The key determinant for high performance is in the feedforward part of the control strategy, the effectiveness of which is only limited by the accuracy of the model. However, electronic throttle control is not necessarily prerequisite to be able to comply with future emissions standards.

A software environment for the analysis and design of engine control systems was developed that provides routines to automate the data management and the tasks during the design process. The concept of discrete parameter-dependent systems which are variable with the sample time was introduced in order to shift seamlessly between system representations in continuous and discrete time. Last but not least, powerful model reduction techniques were used for controller order reduction to enable an efficient implementation.

Robust multi-variable controllers were implemented successfully on a series production engine in a vehicle installation. The development of robust control strategies was accompanied by the development of a rapid prototyping system on the part of the Ford Motor Company which greatly enhanced the flexibility and the computing power of the experimental facilities. A generic and fully transparent approach to implementation was adopted to accommodate a linear time-invariant controller, or a number of gain-scheduled controllers, just as a single LFT parameter-dependent controller in a uniform control scheme.

The interactive design process can be automated to an extent that an iteration can be completed in the test cell on a notebook computer within a couple of hours. A single controller can be optimised to give a high level of performance in a certain operating region, superior to the performance of current engine management systems. However, the extensions to the control scheme that are necessary in order to complete a drive cycle successfully are limited at the moment for a number of reasons, not at least because the latest techniques of gain scheduling still exceed the available computing power. Perhaps only in ten years time, robust control strategies will be put in production, but they start paying off already by reducing the development times. In any case, this is where the future lies.

6.3 Future Research

The experimental requirements for engine testing on transient dynamometer facilities are very demanding. Since the resources are so expensive, they must be shared. Good time management is therefore essential. Moreover, the repeatability of the experiments is limited because of the numerous factors that are not under control. The number of tests that can be conducted during a day is also limited by the necessary recovery times, be it to reach some initial condition or to set up a revised experiment. It would therefore be very desirable and worthwhile to have available a nonlinear simulation model that is not only representative of the engine behaviour on the dynamometer but could actually be used to replace at least some engine tests in practice.

The need for a nonlinear simulation model that would allow for repeatable controller testing over a drive cycle can only be emphasised here. In any case, the behaviour of a control system should be tested under realistic conditions before implementation to ensure the correctness of the implementation as well as safe operation. If simulations were a viable alternative to the experiments in practice, the time constraints would be greatly alleviated and the cost much reduced. However, the task of developing such a model relies on the most accurate experimentation to begin with. The simulation program itself must be verified and maintained before the model can be validated with drive cycle data. Systematic procedures are required for the management of changes and the configuration of both the program and the model.

Much progress has been made in the course of this project in the development of a nonlinear hybrid simulation model that is programmed in SIMULINK. Effective means have been established for version and configuration management via a source code control system. In particular, the model is still to be validated over a drive cycle before it can be used realistically for controller testing. The model is then to be extended to include idle operation and cold start, as the scope of the emissions control problem is increased.

In the future, a more holistic approach to system identification should be adopted, where error analysis is an integral part of the modelling process, the experimentation, and, of course, the subsequent data analysis in order to reveal and quantify the secondary effects of factors such as unmodelled dynamics, noise, or procedural errors. To prove the concept and improve the process quality, the entire process of model development should be repeated, possibly for a different type of engine, so that the overall procedural accuracy can be improved systematically from the beginning. Moreover, alternative techniques of system identification should be explored to identify the dynamics of the engine in realistic driving scenarios rather than in equilibrium at fixed operating points. Separate models for acceleration, deceleration, and at zero load could be treated in the same way as models in different operating points. If the model parameters are derived from several different experiments, new ways of experimentation must be found to ensure the consistency of the operating conditions.

The structure of the parameter-dependent system representation will have to be refined according to the design experience based on the models in fixed operating points. It remains an open question, how large variations in gain across the operating envelope should be represented in an LFT framework without being overly conservative. In addition to the effects of parameter variations on the system's dynamics, the sensitivity of the control system's performance with respect to unmodelled dynamics should be studied in order to assess the significance of different sources of uncertainty. For the same reason, a comprehensive examination to describe process and measurement noise would be very desirable, for example in connection with the sampling of the pressure in the intake manifold. Finally, a statistical analysis over a drive cycle could provide a lot of information about the nature of the parameter variations for a more precise characterisation in terms of maximum deviations and rates of change. More generally, it could be of interest to establish analogies with other kinds of parameter-varying systems which are not necessarily periodic in time but in some other domain, perhaps other rotating machinery.

Before further efforts are invested into control design, the robustness of the current control system's performance should be analysed in more detail using complex and mixed μ calculations on the basis of the revised models. At a later stage a similar analysis including time-varying perturbations can be carried out for a control system that consists of several gain-scheduled controllers. Only then a further attempt should be made to re-design controllers in fixed operating points for maximum performance. After a successful implementation of these controllers, it would seem reasonable to try and extend the high level of performance across the operating envelope via gain scheduling.

In the event that a drive cycle can be completed in this way in principle, a number of direct, yet more difficult, control synthesis techniques for parameter-dependent systems can be applied to reduce potential conservatism. Furthermore, the parameter-dependent control design could be embedded in a μ synthesis procedure to account for unmodelled dynamics as well as time-invariant uncertainty. It would also be possible to incorporate the rates of change of the parameter variations into the design process. A practical comparison of the different techniques would be very worthwhile, especially with regard to the issues of controller complexity and implementation, since some techniques are genuinely based in continuous time while others are based in discrete time. However, all these techniques rely on computationally demanding problem formulations in terms of linear matrix inequalities, for which methods of solution exist, but special-purpose software is not readily available and the algorithms are numerically involved. Because of the computational constraints in the implementation a reduction of the controller complexity will be inevitable, yet for the reasons above model reduction for parameter-dependent systems is not at all a routine task.

The original ideas of $\mathcal{H}_\infty$ loop shaping can always be retained in a problem formulation that is based on the four-block problem, irrespective of the particular method of controller synthesis. Beyond the present application, it could be investigated how the open-loop settings of the plant or, in other words, the varying off-sets of the input and output signals could be integrated in an LFT framework.

As far as the experimental facilities are concerned, the greater the flexibility the better. The experimental set-up should allow for quick programming and exact repeatability of arbitrary transients. Ideally, any subsection of a drive cycle should be available on demand from the control computers of the dynamometer to be executed any number of times. In addition to the implementation of new control strategies on a rapid prototyping system, the functionality of current engine management systems should also be replicated and implemented in a high-level language so that parts of the strategy can be substituted easily and side effects can be overseen and eliminated when the two systems are working in parallel. Last but not least, rigorous test management and support are fundamentally important for smooth test operations.

APPENDICES

A Static Compensation of Actuator Nonlinearities

In Sections 2.2.2 and 2.2.3 the air by-pass and EGR valves were modelled as in Figure A.1(a). The model includes two static nonlinearities F_1 and F_2 at the input and output of the actuator. In a robust control framework, however, a simple linear, possibly uncertain, model from the input u to the output p_2 would be preferable.

Therefore the static behaviour of the actuators was linearised approximately by implementing a nonlinear pre-compensator F^* on the engine, see Figure A.1(c). Assuming an ideal compensator, the behaviour of the actuator is simplified to consist of the nominal valve dynamics G only. Depending on the precision of the linearisation, the gain of the system may vary slightly across the operating envelope.

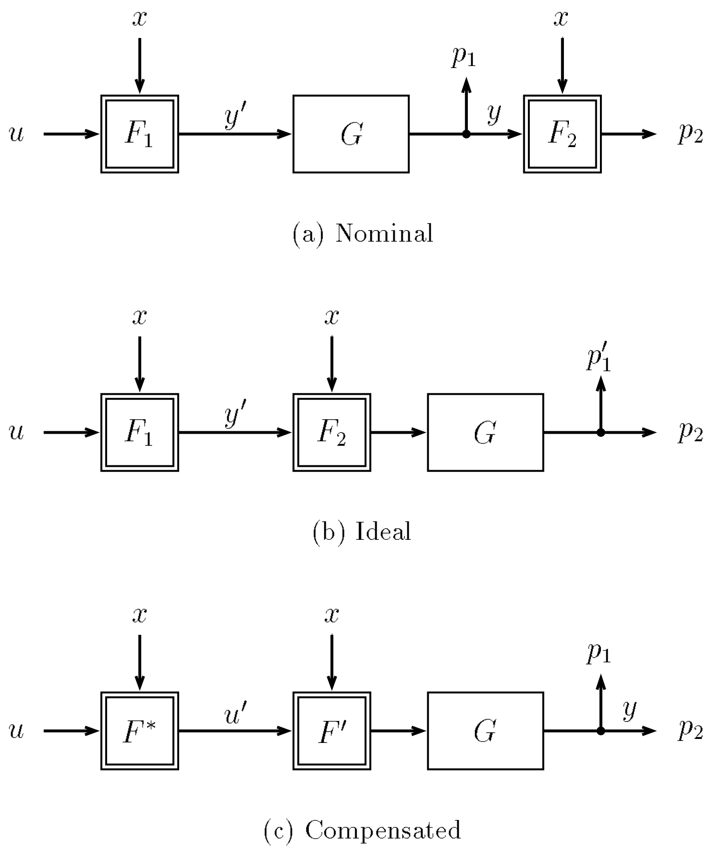

Figure A.1: Actuator Model

Without loss of generality, the system G is assumed to have unity gain; in fact, any physical gain can be absorbed in the input characteristic F_1. Under these circumstances the order of the blocks can be re-arranged as in Figure A.1(b). Strictly speaking, this is valid in steady state only. In the dynamic case the behaviour of the models in Figure A.1(a) and Figure A.1(b) on the page before may be quite different, depending on the nature of the nonlinearities. However, such an approximation may still be appropriate, if the changes in the operating condition x are relatively slow compared to the dynamics of G. After the originally separate nonlinearities are aggregated into a single nonlinearity at the input

$$F' = F_2 \circ F_1 \,, \tag{A.1}$$

the pre-compensator F^* is constructed such that:

$$p_2 = F'(F^*(u,x),x) = Ku \,, \tag{A.2}$$

where K is the nominal gain to be specified. Since the nonlinear function F' is given over a set of discrete operating points, it is separable in the variables x and u and can be inverted for fixed values of x, in fact pointwise, by simple geometric considerations. The revised actuator model can then be written as

$$p_2 = GKu \,. \tag{A.3}$$

For more information on actuator modelling in automotive applications the interested reader is referred to [33, 48].

B Bilinear Transformation with Variable Sample Time

The bilinear transformation for linear time-invariant systems

$$\frac{1}{s} = \frac{h}{2}\frac{z+1}{z-1} \tag{B.4}$$

can be represented in upper LFT form

$$\frac{1}{s}I = \mathcal{F}_u(N, z^{-1}I) \tag{B.5}$$

with the coefficient matrix

$$N = \begin{bmatrix} I & \sqrt{2\alpha}I \\ \sqrt{2\alpha}I & \alpha I \end{bmatrix} , \tag{B.6}$$

where α is half the sample time ($\alpha = h/2$). The continuous-time system

$$G = \left[\begin{array}{c|c} A & B \\ \hline C & D \end{array}\right] = \mathcal{F}_u(M, \frac{1}{s}I) \tag{B.7}$$

can be considered to be equivalent under the following transformation

$$G_d = \mathcal{F}_u(M, \mathcal{F}_u(N, z^{-1}I)) = \mathcal{F}_u(\tilde{M}, z^{-1}I) \tag{B.8}$$

to the discrete-time system G_d as defined by the matrix

$$\tilde{M} = \begin{bmatrix} (I-\alpha A)^{-1}(I+\alpha A) & \sqrt{2\alpha}(I-\alpha A)^{-1}B \\ \sqrt{2\alpha}C(I-\alpha A)^{-1} & D+\alpha C(I-\alpha A)^{-1}B \end{bmatrix} \tag{B.9}$$

in the sense that their frequency responses are the same except for a frequency scaling. The equivalence also holds for the larger class of LFT parameter-dependent systems

$$G = \mathcal{F}_\ell(M, \Delta_p)\,, \tag{B.10}$$

which can be seen from partitioning the coefficient matrix as follows:

$$M = \left[\begin{array}{c|c:c} A & B_1 & B_2 \\ \hline C_1 & D_{11} & D_{12} \\ \hdashline C_2 & D_{21} & D_{22} \end{array}\right]\,. \tag{B.11}$$

This relationship can be generalised to systems where the sample time itself is subject to perturbations

$$h = \bar{h} + \hat{h}\delta h \tag{B.12}$$

or is time-varying by some deterministic mechanism, as in the case of combustion engines, where the sample time is a function of engine speed. For that purpose, the bilinear transformation is re-defined as a function of the sample time

$$\frac{1}{s}I = \mathcal{F}_u(N, \begin{bmatrix} z^{-1}I & 0 \\ 0 & \delta h I \end{bmatrix}) = \mathcal{F}_u(N, \Delta) \tag{B.13}$$

with

$$N = \left[\begin{array}{cc:c} 0 & I & \frac{1}{2}I \\ 0 & I & I \\ \hdashline \hat{h}I & \bar{h}I & \frac{\hat{h}}{2}I \end{array}\right]\,. \tag{B.14}$$

The transformation is then represented by the star product $\mathcal{S}(N, M)$ shown in Figure B.2 on the following page. Re-ordering inputs and outputs, the state-space data of the equivalent discrete system

$$G_d = \mathcal{F}_\ell(\tilde{M}, \begin{bmatrix} \Delta_p & 0 \\ 0 & \delta h I \end{bmatrix}) \tag{B.15}$$

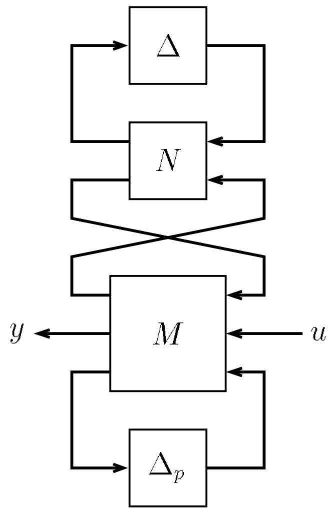

Figure B.2: Bilinear Transformation as Star Product

is given by

$$\tilde{M} = \left[\begin{array}{cc:}
(I-\bar{\alpha}A)^{-1}(I+\bar{\alpha}A) & (I-\bar{\alpha}A)^{-1}B_1 \\
2\bar{\alpha}C_1(I-\bar{\alpha}A)^{-1} & D_{11}+\bar{\alpha}C_1(I-\bar{\alpha}A)^{-1}B_1 \\
\hdashline
2\bar{\alpha}C_2(I-\bar{\alpha}A)^{-1} & D_{21}+\bar{\alpha}C_2(I-\bar{\alpha}A)^{-1}B_1 \\
(I-\bar{\alpha}A)^{-1} & \frac{1}{2}(I-\bar{\alpha}A)^{-1}B_1
\end{array}\right. \cdots$$

$$\cdots \left.\begin{array}{:cc}
(I-\bar{\alpha}A)^{-1}B_2 & 2\hat{\alpha}A(I-\bar{\alpha}A)^{-1} \\
\hline
D_{12}+\bar{\alpha}C_1(I-\bar{\alpha}A)^{-1}B_2 & 2\hat{\alpha}C_1(I-\bar{\alpha}A)^{-1} \\
\hdashline
D_{22}+\bar{\alpha}C_2(I-\bar{\alpha}A)^{-1}B_2 & 2\hat{\alpha}C_2(I-\bar{\alpha}A)^{-1} \\
\frac{1}{2}(I-\bar{\alpha}A)^{-1}B_2 & \hat{\alpha}A(I-\bar{\alpha}A)^{-1}
\end{array}\right] . \tag{B.16}$$

The resulting system is not periodic with the sample time any more, however, the periodic case is recovered for fixed perturbations δh. When dealing with linear parameter-varying systems, we can always assume that such a transformation has already been performed:

$$G_d = \mathcal{F}_\ell(\tilde{M}, \Delta_p)\,. \tag{B.17}$$

C Event-Based Continuous Frequency Domain

In this thesis, the frequency scale of all diagrams is continuous and, as usual, in rad/s. In Chapter 4 the control design is carried out in a continuous frequency domain, although the engine model from Chapter 2 is discrete and event-based. The bilinear transformation was used to switch between continuous and discrete time. First, the discrete-time model was transformed to continuous time to be able to use continuous-time design procedures. The resulting continuous-time controllers were then discretised again to be implemented on the engine, synchronised with engine events.

Because of this approach the continuous frequency scale is somewhat artificial and its relationship with physical time or physical frequencies not immediate. In fact, a frequency on this scale corresponds to different physical frequencies dependent on engine speed, as the corresponding sample time depends on engine speed. For easy reference, the corresponding physical frequencies and time constants are collected in Table C.1 and Table C.2 for a number of operating conditions.

	ω [rad/s]				
N [RPM]	0.01	0.05	0.10	0.50	1.00
870	0.29	1.45	2.90	14.50	29.00
1250	0.42	2.08	4.17	20.83	41.67
2000	0.67	3.33	6.67	33.33	66.67
2750	0.92	4.58	9.17	45.83	91.67
3500	1.17	5.83	11.67	58.33	116.67

Table C.1: Equivalent Physical Frequencies [rad/s]

The tables can be used as follows. There are two events per engine revolution. At 2000 RPM, for example, one revolution takes 30 ms, which corresponds to a frequency of $33.\bar{3}$ Hz or 209.44 rad/s, or equivalently to a time constant of approximately 5 ms. Therefore a frequency of 0.05 rad/s on the artificial frequency scale corresponds to a physical frequency of $209.44/\pi = 3.\bar{3}$ rad/s or a time constant of 0.3 s.

	ω [rad/s]				
N [RPM]	0.01	0.05	0.10	0.50	1.00
870	3.45	0.69	0.34	0.07	0.03
1250	2.40	0.48	0.24	0.05	0.02
2000	1.50	0.30	0.15	0.03	0.02
2750	1.09	0.22	0.11	0.02	0.01
3500	0.86	0.17	0.09	0.02	0.01

Table C.2: Equivalent Physical Time Constants [s]

D Gain Scheduling Schemes

In principle, there are two approaches to control design for systems which exhibit significant changes in dynamics across their operating envelope. One possibility is to consider local representations of such a system and to design controllers for individual operating points. The functionality of the controllers is then to be integrated to cover the entire operating envelope by interpolation. In doing so, it is important to ensure that the data to be interpolated are sufficiently smooth and that the states of the different controllers are always consistent with the state of the system.

Alternatively, a single parameter-dependent controller is designed directly for a parameter-varying system as a continuous function of the parameters which characterise the operating condition.

D.1 Gain Scheduling of Linear Time-Invariant Controllers

Given a number of linear time-invariant controllers

$$K_{ij}\,, \qquad i = 1, \ldots, I\,,\ j = 1, \ldots, J\,, \tag{D.18}$$

of equal state-space dimensions, pertaining to the operating points (n_i, p_j), the behaviour at an intermediate operating point (n^*, p^*) can be calculated as follows. First, the adjacent operating points are determined by searching through the set of operating conditions:

$$i^* = \max_{n_i \le n^*} i\,, \qquad j^* = \max_{p_i \le p^*} j\,. \tag{D.19}$$

If, in fact,

$$n_1 < n^* < n_I\,, \qquad p_1 < p^* < p_J\,, \tag{D.20}$$

then the scheduling parameters $0 \le \alpha \le 1$ and $0 \le \beta \le 1$ are calculated with respect to the operating point (n_{i^*}, p_{j^*}) such that:

$$n^* = (1-\alpha^*)n_{i^*} + \alpha^* n_{i^*+1}\,, \qquad p^* = (1-\beta^*)p_{j^*} + \beta^* p_{j^*+1}\,. \tag{D.21}$$

In all other cases either one or both coordinates of the operating point (n^*, p^*) coincide with the coordinates on the edge of the grid, and the generally two-dimensional interpolation becomes one-dimensional or just a look-up operation. In the general case, the state-space data pertaining to the intermediate operating point

$$M^* = \begin{bmatrix} A^* & B^* \\ C^* & D^* \end{bmatrix} \tag{D.22}$$

are obtained via bilinear interpolation as

$$M^* = (1-\beta^*)\left[(1-\alpha^*)M_{i^*j^*} + \alpha^* M_{i^*+1j^*}\right] + \beta^*\left[(1-\alpha^*)M_{i^*j^*+1} + \alpha^* M_{i^*+1j^*+1}\right]\,. \tag{D.23}$$

Finally, in discrete time the state update and output calculation is performed in a single step:

$$\begin{bmatrix} \dot{x}^* \\ y \end{bmatrix} = M^* \begin{bmatrix} x^* \\ u \end{bmatrix}\,. \tag{D.24}$$

Vector versus Matrix Interpolation

If the following condition for the size of the state-space data holds:

$$n_x + n_u > 4\,, \tag{D.25}$$

it is more efficient to update the adjacent systems $M_{i^*j^*}$, $M_{i^*+1j^*}$, $M_{i^*j^*+1}$, and $M_{i^*+1j^*+1}$ individually and to interpolate between the vectors $\left(\left[\begin{smallmatrix}\dot{x}^* \\ y\end{smallmatrix}\right]\right)_{i^*j^*}$, $\left(\left[\begin{smallmatrix}\dot{x}^* \\ y\end{smallmatrix}\right]\right)_{i^*+1j^*}$, *etc.* , rather than to interpolate the packed state-space matrices. While introducing $3(n_x+n_y)$ extra additions, this trick saves $(n_x+n_y)\times(n_x+n_u-4)$ multiplications.

Alignment of State Trajectories

The controllers that are to be interpolated may not have been intended originally for gain scheduling, or the continuity properties of the plant data may have been insufficient. To ensure that the controller data are sufficiently smooth, the state equations of any two controllers

$$\dot{x}_1 = A_1 x_1 + B_1 u \tag{D.26}$$
$$\dot{x}_2 = A_2 x_2 + B_2 u \tag{D.27}$$

are considered. By a change of coordinates the two systems can be made close, so that their state vectors

$$x_1(0) = \Gamma_1 u = \int_{-\infty}^{0} e^{-A_1\tau} B_1 u(\tau) d\tau \tag{D.28}$$
$$T x_2(0) = T\Gamma_2 u = T \int_{-\infty}^{0} e^{-A_2\tau} B_2 u(\tau) d\tau \tag{D.29}$$

are close at time zero. The output equations need not be considered for that purpose. A change of coordinates such that

$$\inf_T \|T\Gamma_2 - \Gamma_1\| \tag{D.30}$$

is given by

$$T = \Gamma_1 \Gamma_2^* (\Gamma_2 \Gamma_2^*)^{-1} \,. \tag{D.31}$$

Note that the linear operators Γ_1 and Γ_2 map $\mathcal{L}_2(-\infty, 0)$ onto $\mathbb{R}^n$, so that $T \in \mathbb{R}^{n\times n}$. Using the definitions above, the adjoint operator Γ_2^* is given, according to

$$< z, \Gamma_2 u > = z^* \int_{-\infty}^{0} e^{-A_2\tau} B_2 u(\tau) d\tau \tag{D.32}$$
$$= \int_{-\infty}^{0} z^* e^{-A_2\tau} B_2 u(\tau) d\tau \tag{D.33}$$
$$=< B_2^* e^{-A_2^*\tau} z, u >_{\mathcal{L}_2(-\infty,0)} \,, \tag{D.34}$$

by the expression

$$\Gamma_2^* z = B_2^* e^{-A_2^*\tau} z \,, \tag{D.35}$$

yielding the first term

$$\Gamma_1 \Gamma_2^* z = \int_{-\infty}^{0} e^{-A_1\tau} B_1 B_2^* e^{-A_2^*\tau} d\tau \; z \,. \tag{D.36}$$

The expression for the second term $\Gamma_2 \Gamma_2^*$ is very similar. Therefore the matrix T can be computed by solving the Lyapunov equation

$$\begin{bmatrix} A_1 & 0 \\ 0 & A_2 \end{bmatrix} \begin{bmatrix} X_{11} & X_{12} \\ X_{12}^* & X_{22} \end{bmatrix} + \begin{bmatrix} X_{11} & X_{12} \\ X_{12}^* & X_{22} \end{bmatrix} \begin{bmatrix} A_1^* & 0 \\ 0 & A_2^* \end{bmatrix} + \begin{bmatrix} B_1 \\ B_2 \end{bmatrix} \begin{bmatrix} B_1^* & B_2^* \end{bmatrix} = 0 \,. \tag{D.37}$$

T is finally calculated as

$$T = X_{12} X_{22}^{-1} \,. \tag{D.38}$$

D.2 Gain Scheduling via Linear Fractional Transformations

The implementation of a parameter-dependent controller is particularly simple and elegant via linear fractional transformations. If the controller can be represented as a linear fractional transformation of the state-space data

$$\begin{bmatrix} \dot{x} \\ y \\ z \end{bmatrix} = \left[\begin{array}{c|c:c} M_{11} & M_{12} & M_{13} \\ \hline M_{21} & M_{22} & M_{23} \\ \hdashline M_{31} & M_{32} & M_{33} \end{array}\right] \begin{bmatrix} x \\ u \\ w \end{bmatrix} \tag{D.39}$$

with a parameter-varying matrix

$$w = \Delta z = \operatorname{diag}(\delta_1 I_{n_1}, \delta_2 I_{n_2}, \ldots, \delta_f I_{n_f}) z \,, \tag{D.40}$$

which contains the scheduling parameters on the main diagonal, the controller is implemented as follows. Without loss of generality, it can be assumed that the parameter variations are normalised:

$$|\delta_i| \leq 1 \,, \qquad i = 1, \ldots, f \,. \tag{D.41}$$

Then the behaviour of the controller is completely determined by the matrix M, a vector of nonnegative integers

$$\mathcal{N} = \begin{bmatrix} n_1, n_2, \ldots, n_f \end{bmatrix} \,, \tag{D.42}$$

which denote the parameter multiplicities, and the current values of the parameter variations δ_i, $i = 1, \ldots, f$, the state x, and the input u respectively. In discrete time the control calculations take only two steps:

1. the LFT interconnection of the state-space data M with the matrix Δ according to

$$\mathcal{F}_\ell(M, \Delta) = \left[\begin{array}{c|c} M_{11} & M_{12} \\ \hline M_{21} & M_{22} \end{array}\right] + \left[\begin{array}{c} M_{13} \\ \hline M_{23} \end{array}\right] \Delta (I - M_{33}\Delta)^{-1} \left[\begin{array}{c|c} M_{31} & M_{32} \end{array}\right] \,, \tag{D.43}$$

2. the state update and output calculation for the resulting linear time-invariant system

$$\begin{bmatrix} \dot{x} \\ y \end{bmatrix} = \mathcal{F}_\ell(M, \Delta) \begin{bmatrix} x \\ u \end{bmatrix} = \left[\begin{array}{c|c} A & B \\ \hline C & D \end{array}\right] \begin{bmatrix} x \\ u \end{bmatrix} \,. \tag{D.44}$$

In fact, any control scheme which admits such a representation is readily implemented. Although the diagonal structure of Δ can be exploited, it is very demanding to perform a linear fractional transformation in real time, as it involves general matrix multiplications and a matrix inversion. In principle, the computational cost could be reduced to a certain extent by operating step 1 at a lower rate than step 2.

E LFT Realisation of Two-Dimensional Power Series

The two-dimensional power series

$$p(x,y) = \begin{bmatrix} x^0 & x^1 & x^2 & \dots & x^m \end{bmatrix} P \begin{bmatrix} y^0 \\ y^1 \\ y^2 \\ \vdots \\ y^n \end{bmatrix} \tag{E.45}$$

can be represented in upper LFT form

$$M_{22} + M_{21} \begin{bmatrix} xI_m & 0 \\ 0 & yI_n \end{bmatrix} \left(I - M_{11} \begin{bmatrix} xI_m & 0 \\ 0 & yI_n \end{bmatrix} \right)^{-1} M_{12} \tag{E.46}$$

with the coefficient matrix:

$$\begin{bmatrix} M_{11} & M_{12} \\ M_{21} & M_{22} \end{bmatrix} = \begin{bmatrix} \left[\begin{smallmatrix} A & B \\ 0 & C \end{smallmatrix}\right] & S \\ R & Q \end{bmatrix} \tag{E.47}$$

and the matrices A, B, C, Q, R, and S as given below.

Proof. Re-write Equation (E.46) on the current page as

$$\begin{aligned}
&Q + R \begin{bmatrix} xI & 0 \\ 0 & yI \end{bmatrix} \left(I - \begin{bmatrix} Ax & By \\ 0 & Cy \end{bmatrix} \right)^{-1} S = \\
&Q + \begin{bmatrix} R_1 x & R_2 y \end{bmatrix} \begin{bmatrix} I - Ax & -By \\ 0 & I - Cy \end{bmatrix}^{-1} \begin{bmatrix} S_1 \\ S_2 \end{bmatrix} = \\
&Q + \begin{bmatrix} R_1 x & R_2 y \end{bmatrix} \begin{bmatrix} (I - Ax)^{-1} & (I - Ax)^{-1} By (I - Cy)^{-1} \\ 0 & (I - Cy)^{-1} \end{bmatrix} \begin{bmatrix} S_1 \\ S_2 \end{bmatrix} = \\
&Q + R_1 x (I - Ax)^{-1} S_1 + R_1 x (I - Ax)^{-1} By (I - Cy)^{-1} S_2 + R_2 y (I - Cy)^{-1} S_2 \,.
\end{aligned}$$

Note that, if A is nilpotent, then

$$x(I_m - Ax)^{-1} = xI + x^2 A + x^3 A^2 + \dots + x^m A^{m-1} \,. \tag{E.48}$$

Therefore choose

$$S_1 = \begin{bmatrix} P_{10} \\ P_{20} \\ \vdots \\ P_{m0} \end{bmatrix}, \quad \text{and} \quad R_1 = \begin{bmatrix} 1 & 0 & \dots & 0 \end{bmatrix} \quad \text{and} \quad A = \begin{bmatrix} 0 & 1 & & 0 \\ \vdots & \ddots & \ddots & \\ 0 & \dots & 0 & 1 \\ 0 & \dots & 0 & 0 \end{bmatrix}, \tag{E.49}$$

so that

$$R_1\left(x + x^2 A + x^3 A^2 + \cdots + x^m A^{m-1}\right) = \begin{bmatrix} x & x^2 & x^3 & \ldots & x^m \end{bmatrix}. \tag{E.50}$$

Further comparison of the coefficients yields

$$B = \begin{bmatrix} P_{11} & \ldots & P_{1n} \\ \vdots & & \vdots \\ P_{m1} & \ldots & P_{mn} \end{bmatrix} \qquad R_2 = \begin{bmatrix} P_{01} & P_{02} & \ldots & P_{0n} \end{bmatrix} \quad \text{and} \quad S_2 = \begin{bmatrix} 1 \\ 0 \\ \vdots \\ 0 \end{bmatrix}. \tag{E.51}$$

The matrix C is of size $n \times n$, and its structure is that of A^*. Finally, the choice of $Q = P_{00}$ completes the construction. ■

F Notation

$\mathbb{R}$	field of real numbers
$\mathbb{C}$	field of complex numbers
$\in$	belong to
$\blacksquare$	end of proof
$:=$	defined as
$\bar{\alpha}$	mean value
$\hat{\alpha}$	deviation from mean value
I_n	$n \times n$ identity matrix
$[a_{ij}]$	a matrix with a_{ij} as its i-th row and j-th column element
$\mathrm{diag}(a_1, \ldots, a_n)$	an $n \times n$ diagonal matrix with a_i as its i-th diagonal element
A^*	conjugate complex transpose
A^{-1}	inverse of A
$\bar{\sigma}(A)$	largest singular value of A
$\underline{\sigma}(A)$	smallest singular value of A
$\sigma_i(A)$	i-th singular value of A
$\\|A\\|$	norm of A
$\mathcal{L}_2$	Lebesgue space
$\mathcal{H}_\infty$	Hardy space
prefix $\mathcal{R}$	real rational, e.g. $\mathcal{RH}_\infty$
$\left[\begin{array}{c\|c} A & B \\ \hline C & D \end{array}\right]$	shorthand for state-space realisation $C(sI - A)^{-1}B + D$ or $C(zI - A)^{-1}B + D$
$\mathcal{F}_\ell(M, Q)$	lower LFT (See Section 3.1.3 on page 48)
$\mathcal{F}_u(M, Q)$	upper LFT
$\mathcal{S}(M, N)$	star product (See page 48)

G Symbols

A	area	[m^2]
C	coefficient	[-]
G	plant	
K	controller	
N	engine speed	[RPM]
P	generalised plant	
R	radius	[m]
R	gas constant	[kJ/(kgK)]
T	temperature	[K]
V	volume	[m^3]
d	disturbance	
e	error	
h	sample time	[s]
i	current	[-]
m	mass	[kg]
p	pressure	[Pa]
r	radius	[m]
t	time	[s]
u	control input	
w	exogenous input	
x	state	
y	measurement	
z	generic output	

Greek Letters

Δ	uncertainty	[-]
α	throttle plate angle	[deg]
δ	scalar perturbation	[-]
ζ	fuel evaporation rate	[1/s]
η	efficiency	[-]
κ	specific heat ratio	[-]
λ	air-fuel ratio	[-]
τ	time delay	[s]
φ	crank angle	[deg]
χ	fuel fraction	[-]

Indices

0	ambient, or off-set
A	air
exh	exhaust
D	discharge, or displacement
F	fuel
M	manifold
R	ratio
TH	throttle
cal	calibration
cyl	cylinder
inj	injection
p	port
s	stoichiometric
v	volumetric

Acronyms

ABV	air by-pass valve
AFR	air-fuel ratio
(U)EGO	(universal) exhaust gas oxygen (sensor)
EGR	exhaust gas recirculation
FTP	federal test procedure
LFT	linear fractional transformation
LUT	look-up table
MIMO	multiple-input-multiple-output
PFI	port fuel injection
PRBS	pseudo random binary sequence
PWM	pulse-width-modulated
RPM	revolutions per minute
RMS	root-mean-square
SISO	single-input-single-output
TWC	three way catalyst
ULEV	ultra low emissions vehicles

BIBLIOGRAPHY

[1] A. Amstutz, N.P. Fekete, and J.D. Powell. Model-based air-fuel ratio control in SI engines with a switch-type EGO sensor. Technical Paper No. 940972, SAE, 1994.

[2] C.F. Aquino. Transient A/F control characteristics of the 5 liter central fuel injection engine. Technical Paper No. 810494, SAE, 1981.

[3] B.A. Ault. *System Identification and Air-Fuel Ratio Control of a Spark-Ignition Engine*. PhD thesis, Stanford University, 1994.

[4] B.A. Ault, V.K. Jones, J.D. Powell, and G.F. Franklin. Adaptive air-fuel ratio control of a spark-ignition engine. Technical Paper No. 940373, SAE, 1994.

[5] G.J. Balas, J.C. Doyle, K. Glover, A. Packard, and R. Smith. *μ-Analysis and Synthesis Toolbox*. The MathWorks, Inc., Natick, Mass., 1994.

[6] A.J. Beaumont, S.W. Beauchamp, and A.D. Noble. Air fuel ratio control technology for ultra low emissions vehicles. In *Proceedings of the Int. Symposium on Automotive Technology and Automation*, 1993.

[7] C. Beck, J. Doyle, and K. Glover. Model reduction of multi-dimensional and uncertain systems. *IEEE Transactions on Automatic Control*, 41(10):1466–77, 1996.

[8] G. Becker. *Quadratic Stability and Performance of Linear Parameter Dependent Systems*. PhD thesis, University of California, Berkeley, 1993.

[9] G. Becker and A. Packard. Robust performance of linear parametrically varying systems using parametrically-dependent linear feedback. *Systems & Control Letters*, 23(3):205–15, 1994.

[10] S. Boyd, L. El Ghaoui, E. Feron, and V. Balakrishnan. *Linear Matrix Inequalities in System and Control Theory*. SIAM, Philadelphia, 1994.

[11] K.J. Bush, N.J. Adams, S. Dua, and C.R. Markyvech. Automatic control of cylinder by cylinder air-fuel mixture using a proportional exhaust gas sensor. Technical Paper No. 940149, SAE, 1994.

[12] C.-F. Chang. *Air-Fuel Ratio Control in an IC Engine Using an Event-Based Observer*. PhD thesis, Stanford University, 1993.

[13] C.-F. Chang, N.P. Fekete, and J.D. Powell. Engine air-fuel ratio control using an event-based observer. Technical Paper No. 930766, SAE, 1993.

[14] D. Cho and J.K. Hedrick. Automotive powertrain modeling for control. *ASME Journal of Dynamic Systems, Measurement, and Control*, 111:568–76, 1989.

[15] D. Cho and H.-K. Oh. Variable structure control method for fuel-injected systems. *ASME Journal of Dynamic Systems, Measurement, and Control*, 115(3):475–81, 1993.

[16] F.M. Cornford. *Cambridge's Classic Guide to Success in the World, Microcosmographia Academica*. MainSail Press, Cambridge, 1993.

[17] R.A. Davis. *Model Validation for Robust Control*. PhD thesis, University of Cambridge, 1995.

[18] J.C. Doyle, B.A. Francis, and A.R. Tannenbaum. *Feedback Control Theory*. Maxwell Macmillan, New York, 1992.

[19] J.C. Doyle, K. Glover, P. Khargonekar, and B.A. Francis. State-space solutions to standard $\mathcal{H}_2$ and $\mathcal{H}_\infty$ control problems. *IEEE Transactions on Automatic Control*, 34(8):831–47, 1989.

[20] N.P. Fekete. *Model-Based Air-Fuel Ratio Control of a Multi-Cylinder Leanburn Engine*. PhD thesis, Stanford University, 1995.

[21] N.P. Fekete, U. Nester, I. Gruden, and J.D. Powell. Model-based air-fuel ratio control of a lean multi-cylinder engine. Technical Paper No. 950846, SAE, 1995.

[22] P. Gahinet, A. Nemirovski, A.J. Laub, and M. Chilali. *LMI Control Toolbox*. The MathWorks, Inc., Natick, Mass., 1995.

[23] T.T. Georgiou and M.C. Smith. Robust stabilization in the gap metric: Controller design for distributed plants. *IEEE Transactions on Automatic Control*, 37(8):1133–43, 1992.

[24] K. Glover and J. Doyle. State-space formulae for all stabilizing controllers that satisfy an $\mathcal{H}_\infty$-norm bound and relations to risk sensitivity. *Systems & Control Letters*, 11:167–72, 1988.

[25] K. Glover, J. Sefton, and D.C. McFarlane. A tutorial on loop shaping using $\mathcal{H}_\infty$ robust stabilization. In *Proceedings of the 11th IFAC World Congress*, pages 94–103, 1990.

[26] O. Hadded, J. Stokes, A.J. Cartmell, R.J. Brisley, and R. Brück. The achievement of ULEV emission standards for large high performance vehicles. Technical Paper No. 930389, SAE, 1993.

[27] E. Hendricks, M. Jensen, P. Kaidantzis, P. Rasmussen, and T. Vesterholm. Transient A/F ratio errors in conventional SI engine controllers. Technical Paper No. 930856, SAE, 1993.

[28] E. Hendricks and S.C. Sorenson. Mean value modelling of spark ignition engines. Technical Paper No. 90616, SAE, 1990.

[29] E. Hendricks and T. Vesterholm. The analysis of mean value SI engine models. Technical Paper No. 920682, SAE, 1992.

[30] E. Hendricks, T. Vesterholm, P. Kaidantzis, P. Rasmussen, and M. Jensen. Nonlinear transient fuel film compensation (NTFC). Technical Paper No. 930767, SAE, 1993.

[31] J.B. Heywood. *Internal Combustion Engine Fundamentals*. McGraw-Hill, 1988.

[32] J.B. Heywood. Future engine technology: Lessons from the 1980s for the 1990s. *ASME Journal of Engineering for Gas Turbines and Power*, 113(3):319–30, 1991.

[33] R. Isermann and U. Raab. Intelligent actuators — ways to autonomous actuating systems. *Automatica*, 29(5):1315–1331, 1993.

[34] J. Joyce. *Ulysses*. Oxford University Press, Oxford, 1993.

[35] P. Kaidantzis, P. Rasmussen, M. Jensen, T. Vesterholm, and E. Hendricks. Advanced nonlinear observer control of SI engines. Technical Paper No. 930768, SAE, 1993.

[36] U. Kiencke and C.-T. Cao. Regelverfahren in der elektronischen Motorsteuerung, Teil 1. *Automobil-Industrie*, pages 629–36, 1987.

[37] M. Majors, J. Stori, and D. Cho. An adaptive neural network control method for automotive fuel-injection systems. In *Proceedings of the IEEE Symposium on Intelligent Control*, 1993.

[38] D.C. McFarlane and K. Glover. *Robust Controller Design Using Normalized Coprime Factor Plant Descriptions*. Springer-Verlag, Berlin, 1990.

[39] J.J. Moskwa. *Automotive Engine Modeling for Real Time Control*. PhD thesis, MIT, Cambridge, Mass., 1988.

[40] J.J. Moskwa and J.K. Hedrick. Modeling and validation of automotive engines for control algorithm development. *ASME Journal of Dynamic Systems, Measurement, and Control*, 114(2):278–85, 1992.

[41] R. Musil. *Der Mann ohne Eigenschaften*. Rowohlt, Hamburg, 1984.

[42] C.H. Onder. *Modellbasierte Optimierung der Steuerung und Regelung eines Automobilmotors*. PhD thesis, ETH Zürich, 1993.

[43] C.H. Onder and H.P. Geering. Model-based multivariable speed and air-to-fuel ratio control of an SI engine. Technical Paper No. 930859, SAE, 1993.

[44] C.H. Onder and H.P. Geering. Measurement of the wall-wetting dynamics of a sequential injection spark ignition engine. Technical Paper No. 940447, SAE, 1994.

[45] A. Packard. Gain scheduling via linear fractional transformations. *Systems & Control Letters*, 22:79–92, 1994.

[46] A. Packard and J. Doyle. The complex structured singular value. *Automatica*, 29(1):71–109, 1993.

[47] E.M. Phillips and D.S. Pugh. *How to get a Ph.D.* Open University Press, Milton Keynes, Philadelphia, 1992.

[48] U. Raab. *Modellgestützte digitale Regelung und Überwachung von Kraftfahrzeugaktoren.* Nr. 313 in Fortschrittsberichte, Reihe 8. VDI-Verlag, Düsseldorf, 1993.

[49] H. Shiraishi, S.L. Ipri, and D. Cho. CMAC neural network for fuel-injection control. In *Proceedings of the American Control Conference*, pages 1773–7, 1993.

[50] H. Sindano. Phenomenological transient fuelling model for port injected engines. In *Proceedings of the IMechE*, 1990.

[51] R.C. Turin. *Untersuchung modellbasierter, adaptiver Verfahren zur Kompensation der Gemischbildungsdynamik eines Otto-Motor.* PhD thesis, ETH Zürich, 1992.

[52] R.C. Turin, E.G.B. Casartelli, and H.P. Geering. A new model for fuel supply dynamics in an SI engine. Technical Paper No. 940208, SAE, 1994.

[53] R.C. Turin and H.P. Geering. On-line identification of air-to-fuel ratio dynamics in a sequentially injected SI engine. Technical Paper No. 930857, SAE, 1993.

[54] R.C. Turin and H.P. Geering. Model-based adaptive fuel control of an SI engine. Technical Paper No. 940374, SAE, 1994.

[55] J. Updike. *Memories of the Ford Administration.* Penguin, London, 1993.

[56] G. Vinnicombe. *Measuring the Robustness of Feedback Systems.* PhD thesis, University of Cambridge, 1992.

[57] F. Wu. *Control of Linear Parameter Varying Systems.* PhD thesis, University of California, Berkeley, 1995.

[58] F. Wu, X.H. Yang, A. Packard, and G. Becker. Induced $\mathcal{L}_2$-norm control for LPV system with bounded parameter variation rates. In *Proceedings of the American Control Conference*, pages 2379–83, 1995.

[59] K. Zhou, J. Doyle, and K. Glover. *Robust and Optimal Control.* Prentice Hall, 1995.

INDEX